PhD PROGRAM

IN TRANSLATIONAL AND MOLECULAR MEDICINE

(DIMET)

Uptake and Intracellular Trafficking of Nanoparticles for Potential Medical Use

Coordinator : Prof. Andrea Biondi

Tutor : Prof. Giuseppe Miserocchi

Mentor: Prof. Nica Borgese

Dr. Barbara Lettiero

Matr. N° 034706

XXIII CYCLE

ACADEMIC YEAR 2009/2010

Table of contents

Chapter 3:

Chapter 4:

Chapter 5:

Chapter 6:

Chapter 1

General Introduction

1.1 Nanomedicine

In the last years nanotechnology has been undergoing an explosive expansion in many areas, such as cosmetics, electronics, aerospace and computer industry. According to the "National Nanothechology Initiative" (NNI), a multiagency US government program, *Nanotechnology* is defined as "the understanding and control of matter at dimensions of roughtly 1 to 100 nanometers, where unique phenomena enable novel application" [1]. Recently, as the need to define new paradigm especially for pharmacotherapy and diagnosis of incurable diseases, such as cancer, cardiovascular and neurological disorders is still pressing, this concept has been extended to medicine. Indeed, the National Institute of Health (Bethesda, MD, USA) introduced the term *Nanomedicine* to describe the application of nanotechnology to medical field especially for the treatment, diagnosis, monitoring and control of biological systems [2]. Engineered nanoparticles seem to be promising tools to achieve a number of these aims and two main types of nanomedicine products are currently in clinical trials: diagnostic tests and drug delivery devices [2]. The ultimate goal is the creation of combined diagnostic and therapeutic (theragnostic) nanoagents able to deliver molecules of interest to specific organs, tissues or cells, thus providing a personalized medicine which allows the prescription of precise treatments best suited for single patient [3]. However it is noteworthy that the 100 nm limit cannot be applicable to all particles tested for medical purposes. There are a number of literature reports in both basic science and pharmaceutical field which scientifically define dimensions of nanoparticles ranging in size from 1 to 1000 nm [4-6].

For instance, in the area of drug delivery relative large nanoparticles (> 100 nm) may be needed for loading a sufficient amount of drugs onto the nanocarrier [7]. Moreover, after intravenous injection of parenteral formulations, particle size must be below 5 μm to avoid blocking of fine capillaries leading to embolism [8].
Therefore, in this thesis, we consider all nanoparticles for which the size is between 1 and 1000 nm.

1.2 Nanomedicine and Nanoparticles

The increasing optimism towards Nanomedicine can be ascribed to the development of colloidal structures in the nanometer size range, called nanoparticles (NPs) which possess unique and attractive properties different from bulk materials.
The main factor is reasonable related to the small dimension that gives rise to an increased relative surface area and a quantum effect. Indeed, the physical and chemical properties of materials can significantly improve or radically change as their size is scaled down to small clusters of atoms [9]. In particular, these factors are responsible for modification in reactivity, strength and electrical characteristics of the nanostructures. For instance, as a particle decreases in size a greater proportion of atoms are found at the surface compared to those inside [10], thus inducing larger surface area per unit mass than bulk materials. This means that a given mass of NPs will be much more reactive than the same mass of material made up of larger particles [10]. In addition, at the nanoscale level a spatial

confinement of electrons may occur in semiconductor particles, thus generating a complete quantization of energy states [11] which confers them unique optical properties. In this way, particles can be made to emit or adsorb specific wavelength (color) of light, merely by controlling their size [10].

Mostly important being of the same size as biological entities, nanoparticles can readily interact with biomolecules on both the cell surface and within the cells **[fig1].** This property would make them very useful to identify diseases at earlier stage possible, ideally, at the molecular level [10].

Apart from the size other factors such as composition, shape, surface charge and chemistry may predict NPs behavior and effects in the human body, especially regarding their ability to overcome biological barriers of different nature (e.g. enzymatic degradation, uptake by scavenging phagocytic cells, abnormal flow of blood, hydrostatic pressure at target sites and epithelial barriers [12]). For instance, spherical particles were taken up by cells more quickly than rod-shaped particles of similar size [13], because of greater membrane wrapping time required for the elongated particles. Moreover, plasma protein adsorption onto NPs is likely due to a variety of effects including size, surface area and the curvature of NPs surface [14], thus affecting the eventual fate of NPs in the body (e.g. rate of clearance from the bloodstream, organ disposition, biodistribution) [15,16].

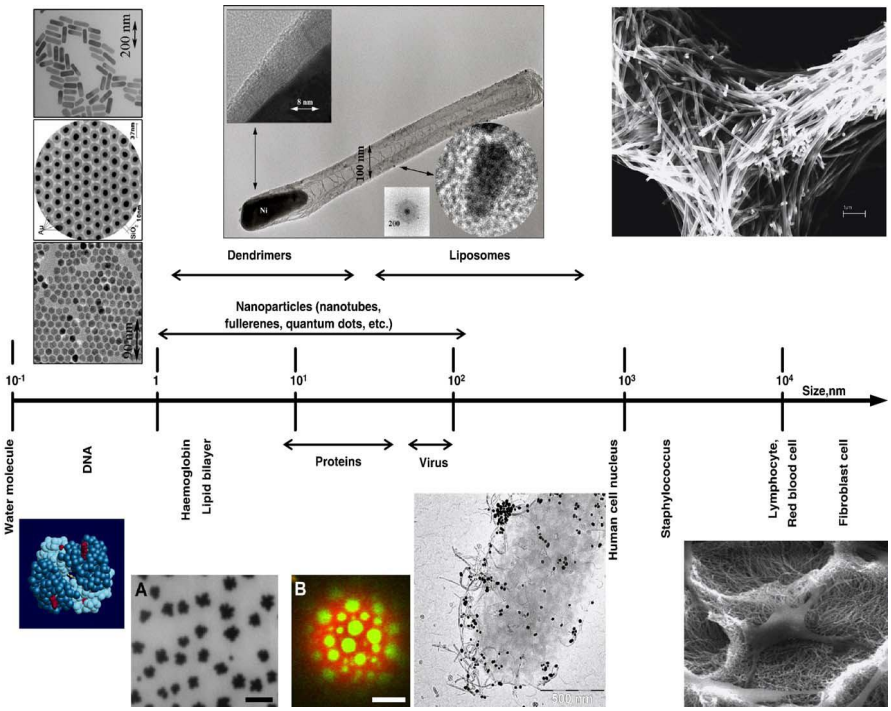

Fig.1: Nanotechnology could produce structures that have the same size than biological systems. Nanostructured material from left to right: gold nanoparticles, 37 nm diameter, and nanorods 200 nm length; carbon nanotubes, 200 nm diameter, with incorporated Ni particle of 8 nm; carbon nanotubes scaffolds. Biological structures from left to right: DNA; pulmonary surfactant vesicles and liposomes; Gram negative bacteria transfected with gold nanoparticles via carbon nanotubes; fibroblast growing on scaffold made of carbon nanotubes. Pison U. et al. 2006 [10].

Finally, the most promising advantage of NPs is based on their ability to entrap, bind, adsorb and carry several compounds like drugs, imaging agents, proteins and peptides. Consequently, the *in vivo* fate of molecules is determined by the properties of the carrier systems rather than those of the loaded agents. For instance, this would be very useful in order to increase the stability of peptides and proteins (cytokines, growth factors, hormones, vaccines), whose therapeutic potential, as well as clinical application, is often hampered by a

number of obstacles [17-18]. Being highly vulnerable molecules, they usually present short in vivo half-lives, due to degradation by enzymes, either at the site of administration or in every anatomical location [19]. Moreover, diffusion transport of large-size pharmaceutical proteins through epithelial barriers is generally slow, unless specific transporters are available. In the gastrointestinal tract the situation is even poorer due to degradation by acidic environment and proteases [20]. Likewise, great attempts have been directed towards development of new formulations for the enhanced delivery of either poor water soluble or cytotoxic drugs, such as paclitaxel and doxorubicin, to target tumors [21-23].

In light of this considerations, *nanoparticles* would have the desirable advantage of improving controlled release of molecules of interest at a specific site of action, thus minimizing any side effects.

1.3 Multifunctional Nanoparticles

1.3.1 "Stealth" Nanocarriers

The crucial step in developing engineered nanoparticles consists of preparing multifunctional nanocarriers with proper chemical moieties simultaneously assembled on their surface [24], in order to achieve various therapeutic and diagnostic purposes, such as passive or active targeting into the specific pathological zone **[fig.2]**. Among such modifications the most relevant result concerns the increase of both NPs stability and longevity in the bloodstream. Indeed, physicochemical parameters (size and surface characteristics) can control the degree of particle self-association [25] in biological fluids as well as particle clearance from the blood circulation. First, large surface area of NPs gives rise to increased reactivity which may determine dramatic changes in the effective size of the carriers upon introduction into a protein-containing medium (e.g. plasma) [26]. For example, dendrimers and quantum dots are well known to flocculate in biological media [26]. Second, since the first generation of colloidal carriers, characterized by variable hydrophobic surfaces, are recognized as foreign compounds by our immune system, they are promptly coated by plasma proteins (opsonins) and removed from the bloodstream by phagocytic cells, especially the liver and spleen macrophages (called *reticuloendothelial cells* or *RES*), within minutes [27]. For instance, intravenously (i.v.) administered polymeric NPs mainly distribute into liver (60-90% of the injected dose), spleen (2-10%), lung (3-20% and more) and bone marrow (>1%) [28].

In this view, several approaches have been proposed for the modification of hydrophobic particle surface by the addition of an emulsifying agent or a surfactant [26]. This is expected to be biocompatible, soluble, hydrophilic and with highly flexible main chain [24]. Such strategy led to production of a second generation of long circulating carriers (*"Stealth NPs"* or *"Sterically stabilized"*). For instance, copolymer non ionic surfactants (poloxamers and poloxamines) absorbed onto particle surfaces have proved to be useful to prolong NPs circulation time in mice and rats [29,30], as well as polysorbates which reduced the liver uptake and yielded the highest accumulation in heart, muscles, kidney and the brain [31]. It is known that the presence of such surfactants on particle surfaces strongly reduces interparticulate attractive Van der Waals forces while increasing repulsive barrier between two approaching particles [32]. However, lack of evidence of poloxamer penetration or adsorption onto liposomes [33] along with reduced biocompatibility of polysorbate 80-coated polybutylcyanoacrylate (PBCA) nanoparticles [34], pointed out the need for an alternative coating, such as Polyethylene glycol (PEG) and its derivatives [35-36].

Polyethylene glycol (PEG) is commonly used for this purpose because it has desirable attributes such as chemical inertness of the polymer backbone, excellent solubility in aqueous solutions, low degree of immunogenicity and antigenicity [37], and its hydroxyl groups are first activated and then reacted with the chosen molecule [26]. The molecular weight of the PEG segment should be between 2000 and 5000, in order to suppress protein adsorption. For instance, PEG-grafted liposomes, in the size range of 70-200 nm showed extended

circulation half lives of 15-24 hours in rodents and up to 45 hours in humans [38], whereas non PEGylated liposomes had half-lives of 2 hours [39].

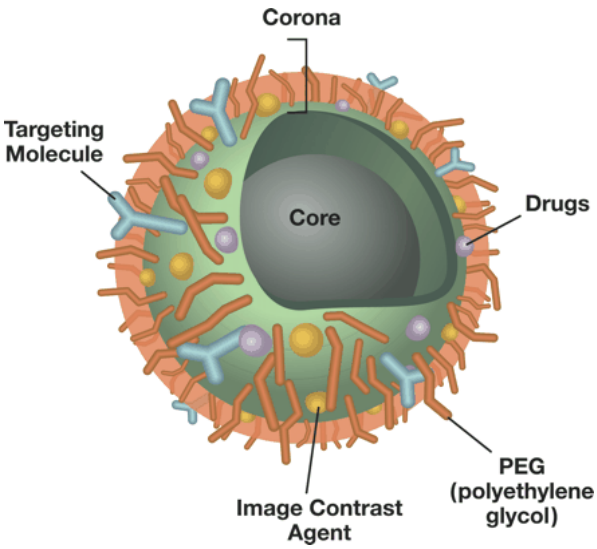

Fig.2: **The multifunctional nanoparticle**. The nanoparticles "corona" can be functionalized with hydrophilic polymers, targeting molecules, therapeutic drugs and image contrast agents. McNeil, S. E.. 2005

In general, it appears that polymer coatings sterically hinder interactions of NPs with blood proteins through the shielding of any surface charge and hydrophobicity, thus reducing NPs opsonization. Consequently, nanocarriers can evade macrophage recognition and gain prolonged residence time in the bloodstream, as widely reported in literature [40- 42].

1.3.2 Combination of polymer coating and targeted ligands

Besides increasing nanoparticle half-life in the circulation system a vast array of intriguing surface modifications, defined *NPs functionalization*, has also been developed to actively delivery the nanocarriers to specific body sites. Ligands (i.e. antibodies, peptides, sugar moieties) that specifically bind to surface epitopes or receptors, preferentially overexpressed at target sites, are coupled to the surface of polymer-coated NPs, such as liposomes [43,44]. In particular, potential ligands were attached to the activated far (distal) ends of some liposome-grafted polymeric chain [45], so that they are extended outside of the dense PEG brush [24], reducing any steric hindrances for their binding to the target.

Nowadays the majority of efforts relates to cancer targeting because of the potency and the citotoxicity of chemotherapeutic agents. Indeed, very attractive strategies are based on better opportunities of long circulating NPs to leak out of the tumor vasculature, which can exhibit pore size up to 700 nm [46], rather than extravasate from normal vessels (defined *passive targeting*). A representative example is Doxil (Ortho Biotech), a PEG-liposome containing the cytotoxic drug doxorubicin [47], which has been used in the clinic for over two decades. However, since the coupling of higher interstitial with lower intravascular pressure could remarkably limit the movement of NPs out of blood vessels in experimental tumors [48], active targeting via the inclusion of targeting molecules on NPs surfaces is considered the most effective strategy to enhance cellular uptake into cancer cells [49]. Different approaches are being pursued for this purpose, which include nanoparticle conjugation either to folate or to antibodies

against tranferrin receptors (TfR), as well as to tranferrin itself [24]. For instance, superparamagnetic magnetite NPs modified with folate demonstrated to be a promising tool for diagnostic applications [50]. Moreover, immunoliposomes coupled with OX26 monoclonal antibody to rat TfR were also successfully found to accumulate in brain microvascular endothelium [51].

Finally, additional components, such as PH-sensitive coatings, might be added to Stealth NPs to generate stimuli-responsive systems able to degrade and release the entrapped drugs or contrast agents only in body's sites or cell compartments with lowered PH, like tumors, infarcts, inflammatory zones, cell cytoplasm or endosomes [24]. A variety of liposomes and polymer based carriers have been described for such purpose in literature [52-53]. However, these smart multifunctional systems still represent a challenge.

1.4 Different types of Nanoparticles for drug delivery and imaging

Among the several colloidal systems produced it is difficult to determine which of them might be the most suitable for biomedical purposes. Indeed, lipid-based NPs, such as Solid Lipid Nanoparticles (SLN) and iron oxide NPs are all examples of promising particulate carriers and their properties, in some case issues, will be summarized below.

1.4.1 Solid Lipid Nanoparticles (SLN)

SLN are particles made of an high melting fat matrix (hydrophobic core) surrounded by phospholipids and physically stabilized by emulsifiers (0,5 to 5%). The lipids used are solid at room temperature and also at body temperature and they include triglycerides (i.e. tristearin, tripalmitin), complex glyceride mixture, steroids (i.e. cholesterol), fatty acids and waxes (i.e. cetyl palmitate) [54-55]. SLN are produced by using several methods based on nature and solubility of the entrapped molecules [54]. This leads to the production of different drug incorporation models: *a solid solution model*, in which lipophilic drugs are completely dispersed in the fat matrix, *a drug-enriched shell model*, where drugs concentrate in the still liquid outer shell of the SLN and *a drug-enriched core model* in which drugs precipitate prior to lipid crystallization [**fig.3**].

Since their first description by Muller et al. [56], SLN have been considered alternative carriers to well-established systems, like liposomes and polymeric nanoparticles. The main advantage of SLN

is related to the expected very low acute and chronic toxicity due to their physiological and biodegradable components and to the avoidance of any organic solvents in the production procedures. Above all, being in the solid state, SLN can reduce drug mobility, thus achieve controlled drug release. Therefore, they might overcome some physical and chemical instabilities described for liposomes, which can compromise the performance of these carriers [57]. For instance, Cavalli et al. [58-59] have reported promising data on sustained *in vitro* release of anticancer drugs paclitaxel, doxorubicin and idarubicin (0,1% after 120 min) in contrast to burst release from reference solutions. Interestingly, an increased doxorubicin uptake was observed in rabbit brains only after i.v. administration of Stealth SLN [60]. In general, despite intensive studies are carried out to optimize the production of Stealth SLN, more *in vivo* and *in vitro* reports are needed to better clarify nanoparticle behavior.

Among SLN disadvantages we may include low loading capacity, limited either by the formation of a perfect lipid crystal matrix during SLN production or by any drug expulsion after polymorphic transition during storage [57]. Moreover, due to their hydrophobic nature, SLN are expected to poorly entrap hydrophilic molecules. Indeed, some reports demonstrated evidence of initial burst release of hydrophilic molecules, due to their adsorption on SLN surfaces, followed by a well-defined slow release [61,62]. Finally, alternative colloidal structures (micelle, liposomes, mixed micelles) may be present in the aqueous dispersion [63]. However, new formulations, called nanostructured lipid carriers (NLC), mixing lipid of different natures, along with new methods of production, such as double emulsion

(w/o/w), with drug encapsulation in the internal water SLN phase, have been developed to overcome some of these drawbacks [57].

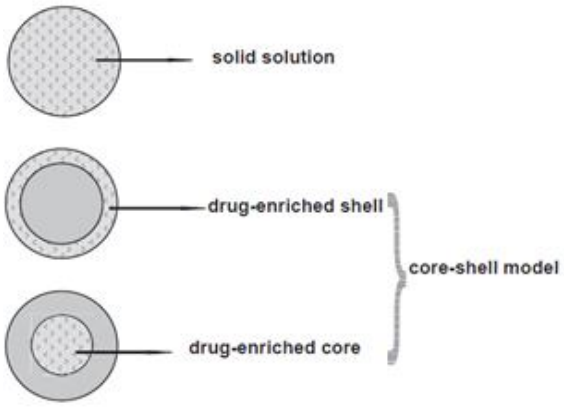

Fig.3: Models of drug incorporation into SLN: homogeneous matrix of solid solution (upper),
drug-free core with drug-enriched shell (middle), drug-enriched core with lipid shell (lower). Üner M. and Yener G 2007 [63].

1.4.2 Iron oxide Nanoparticles

For nearly 40 years much work has been directed towards the production and characterization of superparamagnetic nanoparticles as alternative agents for diagnostic (magnetic resonance imaging, MRI) and therapeutic purposes (local heat source in the case of tumor therapy, called *magnetic hyperthermia*). This increasing interest is related to NPs inducible magnetization, which allow them to be directed to a defined location or heated only in the presence of an externally applied magnetic field [64]. Furthermore, due to their size, magnetic NPs could be smart probes for targeting macromolecules and cells and for tracking biological processes (*molecular imaging*). Two different classes of iron based NPs are currently used in clinical imaging, namely superparamagnetic iron oxide (SPIO) particles with mean diameter of more than 50 nm and ultrasmall superparamagnetic iron oxide (USPIO) particles with smaller hydrodynamic diameter [65].

Iron oxide NPs are composed of a magnemite and magnetite (Fe2O3 and Fe3O4) core coated with biocompatible organic compounds (polysaccharides, i.e. dextran, chitosan, PEG, polyvinyl alcohol, and low- molecular- weight dispersants, such as dopamine). These coating are required to prevent destabilization and aggregation of the colloidal suspension in aqueous solution, thus making the nanoparticles soluble in biological media [66]. Moreover, they could serve for further functionalization of the particles by ligands, in order to facilitate their cell and tissue targeting (e.g. pH- and temperature-sensitive coatings) **[fig.4]**.

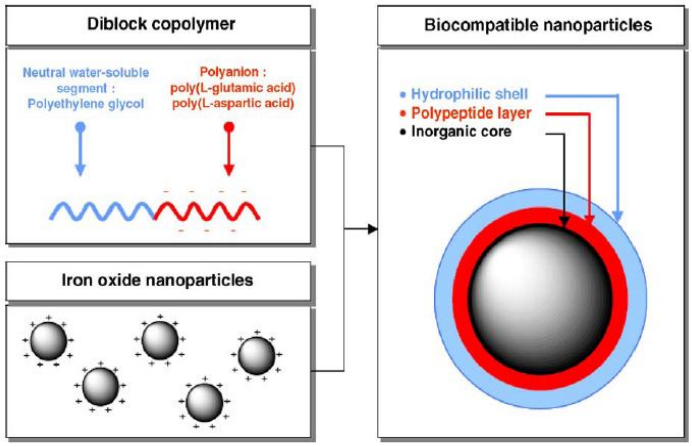

Fig. 4: Iron oxide nanoparticles: the inorganic core provide MRI imaging features, diblock copolymers could be selected to give a hydrophiclic shell and a polypeptide layer sensitive to the environment (pH, temperature, ion content etc.). Pison U. et al. 2006 [10]

The performance and *in vivo* fate of iron oxide NPs are crucially dependent on the nature of the coating and on its ability to relate to the biological environment. Indeed, polymer-coated SPIONs demonstrated to be more stable in water and in phosphate buffered saline (PBS) for months than the uncoated counterpart [64]. However, vinyl alcohol/vinyl amine copolymer coated particles (A-PVA SPIONs), once added in cell medium DMEM (Dulbecco's Modified Eagle's Medium) showed a stable particle size during the first hour but an increase in their diameters from 40 nm up to 110 nm after 2 h [64]. Further studies are needed to better characterized NPs properties gained in more "physiological" fluids (i.e. cell culture media, in presence or in absence of serum).

Moreover, in patients the blood half-life of different iron oxide NPs vary from 1h to 24h/36h and the determining factors are both NPs size and surface properties. Indeed, highly anionic surfaces of USPIO (8.7

nm), usually less prone to liver uptake because of their small size, showed the shortest half-life in humans due to their coating with citrate [66]. Likewise, intracellular metabolism is also related to the chemical composition of these NPs. It's known that iron-based NPs share their predominant internalization by hepatic macrophages (Kupffer cells) and for such reason they are widely use for liver imaging and for diagnosis of inflammatory disorders associated with high phagocytic activity (i.e. atherosclerosis and brain ischemia) [67]. Indeed, dextran coating of iron NPs (i.e. ferumoxtran-10 or SINEREM) was completely degraded in macrophage lysosomes by intracellular dextranases within 7 days [68] and almost exclusively eliminated in the urine (89% in 56 days) due to its low molecular weight.

However, there is some evidence of uncoated iron nanoparticle-induced ROS production in human microvascular endothelial cells (HMVECs), which could directly increase cell permeability trough the remodeling of microtubules [69].

All of these results underscore the importance of the use of polymer coatings for making safe iron NPs, but above all they point out the necessity to better characterize the fate of such iron carriers in different body compartments at later time points, once free iron is eventually released from degraded NPs.

1.5 Nanoparticle interactions in the blood compartment

On exposure to blood, nanoparticles may encounter a plethora of proteins and immune cells responsible for their uptake and clearance from the circulation system, such as monocytes, platelets, leukocytes and dendritic cells (DC). The key role is predominantly attributed to macrophages residing in the liver (Kupffer cells) and in the marginal zone and red pulp of the spleen, which recognize and bind plasma proteins adsorbed onto NPs surface (opsonic molecules) via their scavenger receptors. In particular, this process of protein adsorption, termed *opsonization*, mainly enhance further NPs phagocytosis which consists of engulfment by lamellipodia that project from macrophage surface, internalization by zipper process and subsequent delivery of the particles to acidic endosomes and finally to lysosomes for degradation [70].On the other hand, dysopsonic proteins, like albumin, promote prolonged NPs circulation times in the blood [71,72], once they are bound to NPs surface.

The opsonins comprise various elements, such as different subclasses of immunoglobulins, complement proteins, like C1q and generated C3 fragments (C3b, iC3b), apolipoproteins, von Willebrand factors, thrombospondin, fibronectin and mannose-binding protein [26]. The plasma protein composition on a given nanoparticles, at a given time, depends on several factors, like inter-individual variations in blood opsonic concentration [26] and binding affinities; the latter is closely related to NP properties, like size, surface charge density and curvature.

In general, the number of proteins bound to nanoparticles scales up with increasing hydrophobicity of NPs surface as well as size. For instance, a study showed that apolipoproteins AI, AII, AIV and E as well as albumin and fibrinogen were preferentially bound to the more hydrophobic copolymer particles compared to the hydrophilic ones [73]. Moreover, larger particles (200 nm and above) are more rapidly cleared from the blood than their smaller counterpart [9] and at the same time they are more prone to activate the human complement system.

Likewise, neutral particles have a distinctively slower opsonization rate, thus reduced RES uptake in the liver, compared to negatively charged NPs, as demonstrated for liposomes [74]. Furthermore, positively charged particles have been known to form aggregates in the presence of the negatively charged serum proteins, which often cause transient embolism in the lung capillaries [75].

However, the smaller the NPs (those with a diameter of less than 100 nm) the easier the penetration through the hepatic sinusoidal endothelium, due to the size of its fenestrations which are about 100-150 nm in diameter [76]. Moreover, particles less than 10 nm can leave the systemic circulation through the permeable vascular endothelium in limph nodes [26]. In light of these considerations, several efforts has been directed towards suppression of opsonization events, in order to keep the particles into the vasculature and enhance their delivery to specific body compartments other than macrophages. One of the earliest strategy was the coupling to linear sugars, like dextrans [77] and to sialic and polysialic acids, by mimicking the mammalian cell surfaces [26] up to the employment of polymers and

surfactants like PEG, polyethylene oxide (PEO), poloxamer, poloxamine, polysorbate (Tween 80) [78]. The protective effect of such hydrophilic coatings on carriers is mostly related to their high surface density and long chain-lenghts which adopt a brush-like configuration forming a sterically-uncharged barrier, thereby reducing zeta potential and phagocytosis [78] **[fig.5]**. Indeed, a decrease in the distance between PEG chains from 6.2 nm to 5.1 nm drastically decreases the adsorption of apolipoproteins up to 90% [78]. Moreover, dextran immobilized onto polystyrene substrate through both terminal groups ("side-on conformation") was much more effective in preventing fibrinogen adsorption compared to the counterpart anchored only through one terminal group ("end-on conformation") [79].

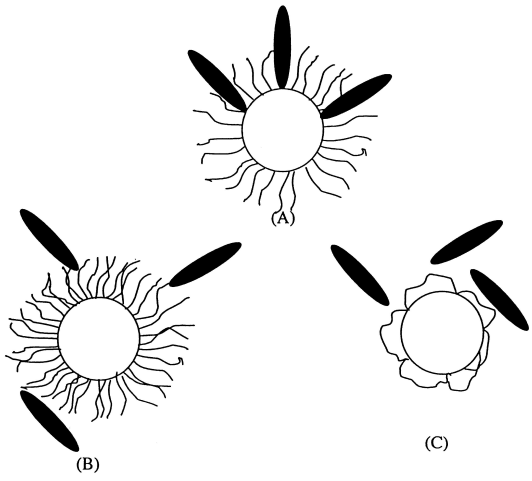

Fig. 5 Effect of surface PEG density and its conformation on the opsonization process: (A) opsonization takes place when the density is low, (B) opsonization is not possible at higher surface density and (C) when both the end groups of PEG participate in surface modification. Kumaresh S. et al. (2001) J. Control. Rel. 70:1-20 [78].

As a rough summary, particles that are in the range of 100-200 nm in diameter with neutral and hydrophilic surface exhibit the best properties to gain prolonged circulation time in the blood.

However, all polymer-grafted NPs are at some point cleared from the blood by macrophages of the RES [26]. Based on their physicochemical properties, these coatings may be plausibly displaced by some plasma proteins or their linkages to NPs surfaces may undergo chemical breakdown in the blood [26]. Nevertheless, some populations of stimulated or activated macrophages are capable of recognizing and internalizing Stealth NPs by an opsonic-independent process [80,81].

Therefore, these above observations probably explain why the residence time of engineered long circulating NPs in the blood never exceeds 3 to 5 days.

1.5.1 The activation of Complement System

Despite the mechanism involved in the opsonization and clearance of particulate carriers after i.v. injection are not well understood [82], the components of the complement system seem to play a role synergetically with the other opsonins in order to prepare particles for phagocytosis.

The complement system comprising at least 35 soluble and membrane-bound proteins, receptors and regulators is one of the most ancient defense mechanism, with a primary function of destroying and removing foreign substances (e.g. pathogens, engineered nanoparticles) along with apoptotic cell debris from the body, either by direct lysis or by mediating leukocyte function in inflammatory and innate immunity [83]. It also serves as an important effector of acquired immunity, through enhancement of B-cell responses to an antigen and promotion of the activation of DC and T-cells [84].

Based on activation triggers, there are three established pathways of the complement cascade, namely the classical, the lectin and the alternative pathways (CP, LP and AP respectively)**[fig.6]**.

They all converge in the central event of the complement activation, that is the cleavage of C3 into C3b and C3a via two enzyme complexes, termed C3 convertases (notably C4b,2a and C3b, Bb for CP/LP and AP pathways respectively).

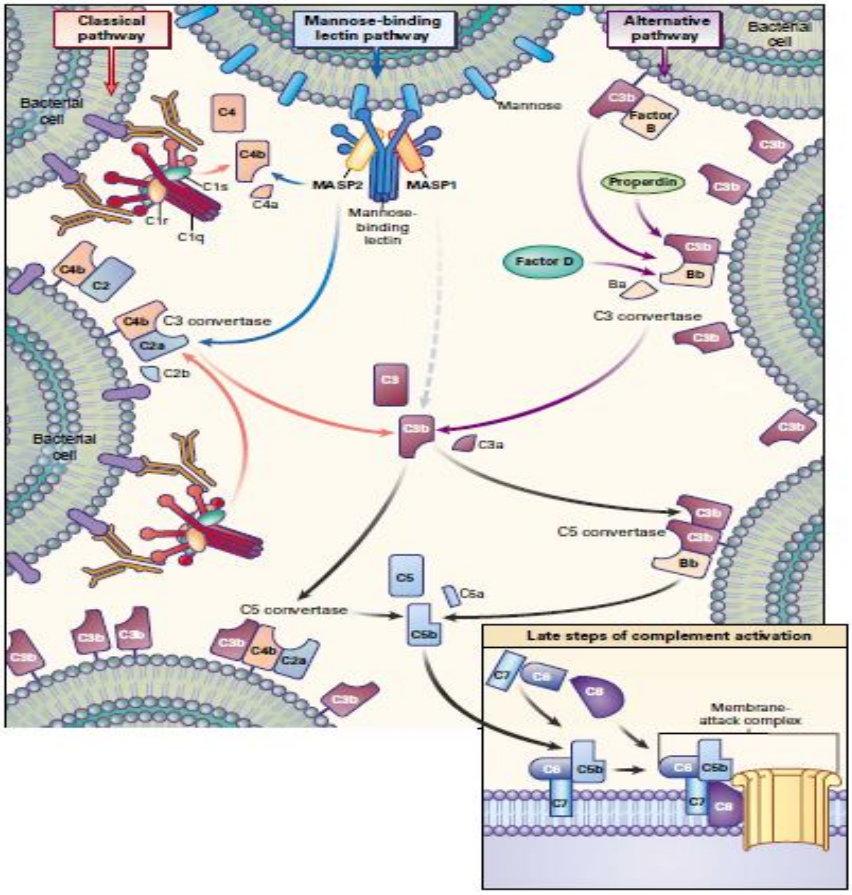

Fig. 6: The Three Activation Pathways of Complement : the Classical, Mannose-Binding Lectin and Alternative Pathways. Walport M.J.(2001) N Engl J Med 344(14): 1058- 1066.

CP is generally triggered by recognition and subsequent binding of the multimeric calcium sensitive C1q component to an antigen-antibody complex on the surface of foreign intruders. However, the direct binding of either C1q or C- reactive protein to certain surfaces may also trigger this enzymatic cascade. It causes the sequential activation

of C4 and C2 factors involving serine proteases C1q subunits, C1r and C1s [85]. LP is usually considered an antibody independent pathway and is activated by the binding of mannose-binding lectin (MBL) or ficolins to high-density carbohydrate arrays presented at the bacterial cell wall (e.g. D-mannose, L-fucose and N-acetylglucosamine) [85].

However, a recent study proposed heavily glycosylated molecules, such as human IgA, as likely candidates for LP activation [84]. Finally AP is triggered by spontaneous hydrolysis of the internal thioester bond within C3 in the fluid phase [86], inducing a conformational change that enables binding to factor B, cleavage by factor D and further formation of the soluble C3 convertase. Moreover, incorporation of NH_3, OH or COOH groups on foreign surfaces influence the activation of AP pathway [83,87]. Indeed, to guarantee immediate response to "non self" substances, the cascade is constantly kept at a low level of activity- "tick over"- by the AP [88]. This pathway also serves as a major amplification loop for C3 conversion (C3 feedback) in any type of complement activation [85,89], by which an initial weak stimulus may be markedly enhanced [83]. In particular, the plasma protein properdin may play a key role in amplifying complement activity, due to its ability to stabilize AP C3 convertase, thus enabling C3b to bind to it and forming the alternative C5 convertase [89].

Several consequences result from complement activation, once the nascent C3b fragments are covalently bound to patches of hydroxyl and amine groups on target surfaces via their reactive thioester bonds **[fig.7]**. The first is a rapid phagocyte clearance of the foreign invaders due to the interaction of C3b and its proteolytic fragments (iC3b and

C3dg) with complement receptors (CR1, CR3, CR4 and CRIg) on Kupffer cells and spleen macrophages [70,85]. Moreover, C3b may up-regulate B-cell mediated response via CR2 [90]. The second is generation of anaphylatoxic peptides (e.g. C3a and C5a), as a result of proteolytic cleavage of C3 and C5, which cause indirect injury by triggering chemotactic and pro-inflammatory responses upon binding to their receptors (C3aR, C5aR and C5L2 [91]) on mast cells, polymorphonuclear cells (PMN), monocyte/macrophages [83,92]. The third regards the assembly of the multiprotein pore complex (termed membrane attack complex, MAC or C5b-9), through the activity of the enzyme C5 convertase, which lead to a direct cell lysis [89,91].

Finally, recent studies have identified additional activation pathways. For instance, some steps of the cascade (especially the cleavage of C3 and C5) can be directly initiated by a series of extrinsic proteases, like kallikrein and thrombin [extrinsic protease pathway] [93] and MBL-associated protease 2 [MASP-2] of the lectin pathway seems to directly attack and cleave C3 without formation of corresponding C3 convertase, C4b,2a [C2 bypass pathway] [94].

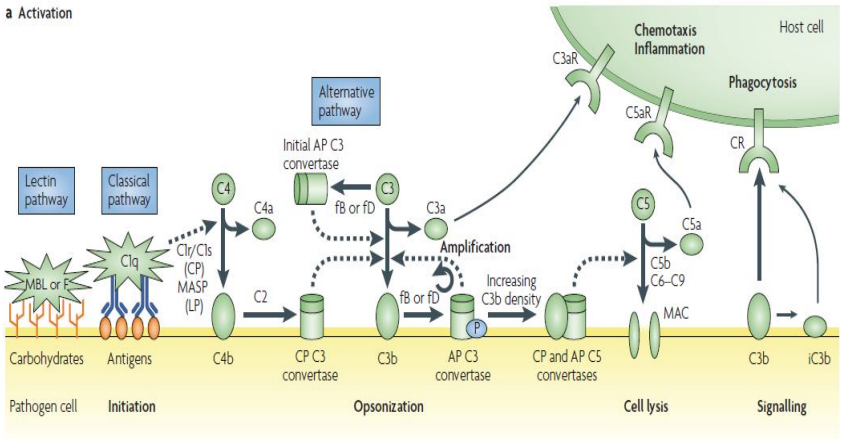

Fig.7: Activation of complement system. Covalent binding of C3b (opsonization) amplifies the cascade and mediates phagocytosis and adaptive immune responses by binding to complement receptors (CRs)Accumulation of deposited C3b also leads to the assembly of C5 convertases that activate C5 to C5a and C5b.Whereas C5b initiates the formation of the lytic membrane-attack complex (MAC), the anaphylatoxins C3a and C5a induce pro-inflammatory and chemotactic responses by binding to their receptors. Lambris J.D et al.(2008) [91].

1.6 Nanoparticle interactions with cells

Improved NPs rely on smart structure design involving spatial arrangement of specific chemical groups on particle surface in order to allow them to interact with cell membranes. Interestingly, several promising applications employ NPs as carriers to deliver molecules to the nucleus and cytosol of cells, such as siRNA [95] or as contrast agents for cell selections and phototherapy [96]. However, due to the nature of the lipid bilayer to act as a selective permeable barrier able to repeal exogenous substances and thus protect the intracellular environment, breaching of cell membranes are one of the major challenges for an efficient drug delivery.

In general the kinetics, amount and mechanism of NPs internalization depend upon several factors, such as type of cells and nanomaterials involved, cell treatment, incubation conditions and purity of the nanomaterials [13]. For instance, it was shown that the uptake rate of NPs decreases with increasing in particle size [97]. Moreover, different studies suggested that cationic surfaces could facilitate NPs penetration into cells over anionic or neutral counterparts owing to the attraction of positively charged NPs to the negatively charged plasma membrane of cells [98,99].

Once NPs reached the cell target site, they can either slowly degrade and deliver their cargo by diffusion [100] or undergo cellular endocytosis, as hypnotized for polymeric NPs [101,102]. Upon endocytic uptake, these nanocarriers may be transferred into early sorting and recycling endosomes (termed “early endocytic structures”) and subsequently moved from such early organelles to late endosomes, late endosomal-lysosomal hybrid organelles and finally to lysosomes (widely named “late endocytic compartments”) [103]. Unfortunately, following lysosomal trafficking NPs degradation and subsequent cleavage of loaded drugs or fluorescent molecules may occur via the enzymes contained within these acidic organelles, making them completely ineffective. This is the scenario for the clathrin- (or receptor)-mediated endocytosis, the most common and characterized route of pynoctosis [**fig.8**], that has been reported to be involved in the internalization of different NPs, such as cationic lipid/DNA or polymer/DNA complexes, useful tools for gene therapy [104].

Therefore, many mechanisms have been reported to evade the traditional endolysosomal pathway. For instance, polymeric NPs made from poly (DL-lactide-co-glycolide) can undergo a selective reversal of their surface charge (from anionic to cationic) in the acidic endosomal compartment, thus resulting in a local NP-membrane interaction and rapid escape into the cytosol [9,105]. Moreover, pH sensitive and fusogenic particles, like liposomes, can be stable at neutral pH or above but become fusion-competent at the acidic pH of late endosomes and release their cargo in the cell cytoplasm [9,106]. Likewise, NPs may mimic the mechanisms exploited by pathogen for escaping their degradation inside the cells. Indeed, caveolae-mediated endocytosis is considered a promising route of uptake as it is successfully used either by non-enveloped simian virus 40 (SV40) [107][**fig.8**] or cholera toxin B (CTB) [108] to reach the endoplasmic reticulum (ER). Interestingly, liposomes made from ER-like phospholipids can enter the cells via an uptake mechanism primarily dependent on caveolae and utilize a retrograde trafficking pathway similar to that exploited by CTB to specifically deliver drugs/markers from the Golgi to ER compartment and its associated membranes, termed lipid droplets [109].

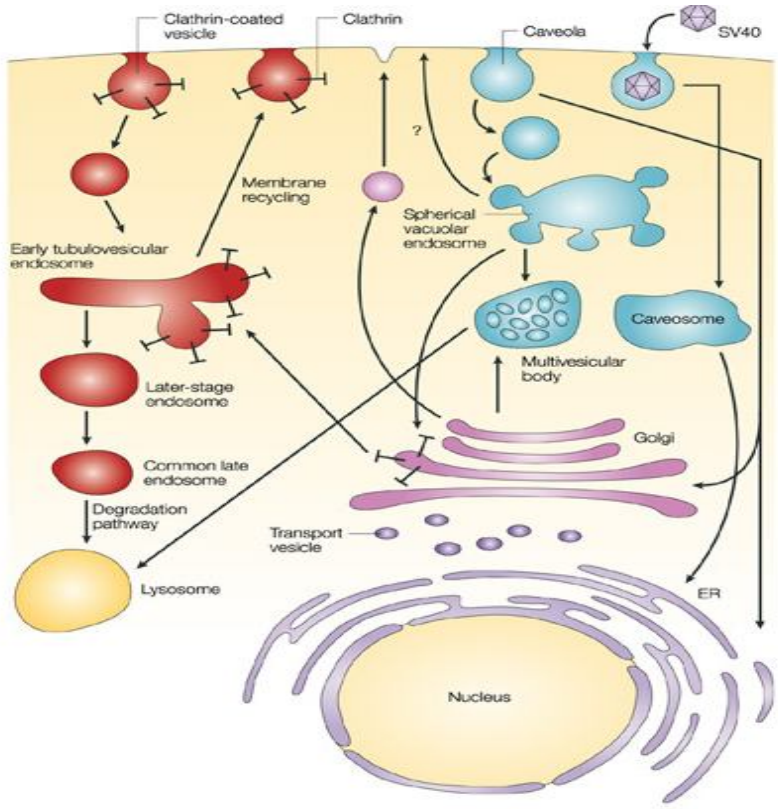

Fig.8: Intracellular trafficking pathways Clathrin-mediated and caveolae-mediated endocytosis. Carver L.A. et al. (2003) Nat Rev Cancer 3: 571-581

Fiinally, macropinocytosis is considered an interestingly alternative pathway for the delivery of NPs to cells. This nonselective endocytic route of extracellular fluid is manly based on actin-driven formation of membrane protrusions (ruffles) which collapse onto and fuse with the plasma membrane, thus resulting in generation of vacuoles with a diameter greater than 0,2 mm, termed macropinosomes [110]. Actin polymerization is usually initiated by the activation of the small family Rho guanosine triphosphatases (GTPases) (Rho, Cdc42 and

Rac) working in concert with phosphoinositide 4,5-bisphosphate [PI(4,5)P2] [111]. The most relevant feature of macropinocytos relies on the ultimate fate of the macropinosomes. Indeed, these vacuoles appear to remain relatively isolated from the rest of the endolysosomal system in different cells lines (e.g. the epidermoid carcinoma cells, A-431 and murine fibroblasts, NIH3T3), eventually fusing back with the plasma membrane [111].

1.6.1 Nanoparicles and pulmonary delivery

The lung is an interesting alternative route for NPs delivery mainly due to its high solute permeability, large surface area for absorption and limited proteolytic activity [112]. Pulmonary targeting is a non-invasive method which can provide local applications for treatment of chronic respiratory disease, like asthma, genetic disorders, like cystic fibrosis, and infections. For instance, it has been demonstrated the slow and sustained-release of antibiotics from SLN to alveolar macrophages in experimental tuberculosis, resulting in a reduction in the total drug dosage required for treatment [113].

Additionally, the thickness of the alveolar epithelium (0,2 μm) and the vast surface of this highly vascularized area (100m^2 in adult human) ensure NPs access to the systemic circulation. In general, after inhalation NPs may be absorbed from the trachea down to the terminal bronchioles and ultimately to the distal alveoli [114], translocate into the interstitial space and reach the bloodstream via lymphatics. Interestingly, insulin-loaded PLGA NPs induced a significant

reduction in blood glucose, with a prolonged effects over 48 h in comparison of insulin solution after delivery to guinea pig lung [115]. However, these attractive properties can also entail potential NPs adverse effects, prominently related to the their long- term accumulation in the lung and subsequent toxicity issues [2].

1.7 Nanoparticles and toxicity issues

The rapid expansion of nanotechnology in the biomedical field points out the need for a thorough evaluation of potential health risks related to NPs exposure. Indeed, the decrease in particle sizes within the nanoscale range entails new physical and chemical properties, thus novel biological effects, other than those of the bulk materials. In particular, the limited data about NPs toxicity have been focused on lung exposure to environmentally produced ultrafine particulate matter (termed PM, having a diameter below 100 nm) and it has demonstrated greater pulmonary inflammation and oxidative stress when compared with larger-sized particles [116,117]. Moreover, ultrafine NPs are not easily phagocytized by macrophages and thus not readily cleared in the alveolar region [118]. However, these data are related to the heterogeneous mixture of ultrafine materials produced incidentally by combustion or friction, which possess different properties from those of synthetic nanoparticles. Each of these types of NPs can trigger unique biological effects related to their own characteristics and thus they must be categorized and investigated separately [119].

Few studies have characterized the potential side effects of engineered NPs, predominantly carbon nanotubes and quantum dots. For instance, single-walled carbon nanotubes (SWCNT) could inhibit the proliferation of kidney cells by inducing apoptosis and decreasing cellular adhesive ability [119] along with increasing the production of markers of oxidative stress *in vitro* and *in vivo* [9,20]. In general, the *in vitro* responses to NPs are mainly dependent upon cells types, cells culture condition, and incubation periods [121] and care should be taken in interpreting data from *in vitro* systems, especially because of the high doses normally used and the impact of a bolus effect [119].

More relevantly, it is needed to investigate the ultimate fate of NPs and their constituents in the body, particularly those which are slowly or not biodegradable [9]. For instance, the cytotoxicity of cadmium selenide (CdSe) quantum dots correlates with the liberation of free Cd^{2+} ions after deterioration of the lattice coating [119]. Moreover, even NPs that are widely accepted as "bioinert", such as polymeric NPs made from PLA, show increased signs of cell damage (e.g. swollen mitochondria, widened endoplasmic reticulum) especially once degradation products are formed [26,122]. Likewise, the cytotoxicity of PACA NPs is clearly dependent upon the length of alkyl side chains, with a significant biocompatibility for the longer chains, that are characterized by a reduced hydrolytic degradation [123]. However, under *in vivo* conditions these products are generally eliminated from the site of degradation, thus the contact with cells would be considerably lower than *in vitro* [123]. Therefore, it should be stressed that *in vitro* tests are only a starting point for complementary *in vivo* and *ex vivo* investigations.

Finally, since the results on ultrafine and engineered NPs are very often different and controversial, it is urgently necessary to standardize approaches and methods for investigation of potential NPs side effects as well as characterize carefully the physicochemical properties of the test materials before any administration.

Scope of the thesis

The research project is aimed at thoroughly characterizing the *in vitro* behaviors of different types of Nanoparticles from the cellular point of view. It addresses the issue of NPs interactions with a model of air-blood barrier, the alveolar epithelial cell line, (*A30 cells)*, especially in terms of biocompatibility, cellular uptake and intracellular distribution. This is of primary interest since NPs inhalation is the most likely route of exposure to humans and a number of literature studies, even sometimes conflicting, have been highlighted adverse effects of nanoparticulate matters on pulmonary cells. The last part of the investigation addresses the issue of the body's immune response to Stealth (Pegylated) Nanoparticles, which can remarkably give rise to acute adverse reactions following intravenous administration.

Chapter 2 discusses the early stages of the interaction of Solid Lipid Nanoparticles (SLN) with alveolar epithelial A30 cells (up to 30 min of incubation), especially comparing the intracellular distribution of a fluorescent lipophilic dye (coumarin-6) either free or loaded on SLN. These data were also confirmed in other commercially available cell lines (HEK-293 and COS-7).

Chapter 3 suggests a possible interpretation, through a biophysical model, for the NPs load perinuclear accumulation in A30 cells observed in Chapter 2.

Chapter 4 presents experimental data on iron oxide NPs coated with L-Dihydroxyphenilalanin (L-Dopa) - TRITC with particular regard to their mechanism of internalization and fate in A30 cells.

Chapter 5 gives a general overview of the molecular mechanisms of Complement activation by different PEGylated entities which are generally assumed to own “stealth” properties to opsonization events.

References

1. **Otilia M**., Koo MS, Israel Rubinstein MD and Onyuksel H (2005) Role of nanotechnology in targeted drug delivery and imaging: a concise review Nanomedicine:nanotechnology, Biology and Medicine 1:193-212
2. **Mansour H.M.**, Rhee YS and Wu X (2009). Nanomedicine in pulomary delivery. Int J Nanomedicine 4: 299-319
3. **Jain K.K.** (2002) Personalized medicine. Curr Opin Mol Ther 4: 548-558
4. **Sung J.C.**, Pulliam BL and Edwards DA (2007). Nanoparticles for drug delivery to the lungs. Trends Biotechnol 25:563-570
5. **Brigger I.,** Dubernet C. and Couvreur P. (2002) Nanoparticles in cancer therapy and diagnosis.Adv Drug Deliv Rev 54: 631-651
6. **Tiwari S.B.** Amiji MM (2006) A review of nanocarrier- based CNS delivery system. Curr Drug Deliv 3: 219-232
7. **De Jong W.H.**, Borm PJA (2008) Drug delivery and nanoparticles: applications and hazards. Int J Nanomedicine 3(2) : 133-149.
8. **Wissing S.A**., Kayser O., Muller R.H. (2004) Solid lipid nanoparticles for parenteral drug delivery. Adv drug Deliv Rev 56 : 1257-1272.
9. **Moghimi S.M**, Hunter AC and Murray JC (2005). Nanomedicine: current status and future prospects. FASEB Journal 19: 311-330
10. **Pison U.,**Welte T., Giersig M., Groneberg DA (2006) Nanomedicine for respiratory diseases. Eur J Pharmacol 533: 341-350.
11. **Bukowski T.J**., Simmons JH (2002). Quantum Dot Research: Current State and Future Prospects Crit Rev Solid State Mater Sci 27: 119-142.

12. **Sanhai W.R**., Sakamoto JH., Canady R and Ferrari M. (2008), Seven challenges for nanomedicine. Nature Nanotechnology 3: 242-244.
13. **Verma A**., Stellacci F.(2010) Effect of surface properties on nanoparticle-cell interaction. Small 6 (1): 12-21.
14. **Aggarwal P**., Hall J.B., McLeland B., Dobrovolskaia M.A., McNeil S.E.(2009). Nanoparticle interaction with plasma proteins as it relates to particle biodistribution, biocompatibility and therapeutic efficacy. Adv Drug Deliv Rev 61: 428-437.
15. **Goppert T.M**., Muller R.H. (2005) Polysorbate – stabilized solid lipid nanoparticles as colloidal carriers for intravenous targeting of drugs to the brain: comparison of plasma protein adsorption patterns. J.Drug Target 13 :179- 187.
16. **Muller R.H**., Heinemann S. Surface modeling of microparticles as parenteral systems with high tissue affinity in: R. Gurny, Junginger H.E. (Eds.), Bioadhesion-possibilities and future Trends, Wissenchaftliche Verlagsgesellschaft , Stuttgart, 1989, pp.202-213.
17. **Frokjaer S.** and Otzen DE. (2005). Protein drug stability: a formulation challenge. Nat. Rev. 4: 298-306.
18. **Hyllery A.M**. Drug delivery, the basic concepts in : Hyllery AM, Lloyd AW., Swarbrick J (Eds.), Drug Delivery and Targeting for Pharmacists and Pharmaceutical Scientists, Taylor &Francis, London 2002, pp.1-48
19. **Almeida A.J**., Souto E.(2007). Solid lipid nanoparticles as drug delivery system for peptides and proteins. Adv Drug Deliv Rev 59(6):478-90
20. **Pettit D.K**., Gombotz WR. (1998) The development of site-specific drug-delivery systems for protein and peptide biopharmaceuticals. Trends Biotechnol. 16:343-349

21. **Kim T.Y**., Kim C., Chung JY., Shin SG., Heo DS., et al. (2004). Phase I and pharmacokinetic study of Genexol-PM, a cremophor-free, polymeric micelle-formulated paclitaxel, in patients with advanced malignancies. Clin Cancer Res 10: 3708-3716.
22. **Ibrahim NK**., Desai N., Legha S., soon-Shiong P., Theriault RL., Rivera E. et al. (2002). Phase I and pharmacokinetic study of ABI-007, a Cremophor –free, protein-stabilized, nanoparticle formulation of paclitaxel. Clin Cancer Res 8: 1038-1044.
23. **Gabizon A**., Peretz T., Sulkes A., Amselem S., Ben-Yosef R., Ben-Baruch N. et al. (1989) Systemic administration of doxorubicin-containing liposomes in cancer patients: a phase I study. Eur J Cancer Clin Oncol 25: 1795-17803.
24. **Torchilin V.P.** (2006). Multifunctional nanocarriers. Adv Drug Deliv Rev 58: 1532-1555.
25. **Ahl P.L**., Bhatia SK., Meers P., Roberts P., Stevens R., Dause R., Perkins WR., Janoff AS (1997) Enhancement of the in vivo circulation lifetime of L-distearoylphosphatidylcholine liposomes : importance of liposomal aggregation versus complement activation. BiochimBiophys Acta 1329: 370-382
26. **Moghimi S.M.**., Hunter C. and Murray J.C.(2001).Long-circulating and Target-Specific Nanoparticles : Theory to Practice. Pharmacol. Rev. 53: 283-318.
27. **Blasi P.**, Giovagnoli S., Schoubben A., Ricci and M., Rossi C.(2007). Solid lipid nanoparticles for targeted brain drug delivery. Adv Drug Deliv. Rev. 59 (6) : 454-477
28. **Kreuter J.** Nanoparticles, in: J. Kreuter (Ed.), Colloidal Drug Delivery Systems, Marcel Dekker, New York, 1994, pp. 219–342.
29. **Storm G.**, Belliot S.O., Daemen T. and Lasic DD (1995) Surface modification of nanoparticles to oppose uptake by the mononuclear phagocyte system. Adv Drug Deliv Rev 17:31–48

30. **Moghimi S.M.** and Hunter C. (2000b). Poloxamers and poloxamines in nanoparticle engineering and experimental medicine. Trends Biotechnol 18: 412-420
31. **Tröster S.D**., Müller U., Kreuter J. (1990) Modification of body distribution of poly(methyl mathacrylate) nanoparticle in rats by coating with surfactants. Int J Pharm.61: 85-100.
32. **Moghimi S.M.** and Szebeni J. (2003). Stealth liposomes and long circulating nanoparticles : critical issues in pharmacokinetics, opsonization and protein-binding poperties. Progress in Lipid Research 42:463-478.
33. **Moghimi S.M.** ,Porter C.J.H., Illum L. and Davis S.S. (1991) The effect of poloxamer-407 on liposome stability and targeting to bone marrow: comparison with polystyrene microspheres. Int J Pharm.68(1-3):121-126
34. **Oliver J.C**., Fenart L., Chauvet R., Pariat C., Cecchelli R. and Couet W. (1999) Indirect Evidence that Drug Brain Targeting Using Polysorbate 80-Coated Polybutylcyanoacrylate Nanoparticles Is Related to Toxicity. Pharm. Res. 16:1836-1842.
35. **Ryan S.M**., Mantovani G., Xuexuan W., Haddleton D.and Brayden D. (2008). Advances in PEGylation of important biotech molecules: delivery aspects. Expert Opin.Drug Deliv. 5(4):371-383
36. **Gref R.,** Minamitake Y., Peracchia M.T., Trubetskoy V., Torchilin V. and Langer R. (1994) Biodegradable long-circulating polymeric nanospheres. Science 263 (5153) : 1600-1603.
37. **Abuchowski A**., Van Es T., Palczuk N.C. and Davis F.F.(1977). Alteration of immunological properties of bovine serum albumin by covalent attachment of polyethylene glycol. J Biol Chem 252: 3578-3581.

38. **Klibanov A.L.**, Maruyama K., Torchilin V.P. and Huang L. (1990) Amphipatic polyethyleneglycols effectively prolong the circulation time of liposomes. FEBS lett 268: 235.237.
39. **Allen T.M.** and Everest J.M. (1983) Effect of liposome size and drug release properties on pharmacokinetics of encapsulated drug in rats. J Pharmacol Exp Ther 226: 539-544
40. **Gref R.**, Luck M., Quelec P., Marchand M., Dellacherie E., Harnisch S., Blunk T. and Muller R.H. (2000)"Stealth" corona-core nanoparticles surface modified by polyethylene glycol (PEG): influence of the corona (PEG chain length and surface density) and of the core composition on phagocytic uptake and plasma protein adsorption. Colloids and surface B: Biointerfaces 18:301-313
41. **Peracchia M.T**., Harnish S., Pinto-Alphandary H., Gulik A., Dedieu J.C., Desmaele D., d'Angelo J., Muller R.H. and Couvreur P. (1999) Visualization of in vitro protein-rejecting properties of PEGylated stealth polycyanoacrylate nanoparticles. Biomaterials 20: 1269-1275.
42. **Papahadjopoulos D.,** Allen T.M., Gabizon A., Mayhew E., Matthay K., Huang S.K., Lee K.D., Woodle M.C., Lasic D.D. and Redemann C. (1991) Sterically stabilized liposomes: improvements in pharmacokinetics and antitumor therapeutic efficacy. Proc Natl Acad Sci USA 88 : 11460-11464.
43. **Zalipsky S.**, Mullah N., Harding J.A., Gittelman J., Guo L. and DeFrees S.A. (1997) Poly(ethylene glycol)-grafted liposomes with oligopeptide or oligosaccharide ligands appended to the termini of the polymer chains. Bioconjug. Chem. 8: 111–118**.**
44. **Sapra P.** and Allen M.T. (2002). Internalizing antibodies are necessary for improved therapeutic efficacy of antibody-targeted liposomal drugs. Cancer Res 62:7190-7194

45. **Blume G.**, Cevc G., Crommelin M.D., Bakker-Woudenberg I.A., Kluft C. and Storm G. (1993), Specific targeting with poly(ethylene glycol)-modified liposomes: coupling of homing devices to binding with long circulation times, Biochim. Biophys. Acta 1149 (1):180–184.
46. **Hobbs S.K.,** Monsky W.L., Yuan F., Roberts W.G., Griffith L. and Torchilin V.P.(1998) Regulation of transport pathways in tumor vessels: role of tumor type and microenvironment. PNAS USA 95: 4607-4612.
47. **O'Brien M.E.** (2008) Single- agent treatment with pegylated liposomal doxorubicin for metastatic breast cancer. Anticancer Drugs 19;1-7
48. **Jain R.K.** (1989) Delivery of novel therapeutic agents in tumors: physiological barriers and strategies. J Natl Cancer Inst 81: 570-576
49. **Davis M.E**., Chen Z.G. and Shin D.M. (2008) Nanoparticle therapeutics: an emerging treatment modality for cancer. Nat Rev Drug Disc 7: 771-782.
50. **Zhang Y**., Kohler N. and Zhang M. (2002) Surface modification of superparamagnetic magnetite nanoparticles and their intracellular uptake. Biomaterials 23: 1553-1561.
51. **Huwyler J.**, Wu D. and Pardridge W.M.(1996) Brain drug delivery of small molecules using immunoliposomes. PNAS USA 93: 14164-14169.
52. **Roux E.**, Passirani C., Scheffold S., Benoit J.P. and Leroux J.C (2004). Serum-stable and long-circulating, PEGylate, pH-sensitive liposomes. J. Control Rel 94:447-451.
53. **Roux E.**, Francis M., Winnik F.M. and Leroux J.C. (2002) Polymer based pH-sensitive carriers as a means to improve the cytoplasmic delivery of drugs. Int. J. Pharm. 242: 25-36.

54. **Wissing S.A.,** Kayser O. and muller R.H. (2004) Solid lipid nanoparticles for parenteral drug delivery. Adv. Drug Deliv Rev 56 : 1257-1272
55. **Mehnert W.** and Mader K (2001). Solid lipid nanoparticles: production, characterization and applications. Adv Drug Del Rev 47: 165-196.
56. **Müller R.H.**, Mehnert W., Lucks J.S., Schwarz C., zur Mühlen A., Weyhers H., Freitas C. and Rühl D. (2002) Solid lipid nanopaticles (SLN) – an alternative colloidal carrier system for controlled drug delivery. Eur. J. Pharm. Biopharm. 41: 62-69.
57. **Almeida A.J.** and Souto E. (2007). Solid lipid nanoparticles as a drug delivery system for peptides and proteins. Adv Drug Del Rev 59:
58. **Cavalli R.**, Caputo O. and Gasco M.R. (1993). Solid lipid liposphere of doxorubicin and idarubicin . Int J Pharm 89 : R9-R12.
59. **Cavalli R.**, Caputo O. and gasco M.R. (2000) Preparation and characterization of solid lipid nanosphere containing paclitaxel. Eur J. Pharm. Sci 10 : 305-309.
60. **Zara G.P.,** Cavalli R., Bargoni A., Fundarò A., Vighetto D. and Gasco M.R. (2002) Intravenous administration to Rabbits of Non-stealth and Stealth Doxorubicin-loaded Solid Lipid Nanoparticles at increasing concentration of stealth agents: pharmacokinetics and distribution of doxorubicin in brain and other tissues. J Drug Target 10(4) : 327-335.
61. **Garcia-Fuentes M.,** Torres D. and Alonso M.J. (2005) New surface-modified lipid nanoparticles as delivery vehicles for salmon calcitonin. Int. J. Pharm. 296: 122-132.
62. **Hu F.Q.** and Hong Y. (2004) Preparation and characterization of solid lipid nanoparticles containing peptide. Int. J. Pharm. 273 : 29-35.

63. **Martins S.**, sarmento B., Ferreira D.C and Souto E. (2007) Lipid-based colloidal carriers for peptide and protein delivery-liposomes versus lipid nanoparticles. Int. J Nanomedicine 2(4) :595-607.
64. **Hofmann-Amtenbrink M**., Von Rechenberg, B. and Hofmann H.(2009) Superparamagnetic nanoparticles for biomedical applications. Tan,M.C.(ed.) Nanostructured Materials for Biomedical Applications, p. 119-149.
65. **Benderbous S**., Corot C. and Jacobs P. and Bonnemain B. (1996) Superparamagnetic agents: physicochemical characteristics and preclinical imaging evaluation. Acad.Radiol 3 (Suppl.2): S292-S294.
66. **Corot C**., Robert P., Iddè J.M and Port M. (2006) Recent advances in iron oxide nanocrystal technology for medical imaging. Adv. Drug Del Rev 58: 1471-1504.
67. **Corot C.**, Petry K.G., Trivedi R., Saleh A., Jonkmanns C., Le Bas J.F., Blezer E., Rausch M., Brochet B., Foster-Gareau P., Baleriaux D., Gaillard S. and Dousset V. (2004) Macrophage imaging in central nervous system and carotid atherosclerotic plaque imaging using superparamagnetic iron oxide in magnetic resonance imaging. Invest. Radiol. 39 : 619-625.
68. **Schulze E**., Ferrucci Jr. J.T., Poss K., Lapointe L., Bogdanova A. and Weissleder R. (1995) Cellular uptake and trafficking of a prototypical magnetic iron oxide label in vitro. Invest. Radiol. 30:604-610
69. **Apopa P.L.**, Qian Y., Shao R., Lan Guo N., Schwegler-Berry D., Pacurari M., Porter D., Xianglin S., Vallyathan V., Castranova V. and Flynn D.C. (2009) Iron oxide nanoparticles induce human microvascular endothelial cell permeability through reactive oxygen species production and microtubule remodeling. Particle and Fibre Toxicology 6(1): 1-14

70. **Moghimi S.M.** and Hunter A.C. (2001)Recognition by macrophages and liver cells of opsonized phospholipid vesicles and phospholipid headgroups. Pharm. Res.18:1-8
71. **Aggarwal P.**, Hall J.B., McLeland C.B., Dobrovolskaia M.A. and McNeil S.E. (2009) Nanoparticle interaction with plasma proteins as it relates to particle biodistribution, biocompatibility and therapeutic efficacy. Adv. Drug Deliv. Rev 61:428-437.
72. **Moghimi S.**M., Muir L.S., Illum I., Davis S.S. and Bachofen V.K. (1993) Coating particles with block co-polymers (poloxamine 908) suppress opsonization but permits the activity of dysopsonins in the serum. Biochim. Biophys. Acta 1179: 157-165.
73. **Cedervall T.**, Lynch I., Foy M., Beggard T., Donnely S.C., Cagney G., Lines S., and Dawson K.A. (2007) Detailed identification of plasma proteins adsorbed on copolymer nanoparticles. Angew. Chem. Int. Ed Engl. 46: 5754-5756.
74. **Levchenko T.S.**, Rammohan R., Lukyanov A.N., Whiteman K.R and Torchilin V.P. (2002) Liposomes clearance in mice: the effect of separate and combined presence of surface charge and polymer coating. Int. J. Pharm 240: 95-102.
75. **Zhang J.S**., Liu F. and Huang L. (2005) Implications of pharmacokinetic behavior of lipoplex for its inflammatory toxicity. Adv. Drug Deliv. Rev. 57: 689-698
76. **Braet F.,** Dezangen R., Baekeland M., Crabbe E., van der Smissen P and Wisse E. (1995) Structure and dynamics of the fenestrae-associated cytoskeleton of rat-liver sinusoidal endothelial cells. Hepatology 21: 180-189.
77. **Pain D**., Das P.K., Ghosh P.C., and Bachhawat B.K.(1984) Increased circulatory half-lifr of liposomes after conjugation with dextran. J Biosc. 6: 811-816.

78. **Kumaresh S.,** Soppimath S., Aminabhavi T.M., Kulkarni A.R. and Rudzinski W.E. (2001) Biodegradable polymeric nanoparticles as drug delivery devices. J Control. Rel. 70: 1-20
79. **Osterberg E.,** Bergström K., Holmberg K., Schuman T.P., Riggs J.A., Burns N.L., Van Alstine J.M. and Harris J.M.(1995) Protein-rejecting ability of surface-bound dextran in end-on and side-on configurations: comparison to PEG. J. Biomat. Sci. Polym. Ed. 6: 123-132.
80. **Szbeni J.** and Moghimi S.M. (2009) Liposome triggering of innate immune responses: A perspective on benefits and adverse reactions. J Liposome Res 19(2): 85-90.
81. **Liu F.**, and Liu D. (1996) serum independent liposome uptake by mouse liver. Biochem Biophys. Acta 1278: 5-11.
82. **Patel H.M.** (1992) Serum opsonins and liposomes: their interaction and opsonophagocytosis. Crit Rev Ther Drug Carrier Syst. 9(1):39-90.
83. **Nilsson B.**, Nilsson Ekdahl K., Mollnes T.E. and Lambris J.D. (2007) The role of complement in biomateila-induced inflammation. Mol. Immunol. 44:82-94.
84. **Knopf P.M.**, Rivera D.S., Hai S.H., McMurry J., Martin W. and De Groot A.S.(2008) Novel function of complement C3d as an autologous helper T-cell target. Immunol Cell Biol. 86(3):221-225.
85. **Anderses A.J.,** Hashemi S.H., Andresen T.L., Hunter A.C. and Moghimi S.M. (2009) Complement: alive and kicking nanomedicines. J. Biomed. Nanotechnol. 5(4): 364-372.
86. **Roos A.,** Bouwman H., van Gijlswijk-Jansen D.J., Faberkrol M.C., Sthal G.L. and Daha M.R. (2001) Human IgA activates the complement system via the mannan-binding lectin pathway. J Immunol. 167:2861-2868.

87. **Ekdhal K.N.,** Nilsson B., Golander C.G., Elwing H., Lassen B. and Nilsson U.R. (1993) Complement activation o radiofrequency plasma modified polystyrene surfaces. J. Colloid Interface Sci. 158:121-128
88. **Rickling D**. and Lambris J.D (2007) Complement-targeted therapeutics. Nat Biotechnol 25(11):1265-1275.
89. **Moghimi S.M**. and Hamad I. (2008) Liposome-mediated triggering of complement cascade. J. Liposome Res 18: 195-209.
90. **Dempsey P.W.**, Allison M.E., Akkaraju S., Goodnow C.C. and Fearon D.T. (1996) C3d of complement as a molecular adjuvant: bridging innate and acquired immunity. Science 271:348-350.
91. **Lambris J.D**., Rickling D. and Geisbrecht V. (2008) Complement evasion by human pathogens. Nat Rev Microbiol 6: 132-142.
92. **Szebeni J.** (2005) Complement activation-related pseudoallergy: A new class of drug-induced acute immune toxicity. Toxicology 216: 106-121.
93. **Markiewsky M.M,** Nilsson B., Nilsson Ekdhal K., Mollnes T.E. and Lambris J.D. (2007) Complement and coagulation: strangers or partners in crime? Trends Immunol. 28:184-192
94. **Atkinson J.P.** and Frank M.M (2006) Bypassing complement: evolutionary lessons and future implications. J.Clin. Invest 116: 1215-1218.
95. **Whitehead K.A**., Langer R. and Anderson D.G. (2009) Knocking down barriers: advances in siRNA delivery. Nat.Rev.Drug Discovery 8:129-138.
96. **El-Sayed, I.H**., Huang X. and El-Sayed M.A (2006) Selective laser photo-thermal therapy of epithelial carcinoma using anti-EGFR antibody conjugated gold nanoparticles. Cancer Lett. 239:129-135.

97. **Rejman J.,** Oberle V., Zuhorn I.S. and Hoekstra D. (2004) Size dependent internalization of particles via pathways of clathrin- and caveolae- mediated endocytosis. Biochem J 377:159-169.
98. **Rabinovich-Guilatt** L., Couvreur P., Lambert G. and Dubernet C.(2004) Cationic vectors in ocular drug delivery. J Drug Target. 12(9-10): 623-33.
99. **Labhasetwar V.,** Song C., Humphrey W., Shebuski R. and Levy R.J. (1998) Arterial uptake of biodegradable nanoparticles: effect of surface modifications. J Pharm Sci.87(10):1229-34.
100. **Andresen T.L.**, Jensen S.S. and Jongersen K.(2005). Advanced strategies in liposomal cancer therapy: problems and prospects of active and tumor specific drug release. Prog. Lipid Res. 44:68-97
101. **Kin H.R.,** Gil S., Andrieux K., Nicolas V., Appel M., Chacun H., Desmaele D., Taran F., Georgin D. and Couvreur P. (2007) Low-density lipoprotein receptor-mediated endocytosis of Pegylated nanoparticles in rat brain endothelial cells. Cell. Mol. Life Sci. 64: 356-364.
102. **Lai S.K.,** Hida K., Man S.T., Chen C., Machamer C., Schroer T.A. and Hanes J. (2007) Privileged delivery of polymer nanoparticle to perinuclear region of live cells via a non-clathrin, non-degradative pathway. Biomaterials 2876-2884.
103. **Richardson. S.C.W.,** Wallom K.L., Ferguson E.L., Deacon S.P.E., Davies M.W., Powell A.J., Piper R.C. and Duncan R. (2008) The use of fluorescence microscopy to define polymer localization to the late endocytotic compartments in cells that are targets for drug delivery. J. Control Rel. 127: 1-11.
104. **Zuhorn I.S.,** Kalicharan R., and Hoekstra D. (2002). Lipoplex-mediated transfection of mammalian cells occurs through the cholesterol-dependent clathrin-mediated pathway of endocytosis. J. Biol. Chem. 277: 18021 – 18028

105. **Panyam J**., Zhou W.Z., Prabha S., Sahoo S.K., and Labhasetwar V. (2002) Rapid endo-lysosomal escape of poly(DL-lactide-co-glycolide) nanoparticles: implications for drug and gene delivery. FASEB J. 16: 1217-1226

106. **Drummond D.C**., Zignani M., and Leroux J.C. (2000) Current status of pH-sensitive liposomes in drug delivery. Prog. Lipid Res. 39: 409-460.

107. **Carver L.A.** and Schnitzer J.E. (2003) Caveolae miming little caves for new cancer targets. Nat. Rev. Cancer 3: 571- 581

108. **Sharma D.K.,** Brown J.C., Choudhury A., Peterson T.E., Holicky E., Marks D.L., Simari R., Parton R.G. and Pagano R.E.(2004) Selective Stimulation of Caveolar Endocytosis by Glycosphingolipids and cholesterol. Mol. Biol. Cell. 15(7): 3114-3122.

109. **Pollock S.,** Antrobus R., Newton L., Kampa B., Rossa J., Latham S., Nichita N.B., Dwek R.A. and Zitzmann N. (2010) Uptake and trafficking of liposomes to the endoplastic reticulum. FASEB J. 24:1866-1878.

110. **Conner S.D.** and Schmid S.L. (2003) Regulated portals of entry into the cell. Nature 422: 37-44.

111. **Kerr M.C**. and Teasdale R.D. (2009) Defining macropinocytosis. Traffic 10: 364-371.

112. **Patton J.S.** (1996) Mechanisms of macromolecule absorption by the lungs. Adv Drug. Rev 19: 3-36.

113. **Pandey R**. and Khuller G.K.(2005) Solid lipid particle-based inhalable sustained drug delivery system against experimental tuberculosis. Tuberculosis (Edinb) 85: 227-234.

114. **Sung J.C.,** Pulliam B.L. and Edwards D.A. (2007) Nanoparticles for drug delivery to the lungs. TRENDS in Biotechnology 25(12):563-570

115. **Kawashima Y.**, Yamamoto H., Takeuchi H,Fujioka S. and Hino T.(1999) Pulmonary delivery of insulin with nebulized DL-lactide/glycolide copolymer (PLGA) nanospheres to prolong hypoglycemic effect. J. Control. Rel. 62:279:287.
116. **Oberdorster G.** (2000) Toxicology of ultrafine particles: in vivo studies. Phil Trans R Soc London A 358: 2719-2740.
117. **Donaldson K.,** and MacNee W. (2001) Potential mechanisms of adverse pulmonary and cardiovascular effects of particulate air pollution (PM10). Int J Hyg Environ Health 203:411-415.
118. **Ferin J**., Oberdorster G., Soderholm S.C. and Gelein R. (1991) Pulmonary tissue access of ultifine particles. J. Aerosol Med. 4:57-68.
119. **Oberdorster G.,**Maynard A., Donaldson K., Castranova V., Fitzpatrick J., Ausman K., Carter J., Karn B., Kreyling W., Lai D., Olin S., Monteiro-Riviere N., Warheit D., Yang H. and A report from ILSI Research Foundation/Risk Science Institute Nanomaterial Toxicity Screening Working Group (2005). Principles for characterizing the potential human health effects from exposure to nanomaterials: elements of a screening strategy. Particle and Fiber Toxicology 2(8):1-35.
120. **Shvedova A.A.,** Castranova V., Kisin E.R., Schwegler-Berry D., Murray A.R., Gandelsman V.Z., Maynard A. and Baron P. (2003) Exposue to carbon nanotube material:assessment of nanotube cytotoxicity using human keratinocyte cells. J. Toxicol. Environ. Health 66:1909-1926.
121. **Warheit D.B**., Sayes C.M., Reed K.L and Swain K.A. (2008) Health effects related to nanoparticle exposures: environmental, health and safety considerations for assessing hazard and risks. Pharmacol Ther. 120(1):35-42.

122. **Lam K.H**., Schakenraad J.M., Esselbrugge H., Feijen H. and Nieuwenhuis (1993) The effect of phagocytosis of poly(L-lactic acid) fragments on cellular morphology and viability. J Biomed Mat Res 27: 1569-1577.

123. **Vauthier C.**, Dubernet C., Fattal E., Pinto-Alphandary H., and Couvreur P. (2003) Poly(alkylcyanoacrylates) as biodegradable materials for biomedical applications. Adv. Drug Deliv.Rev.55:519-548.

Chapter 2

Cellular uptake of coumarin-6 as a model drug loaded in Solid Lipid Nanoparticles (SLN)

Rivolta I.[1], Panariti A.[1], Lettiero B.[1], Sesana S.[1], Gasco P.[2], Gasco MR.[2], Masserini M.[1], Miserocchi G[1].

[1] Dept of Experimental Medicine, University of Milano Bicocca, 20052 Monza, Italy

[2] Nanovector, 10144 Turin, Italy

Journal of Physiology and Pharmacology, 2011 (In press)

Keywords: Solid Lipid Nanoparticles, nanoparticles uptake, differential scanning calorimetry, effect of temperature on uptake.

Abstract

The aim of present work was to elucidate the interaction of Solid Lipid Nanoparticles (SLNs) with cellular plasma-membrane to gain insight of intracellular drug delivery. To this aim we followed the uptake of coumarin-6 (a drug model) either free in the extracellular medium or loaded on SLN (c-SLN). Alveolar epithelial cells were exposed to a biocompatible concentration of c-SLN (0.01mg/ml of tripalmitin) prepared by warm microemulsion whose lipid matrix was constituted by low melting point molecules (fatty acids, triglycerides). Intracellular fluorescence and preferential accumulation in the perinuclear region were increased by 54.8% on comparing c-SLN to the same amount of free coumarin-6 in the medium. Lowering temperature from 37° to 4°C decreased the intracellular signal intensity by about 48% equally for the free as well as for loaded drug, thus suggesting the inhibition of a similar non–endocytotic entrance pathway. No specific co-localization of the fluorescence with intracellular organelles was found. The c-SLN calorimetric profile obtained with differential scanning calorimetry (DSC), revealing transition within the range 58-62 °C, altered remarkably upon incubation with cells, suggesting a change in SLN structure after association with cells membranes.

We propose that the uptake of the model drug loaded on SLN is only partly related to the endocytotic pathway; it occurs despite the loss of integrity of the original SLN structure and it appears to be more efficient when the drug is vehicled rather than being free in the culture medium.

Introduction

The epithelial surface of the lungs is the largest surface area of the human body in direct contact with the environment and, furthermore, its thickness, in the so called thin part, is in the range 0.1 - 0.3 μm, reaching about 3 μm in the thick part that includes the fibrous components. Accordingly, the alveolar surface represents an important pathway for inhalation drug delivery being routinely used to treat allergic, genetic, infective or chronic diseases of the respiratory system (1). Only recently, though, the delivery to the lung has been considered for administering drugs not only for local pathology, but also for systemic diseases. The pulmonary route, in fact, is attractive for several reasons. It is non-invasive, it might allow drug absorption from a large, highly vascularized surface area, the flow of blood perfusing the lungs is ~5 L/min at rest and drugs that reach the circulation avoid the first-pass metabolism, actually the main disadvantage of orally administration route (2).

The advent of nanotechnology has introduced a great variety of nanoparticles (NPs), defined as “objects” with at least one dimension in the nanometer range. This has provoked great expectations for new inhalation-targeted drug delivery strategies including the application of therapeutics, vaccines and diagnostics. On the other hand, the different physico-chemical properties of nano-sized particles have raised substantial concerns about the safety of organic and inorganic nano-sized material (3). Nevertheless, the application of nanoparticle-based drug delivery in respiratory diseases has been somewhat limited by the ability of nanoparticles to reach the alveolar compartment; in fact, the delivery to the most peripheral lung portions, requires particle

size within a very narrow range, about 1 μm for Poly(Lactic-co-Glycolic Acid) composites (PLGA) (4,5), and in the nanometer range, less than 250 nm, for biodegradable particles (6).

Some reports highlight the efficacy of nanoparticles delivery to the alveolar compartment using either aerosol inhalation (7) and an air-liquid interface exposure system (8, 9, 10).

Of course, the ideal approach of a therapeutic carrier that targets a potent drug specifically at site of pathology is still quite far. This approach requires, in fact, the recognition by NPs of a highly specific molecular epitope on the plasma-membrane surface, in order to deliver the drug to the target site minimizing any effect elsewhere. The identification of the epitope is still a major unsolved problem preventing, so far, the specific targeting of diseased or cancer cells. The case of drug delivery system in inflammatory disease, as for tuberculosis (11), is in principle easier as it resides in phagocytosis by macrophages.

A further problem in alveolar delivery is due to overcoming the surfactant layer. There is a report indicating that metal NPs alter the surface properties of semi-synthetic surfactant and interfere with cyclic changes in surface tension on compression/expansion of the surface film (12). Another report confirms an alteration in fatty distribution within the surfactant layer in presence of poly(amidoamine) dendrimers (13).

A further criticism concerns the toxicity of nanomaterials. It is known that NPs inhaled from the ambient or at the work place may trigger inflammatory reactions: NPs translocation may decrease the immune defences, cause pulmonary endothelial disfunction and general

systemic effects (3). In this context it is of interest to recall the attempt to use carbon nanotubes, extremely toxic by nature (14 ,15), as biocompatible drug carrier after coating them with a naturally derived surfactant (16).

Solid Lipid Nanoparticles (SLN) represent an interesting drug delivery system as an alternative to liposomes and polymeric nanoparticles. SLN are constituted of biocompatible components similar to plasma membrane as well as to the lipidic part of alveolar surfactant and can be prepared by several methods (high pressure homogenization, warm microemulsions, solvent emulsification–evaporation-diffusion, high speed stirring, and or sonication) (17).

Our interest is based on previous results indicating the relatively easy uptake of SLN by alveolar cells (18). Therefore, the aim of present work is to elucidate the interaction of SLN with plasma membrane of alveolar epithelial cells to gain insight concerning the process of intracellular drug delivery. To this aim we followed the uptake of coumarin-6 used as a lipophilic drug model either free in the extracellular medium or loaded on SLN.

Materials and Methods

Preparation and characterization. Solid Lipid Nanoparticles (SLN) were produced by NANOVECTOR, in the terms of the CE Contract STREP N° LSHB-CT-2006-037639-BONSAI (Bio-imaging with Smart Functional Nanoparticles) by choosing tripalmitin as lipidic matrix.

SLN have been loaded with coumarin-6 (3-(2'-Benzothiazolyl)-7-diethylaminocoumarin -MW 350,4 Da), c-SLN, to allow their

visualization by means of fluorescent microscope (λ_{exc} 450 nm, λ_{em} 505 nm). c-SLN were prepared by dispersing in cold water (2°C) a warm microemulsion consisting of tripalmitin (Sigma), Epikuron 200 (Cargill), Sodium Taurocholate (PCA-Italy) and ultrapure water (Millipore- Milliq). Coumarin-6 (Acros) was added to the lipid phase of microemulsion. 2-phenylethanol (Fluka) was present as preservant.

c-SLN dispersion has been washed four times by tangential flow filtration (Sartorius ,Vivaflow 50 Cassette, RC Membrane, Cut Off 100 kDa), followed by heat sterilization and final storage overtime at 4°C until use.

The concentration of coumarin-6 in c-SLN dispersion was determined by fluorimetry (Jasco FP2020 Plus Fluorimeter, λ_{exc} 450 nm and λ_{em} 505 nm) after dissolving SLN dispersion in chloroform/methanol (6/4). In experiments where coumarin-6 was used as free drug, we prepared a stock solution at a concentration of 20 μg/ml in Dimethylsulfoxide (DMSO) to be diluted at the working solution desiderated.

The hydrodynamic diameter (Zave), polydispersity index (PI) and Zeta Potential (Zpot) of SLN dispersion was characterized by photon correlation spectroscopy (PCS) using a Malvern Zetasizer 3000 HSA instrument at a fixed angle of 90° and a temperature of 25°C (Laser λ 633 nm). Each value was the average of ten measuraments.

To evaluate the stability of c-SLN in physiological medium, NPs were incubated up to 24 hours in the cell culture medium supplemented with Pen/Strep and L-Glutamine.

Cell culture. Human Embrionic Kidney (HEK), African Green Monkey SV40-transfected kidney fibroblast cell line (COS-7) and A30 cells were grown on Petri dishes in Dulbecco's Modified Eagle's Medium (DMEM) supplied with 10% Fetal Bovine Serum (FBS), 1% of L-Glutamine and 1% of Penicillin/Streptomycin (Pen/Strep) and incubated in a controlled environment at 37°C with 5% CO_2. During all the experiments cells were incubated with medium supplemented with 1% FBS to prevent serum interference in the toxicity assay. A30 cells (19) represent a continuous alveolar cell line (A30) obtained from lung specimens from patients who underwent lobectomy in the Thoracic Surgery Unit of S. Gerardo Hospital, Monza. These cells were isolated from the apparently healthy portion of the excised lung lobe.

Toxicity. The evaluation of biocompatibility of c-SLN on A30 was analyzed by Lactate Dehydrogenase (LDH) release assay and by MTT ((3-(4,5-Dimethylthiazol-2-yl)-2,5-diphenyltetrazolium bromide) test according to the direction of the manufacturer (Clonetech and Sigma Aldrich) . A dose-response curve, from 0.9 ng/ml up to 9 mg/ml, was performed to determine the cell damage.

Time course of fluorescence intracellular distribution. The experimental set up consisted in a wide field fluorescence microscope NIKON Eclipse FN1, equipped with motorized table PRIOR and Metamorph software for imaging acquisition and analysis. In order to obtain the images of the c-SLN we used a Fluorescein Isothiocyanate (FITC) filter (λ_{max} 488 nm). The kinetic of the internalization up to 30

minutes, was studied on cells kept under the microscope at 32°C . During the experiment c-SLNs were added at a concentration of 9 µg/ml, in a way to guarantee no toxicity for the cells for the time of the exposure. The magnification of the objective was 63x and allowed a field view of at least 5 cells. The acquisition time was 400 ms. Intracellular fluorescence was expressed as percentage of a maximum value detected or as arbitrary units (a.u.), as described in figure legends.

Effect of temperature on fluorescence intracellular distribution. Cells were exposed for 45 minutes to c-SLN 9 µg/ml either at 37°C, or at 4°C. In this latter case cells were pre-cooled at 4°C for 30 min before the incubation. Images were acquired along the Z axis at 0.5 µm distance starting from top of the cell; on the average we acquired images over 40 Z planes. We considered the overall fluorescence acquired in wide field as well as, through a deconvolution process (Autodeblur), the fluorescence estimated on a Z plane corresponding to the mid cell height.

Immunocytochemistry. Cells were plated on glass coverslips and, at confluence, they were incubated with or without c-SLN 9 µg/ml. After 45 minutes, cells were fixed with paraformaldehyde 4% in PBS at room temperature for 20 min. Cells were washed three times in Phosphate Buffered Saline (PBS), LS (Low Salt PBS) and in HS (High Salt PBS) respectively and then permeabilized with digitonin 0.01% in GDB for 30 min. Fixed and permeabilized cells were incubated with primary antibody diluted in GDB at room temperature

(RT) for 2 hours. After washing with HS for three times, cells were incubated with Alexa conjugated secondary antibody (Alexa Fluor 594, Invitrogen), diluted in Gelatin Detergent Buffer (GDB) (1:100). Actin filaments were visualized with Texas Red-conjugated phalloidin (Invitrogen). Cells were then washed with HS and LS three times respectively. DAPI (4'-6-Diamidino-2-Phenylindole) was used to stain cell nuclei at a concentration of 1μM in PBS for 5 min. Coverslips were mounted with glycerol.

Differential scanning calorimetry (DSC) experiments. Measurements were performed with a VP-DSC high sensitivity differential scanning calorimeter (Microcal, Amherst, MA), equipped with twin 0.6 ml cells, interfaced to a personal computer for automatic data collection and analysis. All samples and buffers were degassed (10 min; 20°C) in a MicroCal Thermovac immediately before loading. The calorimetric scans were performed at a rate of 20°C/h starting from 1°C to 80°C. Analysis of the resulting thermograms was performed using MicroCal Origin software.

c-SLN were suspended in PBS buffer at a concentration of 9 μg/ml tripalmitin and then submitted to DSC. DSC experiments were also carried out with A30 cells. For this purpose, the cell cultures were incubated o/n with or without c-SLN 9μg/ml diluted in medium 1%FBS. After incubation, cells were washed twice with PBS, collected and centrifugated for 10 min at 1000 rpm at RT. The pellet was resuspended in 500 μl of PBS and sonicated with a vibrating probe (Vibra cell, Sonics and Materials) for a total duration of 2 min at 40 kHz. Homogenates, corresponded to 23E6 cells, were then submitted to DSC.

Statistical analysis

Statistical analysis was carried out by t-test and significance level was set at $p<0.001$ (in the figures indicated with *) Values are reported as means ± SD

Results

SLN

In c-SLN, the concentration of tripalmitin, chosen as the most representative lipid, was 9 mg/ml of dispersion, while the concentration of coumarin-6 in was 3,42 μM (corresponding to 50 μg/mL dispersion of coumarin-6). The molar ratio 6-coumarin:tripalmitin was about 79.

Zave of heat sterilised c-SLN dispersion was 116.1±15 nm, the polydispersity index was 0.31±0.05, while Zpot was -24.5mV. The average hydrodynamic diameter of the particles dispersed in buffer remained essentially stable (130 nm) for the three time determinations (0, 6 and 24 hrs) on varying their concentration by two order of magnitude. Similar results were obtained by adding 1% FBS to the medium.

c-SLN and cells penetration

c-SLN may represent a good vehicle for drugs because of their lipophilic nature. In fact they penetrate different mammalian cell lines (Fig.1), showing the same pattern of fluorescence distribution: a labelling of the plasma membrane whose intensity may depend on the composition of the lipid bilayer and an involvement of the cytoplasm while the nucleus appeared never labelled.

We focused our attention on A30 cell line since they are continuous cells from native tissue revealing greater sensitivity to stress, such as hypoxia (19), compared to the commercial A549 cells. Moreover A30 show a higher mobility of lipid microdomains with respect to A549 (19) that has been proposed as a mechanism to promote a rapid receptor response as well as turnover in the cellular signalling in response to exogenous agents. In our opinion they represent a sensitive system to study drug delivery to the lungs.

Biocompatibility

The biocompatibility of c-SLN was estimated by assessing the integrity of the plasma membrane and the metabolic activity of the cells following the incubation to nanoparticles for 24 hours. The LDH assay is based on the consideration that when the membrane is damaged, this cytosolic enzyme is released at increased amount in the medium. MTT assay evaluates the amount of cellular MTT that mirrors the activity of mitochondrial dehydrogenase, whose production decreases with increasing cellular distress. We therefore assume that the increase in LDH in the medium and a decrease of MTT represent cytotoxicity markers. In Fig.2, open circles refer to LDH release assay, while filled circles show the percentage decrease in MTT production assay: it can be appreciated that above a tripalmitin concentration of 0.9 μg/ml, the MTT test appears more sensitive than the LDH to unravel cellular distress. Indeed, for a 5 order of magnitude increase in c-SLN concentration (90 μg/ml), LDH increased by less than 10%, while the MTT production decreased by as much as 45±4% At a concentration of 4.5 mg/ml, both LDH and MTT provided the same percentage of cellular distress.

SLN are loaded with coumarin-6, in a molar lipids to coumarin-6 ratio of about 1/182. We therefore evaluated the toxicity of the fluorophore itself considering this ratio. No toxicity was found for the concentration of coumarin-6 corresponding to 0.9 mg/ml of SLN (data not shown). Thus, we conclude that the fluorescent dye is not the cause of distress for the cells.

Based on the above toxicity data, we performed the study using SLN concentration of 9 μg/ml that is in the range where we may suppose no lesional effects on the plasma membrane (1.56 ±1.11 % of LDH release) and a minor reduction in MTT (31 ± 2.5 %).

Intracellular coumarin-6 uptake and distribution

We performed a dose-response curve incubating A30 cells to different bath concentration of coumarin-6 and verified that the measure of intracellular fluorescence emission increases with the increase of the extracellular concentration of the fluorophore chosen (Table 1). We thus considered the cytoplasmic fluorescence as a function of the cellular uptake of coumarin-6. Intracellular fluorescence was evaluated based on a general pattern of distribution, namely a progressive increase in emission from plasma membrane towards the nucleus. Perinuclear accumulation was not homogenous, but occurred preferentially at one location where the distance from plasma membrane to nuclear membrane was the greatest. In order to analyze the intracellular distribution we selected a line on the acquired images, indicated as Emission Line (EL) running from the extracellular space (just outside of the plasma membrane, indicated as 0% of the overall distance to the perinuclear region), up to the nuclear membrane (100%

of the distance) (Fig.3 Inset). We selected four cytoplasmic regions of interest (ROI) along EL at 0%, 25%, 50% and 75% of the total length. We considered the averaged emission of each ROI, whose length averaged 10 pixels, acquired at 3, 9, 15 and 30 minutes from the beginning of exposure to NPs.

Starting from the third minute of incubation, fluorescent signal increased over time in the cytoplasm showing a maximal fluorescence in the perinuclear region. After the 9^{th} minute of exposure to SLN, the fluorescence of the cytoplasm was increased so as to allow a clear distinction between the intracellular and the extracellular compartment. Within the time frame of observation, the plasma membrane also labelled while this was never observed for the nucleus (Fig.1 and 3).

Effect of temperature

To gain insight about the mechanism responsible for the transmembrane transport and uptake of the fluorophore, we evaluated how intracellular fluorescence distribution was affected by changing the incubation temperature. Cells were exposed either to c-SLN or to free coumarin-6 for 45 minutes at 37° or at 4°C, a temperature at which endocytosis is strongly inhibited (20). In this case a single acquisition was obtained along the EL line at the end of the exposure time. Data in Fig.4 show that the decrease in temperature significantly decreased, but did not abolish, the cellular uptake, thus suggesting that the uptake process is not entirely mediated by endocytosis. Interestingly, coumarin-6 intake was decreased by 44% either when the fluorophore was free in the medium or loaded on SLN (Fig.4B).

Since the community's interest in SLN is mainly driven by the possibility to use them as drug delivery systems, we evaluated the cellular uptake of coumarin-6 when loaded on SLN or when free in the medium. To this aim, we compared the average cytoplasmic emission of A30 cells after 30 minutes of exposure to either c-SLN or free coumarine-6 at the same fluorophore concentration. The absolute value of the fluorescence signal detected in the perinuclear region when cells were exposed to c-SLN was 1.5 fold higher compared to the one obtained with free coumarin-6 (Fig.5A). This result may suggest that the fluorophore uptake was favoured when it was linked to SLN as a carrier. Moreover, when we focused our attention to a single region of interest, for example 50% of the EL, we found the and the slope of the fluorescence intensity versus time profile, in the time frame 9-30 minutes, was doubled for loaded, compared to free coumarin-6 (Fig.5B). This result suggests that the rate of intracellular accumulation was increased when the drug model was loaded in SLN.
In view of the marked perinuclear and cytoplasmic typical granulation of the emission signal, we investigated whether the emission could co-localize with known intracellular organelles or cytoplasmic protein. Fig.6 shows that no specific co-localization of fluorescence was found with known markers for Golgi apparatus, endosomes, lysosomes and peroxisomes. We also labelled the c-SLN incubated cells with antibodies against a cytosolic structural protein such as actin, and a cytosolic soluble Glyceraldehyde-3-Phosphate Dehydrogenase (GAPDH). In the first case we observed no co-localization, while in the latter, due to widespread cytosolic distribution of GAPDH, a partial signals overlap was found in the perinuclear region.

DSC

The DSC scan of c-SLN resuspended in PBS showed a series of endothermic transitions (Fig.7a) within the range 58-62 °C, likely corresponding to the phase transition of the SLN lipidic component (21). A30 cell homogenates, submitted to DSC, showed the presence of endothermic transitions with a main prominent peak centered at a temperature of 61°C (Fig.7b). The overall transition observed by DSC appears to be irreversible, since no significant transition was detected during a second heating cycle (Fig.7c), likely reflecting the thermal denaturation of cell proteins (22). Also, the first heating DSC scan of homogenates of A30 cells, previously incubated with c-SLN, showed the presence of an endothermic transition centered at about 61°C (Fig.7d). Contrary to untreated cell homogenates, the second heating scan showed the presence of a series of small endothermic transitions in the range from 57 to 62 °C (Fig.7e). These transitions were reversible, as they were detected also in successive scans (not shown). Since these transitions were not present in untreated A30 cells, and showed up only after cell incubation with c-SLN, they likely correspond to nanoparticles lipids present within the cell homogenate or to the association of c-SLN to the cells.

It is noteworthy to say that the plasma membrane phospholipids lack of phase transition in DSC, is due to the high proportion of very low melting (poly)unsaturated lipids and cholesterol in cell membranes (23).

Discussion

A drug delivery system can be defined as any method used to incorporate drugs to improve their pharmacokinetics parameters (22). SLN might represent a good delivery system because of their lipophilic nature. They show high specific surface area that facilitates the contact with the plasma membrane. As far as in vivo application is concerned, SLN have been used to improve skin/dermal uptake of several drugs, thus they can be employed as the carrier for the topical delivery (24,25,26,27). Moreover they have been used to improve the bioavailability of drugs via duodenal or oral administration in rats or mice (28,29,30,31,32). Furthermore, they have been administered intravenously in rats for anticancer drug delivery (33). Finally, they have been used as carriers for topical ocular delivery of tobramycin and administered by ocular route as eye-drops in rabbits (34).

At cellular level SLN have already been used as non viral system for DNA (35) or for anticancer drugs delivery (36,37,38).

In the present study we consider SLN, prepared by warm microemulsions, whose lipidic matrix is made of biocompatible molecules, with medium-low melting point (fatty acids, triglycerides). Other components of microemulsions are phospholipids as surfactant, water, biliar salts or short chain fatty acids as co-surfactant. SLN obtained from warm microemulsions can incorporate hydrophilic and lipophilic drugs; they can be freeze dried and sterilized by filtration or by heat according to the properties of the molecule incorporated. (39)

As other groups did, we used fluorescently labelled SLN to follow their ability to interact with mammalian cells and in particular with lung epithelial cells. However, the novelty of our approach was that to

compare the uptake of the model lipophilic drug (coumarin-6), for the same extracellular concentration, either free in the medium or loaded in SLN. This comparison allows indeed to interpret interesting aspects concerning the mechanism of SLN-plasma membrane interaction.

Biocompatibility

Our data demonstrate that the SLN prepared for this study are in line with the ones already known (40,41,42). In fact, for c-SLN concentration up to 90 μg/ml, membrane damage, based on LDH activity in the medium, was minor, while MTT production was ~ 30%. Plasma membrane lesions and alteration in metabolic activity may be due to several factors including oxidative and/or osmotic stress. Indeed NPs may generate Reactive Oxigen Species (ROS) in cells (43,44) and the uptake of osmotic active molecules may result in an hyperosmotic cytosolic condition leading to an increase in intracellular water (45).

Uptake and intracellular distribution

We can consider that the fluorescent cytoplasmic emission recorded is actually a mirror of the coumarin-6 transport due to the relationship between the fluorophore concentration in the cell bath and the intensity of the cytosolic fluorescence emission (Table 1).

Our data showed that lung pulmonary alveolar cells took up a significant fraction of the administered dye: the green fluorescence, in fact, was detected already after 9 minutes of exposure to the fluorophore, in agreement with previous work (41,42). The specific feature of intracellular emission distribution was a progressive increase of fluorescence along the major axis of the cytoplasm with preferential accumulation in the corresponding perinuclear region, the

nucleus being asymmetrically placed within the cell. A permanent, though weak, emission was also present on the plasma membrane, as can be appreciated from Fig.1, 3, in line with the indications of Teskac and Kristl who were able to provide a picture “freezing” coumarine-6 loaded SLN passing through the cell membrane suggesting a transport by SLN (46). Yet, it appears difficult to assess whether intracellular coumarin-6 transport is always vehicled through intact SLN. To attempt an answer to this issue we should discuss the mechanism of membrane transports that include a concentration dependent passive exchange and active endocytosis. The former is typical of amphipathic, hydrophobic molecules, such as cholesterol, that is easily found within all intracellular membranes when cells are exposed to it in the medium. Concerning endocytosis, it is reported in the literature that the peculiar vescicular system activated by the cell reflects the size of the matter that has to be internalized (47). Both type of processes are inhibited by decrease in temperature, but endocytosis is notably abolished at 4°C (20). Our data show that the decrease in the incubation temperature from 37° to 4°C drops the intracellular fluorescence signal both for free coumarin-6 and for c-SLN by about 50% (Fig 4). It remains now to be established the role of the above two transport mechanisms to account for this decrease. One can note that coumarin-6, a hydrophobic small molecule, is likely to undergo mostly to plasma membrane exchange, caused, as already proposed (48), by a “collision-induced process” that facilitates the transfer of lipophilic fluorescent markers through the formation of a complex with the cell membranes. Moreover the decrease in coumarin-6 uptake at 4°C is likely to reflect the increase in viscosity

of the plasma membrane that shifts from a highly fluid liquid crystal to a highly ordered crystalline state, thus decreasing the plasma membrane exchange processes.

As far as concerned c-SLN, they are also amphipathic and hydrophobic entities though of much larger dimension (130 nm). The decrease in c-SLN uptake at 4°C may suggest that both plasma membrane exchange as well as active endocytosis may be involved, the latter mechanism not exceeding 50%. However, we should note that the percentage decrease of uptake of coumarin-6 was very similar to that of c-SLN, despite the large size difference, suggesting that the main mechanism allowing fluorescence to enter the cells was the plasma membrane exchange leaving a minor share to the endocytotic pathways even at 37°C.

In favour of this interpretation are the findings from DSC showing that there are differences on considering the endothermic transition profile of pure c-SLN in PBS (Fig.7a) rich in polysaturated lipids, the profile referred to cell lysate after protein denaturation (Fig.7c), and the one referred to cell lysate after c-SLN incubation (again after protein denaturation, Fig.7e). These differences reveal that SLNs undergo a modification upon interaction with the plasma membrane, since the profile of Fig.7a differs from that of Fig.7e, at least in our experimental conditions. In fact, on comparing the Fig.7c with 7e, one may hypothesize that the adsorption of SLN results in a complex interaction and reorganization of the phospholipids both on SLN structure as well as in the cell membranes. Furthermore, the persistent uptake of fluorophore at 4°C (Fig.4) and the qualitative non specific co-localization with intracellular organelles (Fig.6) suggest a minor

role of direct incorporation of SLN through an endocytotic pathway. Our interpretation is in keeping with data from scanning electron microscopy revealing that SLN interacting with epidermal cells (pig skin), spread over the surface and loose their primary shape (40). This suggests that a major change occurs to the particle structure during the chemico-physical interaction process (49) and such modification may account for a “functional burst” of SLN and subsequent release of the loaded drug rapidly labelling the cytosol. Our data support a direct cytoplasmic delivery into the cells of the model drug, sharing an idea already developed by Partlow et al. (50). One can indeed envisage a direct mixing or exchange of phospholipids between the target cell plasma membrane and particle. In fact, since SLN have a strong chemical and structural similarity with the plasma membrane, its structural lipids may merge with cell membranes and facilitate drug delivery into the interior of the cell.

The other interesting point emerging from our study is that, for the same amount of the model drug coumarin-6 present in the medium, its uptake was higher and faster when loaded on SLN, compared to when it was free in the medium (Fig.5A, B). Thus we may suggest that, although SLN do not necessarily reach the cell cytoplasm through an endocytotic pathway, yet, they represent a capacity reservoir for the loaded drug as they add efficiency to endocellular drug delivery through a quantum-like release process.

Figure Legends

Figure 1: c-SLN cells penetration. A30, HEK and COS-7 were incubated with c-SLN 9 μg/ml for 45 minutes at 37°C. Fluorescent images were taken using FITC filter.

Figure 2: Biocompatibility of c-SLN. Dose-response curve for A30 cells incubated with progressively increasing c-SLN concentration from 0.9 ng/ml up to 9 mg/ml for 24hrs (n=6). Open circles refer to LDH release assay, filled circles show the percentage decrease in MTT production assay.

Figure 3: Fluorescence analysis of intracellular distribution. The plot shows the cytoplasmic emission in A30 cells exposed with c-SLN for 9 (empty circles) and 30 (filled circles) minutes. The fluorescence is expressed as percentage of the maximum value measured at 30 min and it is calculated from the ROIs placed at 0, 25, 50, 75% of EL (see inset), averaged from 6 cells. In the inset a typical image of A30 cells incubated with c-SLN

Figure 4: **Effect of temperature on uptake and intracellular distribution of c-SLN and coumarin-6**. The two plots illustrate the fluorescent distribution of c-SLN (panel A) or coumarin-6 (panel B) after 45 minutes of incubation at 32°C (filled symbols) and 4°C (open symbols). The fluorescence is expressed as percentage of the maximum value measured at 45 min and at 75% of EL. For all experiments, n=6 ($p<0.001$, t-Student Test).

Figure 5: Comparison between the intensity and the rate of accumulation of the fluorescence signal in cells incubated with c-SLN (filled circles) or with coumarin-6 (open circles). Panel A represents the average of fluorescent intensity expressed as absolute value obtained after 30 minutes of incubation in the two conditions respectively (113.27+16.6 a.u. for c-SLN vs 73.17+11 a.u. for cum-6, $p<0.001$, n=8). Panel B show that the kinetics of accumulation analyzed at 50% of EL is faster in the presence of SLN as vector of the fluorophore: the slope calculated for perfusion interval between 9 and 30 minutes is 1.24 for coumarin-6 and 2.47 for c-SLN ($p<0.001$, n=8).

Figure 6: Evaluation of co-localization of c-SLN with subcellular organelles and cytoplasmic proteins. A30 cells incubated with c-SLN, after immunocytochemistry protocol with antibodies against selected markers of Golgi apparatus (GM130), endosomes (EEA1), Lysosomes (Lysotracker), peroxisomes (PMP70), actin (phalloidin) and GAPDH. C-SLN cytoplasmic labelling (in green) is shown in the first column, the antibodies labelling (in red) in the central column and the merged images in the third one. In all the images, nuclei are stained in blue. Scale bar, 20 □m

Figure 7: The experimental curve of DSC scan. Baseline-subtracted DSC recording of SLN (a), of A30 cell homogenates (b = first scan; c= second scan) and homogenates of A30 cells incubated with SLN (d = first scan; e= second scan). The scan was carried out at a scan speed 20°C/h in PBS. The scans are displaced on the *y* axis to facilitate visualization.

Table

Table 1. Dose-response relation between the concentration of the fluorophore in the bath and the fluorescence cytoplasmic emission, measured in arbitrary units (a.u.) in A30 cells.

Coumarin-6 (μg/ml)	Fluorescence (a.u.)	SD
25	11,4	1.8
50	27,6	5.3
250	61,8	6.1

Figures:

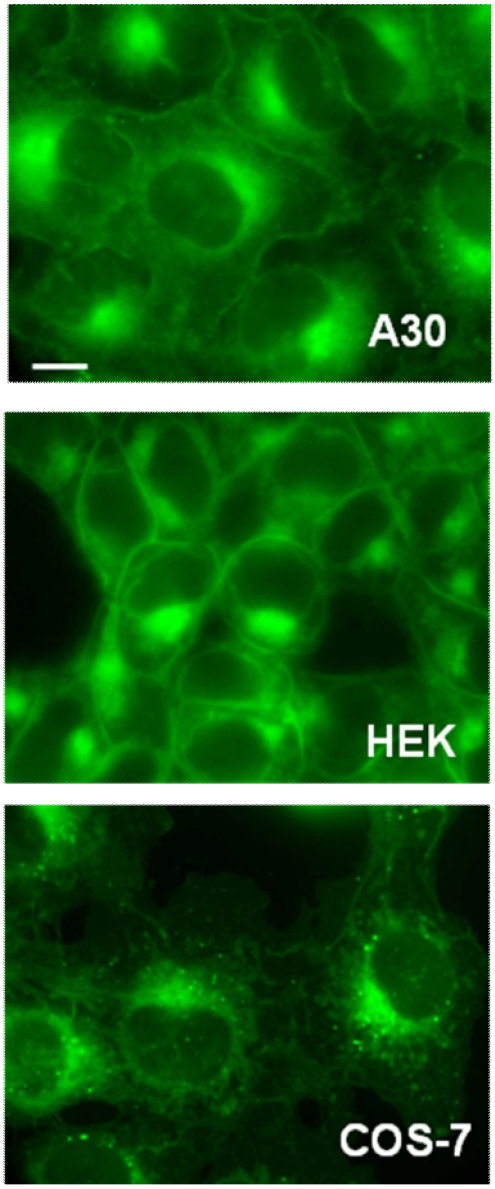

Figure 1: c-SLN penetration into A30, HEK and COS-7 cells.

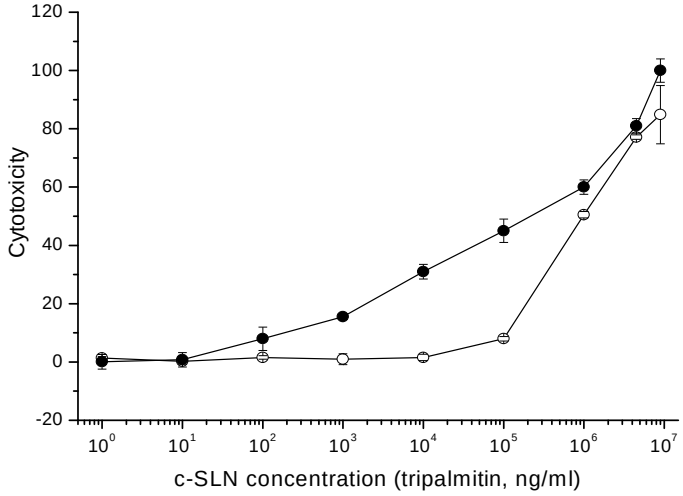

Figure 2: Biocompatibility of c-SLN over time

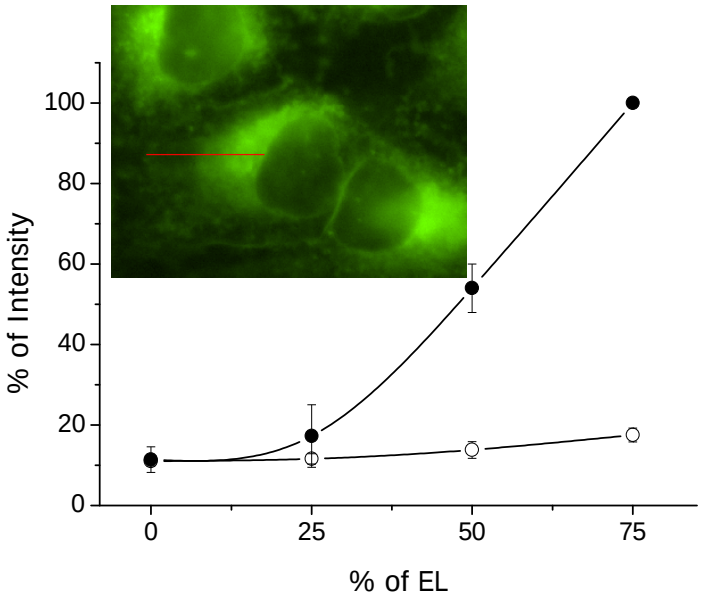

Figure 3: Fluorescence analysis of intracellular distribution.

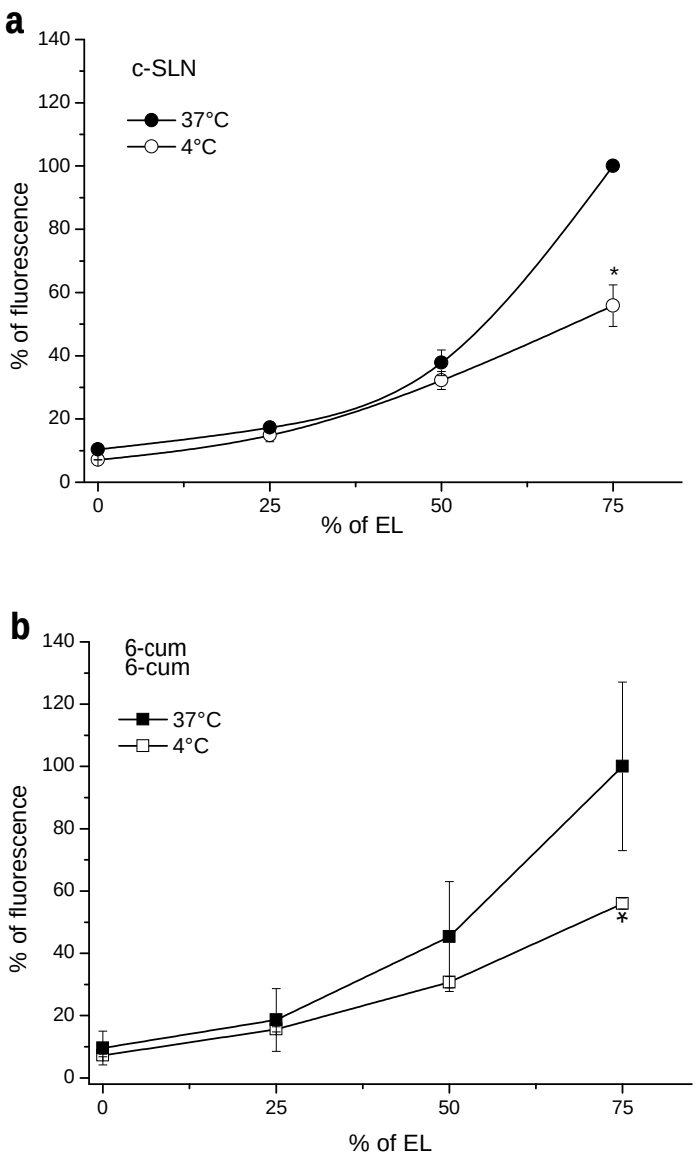

Figure 4: Effect of temperature on uptake and intracellular distribution of c-SLN and coumarin-6

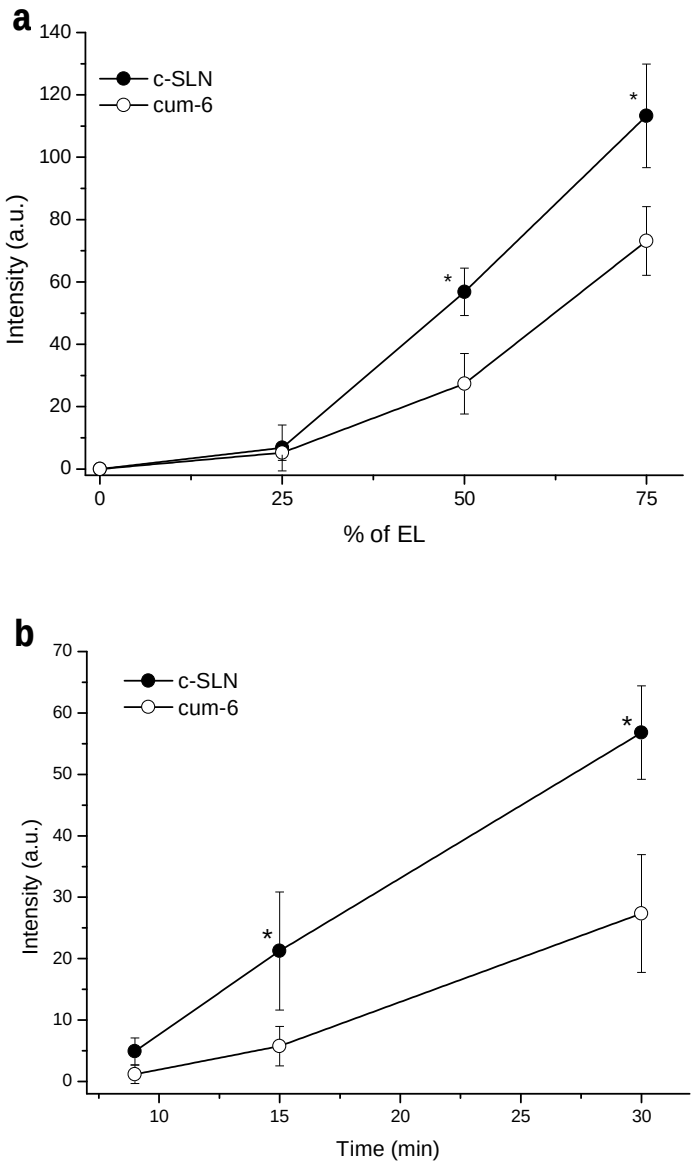

Figure 5: Comparison between the intensity and the rate of accumulation of the fluorescence signal in cells incubated with c-SLN (filled circles) or with coumarin-6 (open circles).

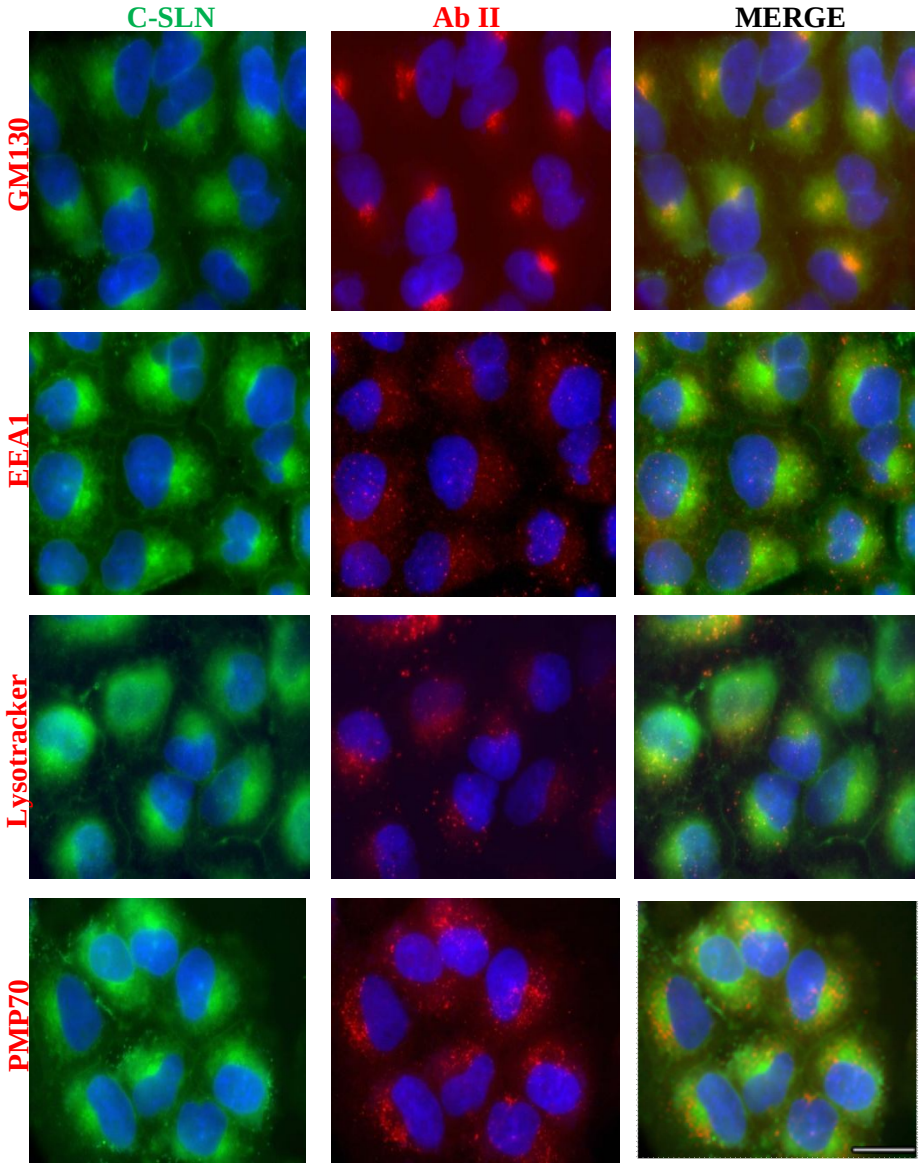
C-SLN
Ab II
MERGE
GM130
EEA1
Lysotracker
PMP70

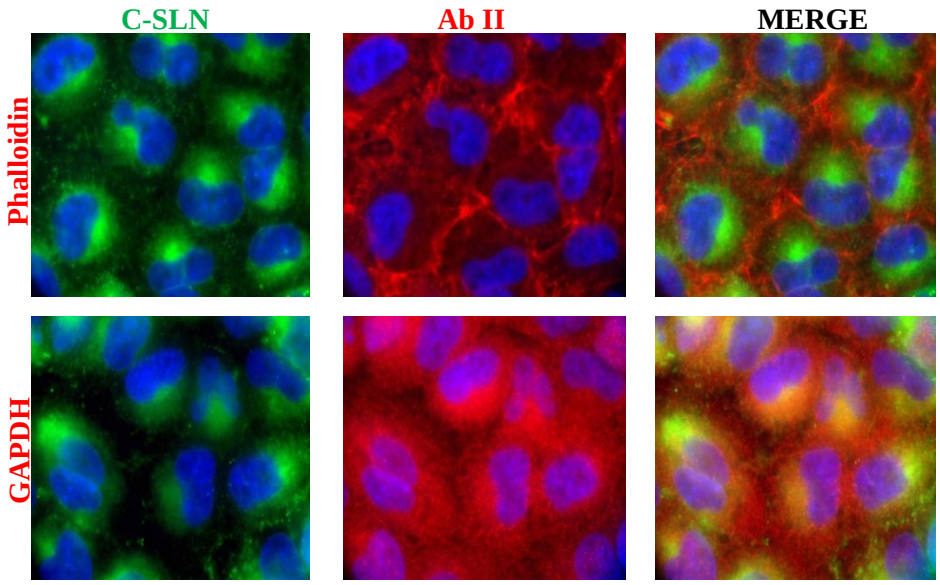

Figure 6: Evaluation of co-localization of c-SLN with subcellular organelles and cytoplasmic proteins.

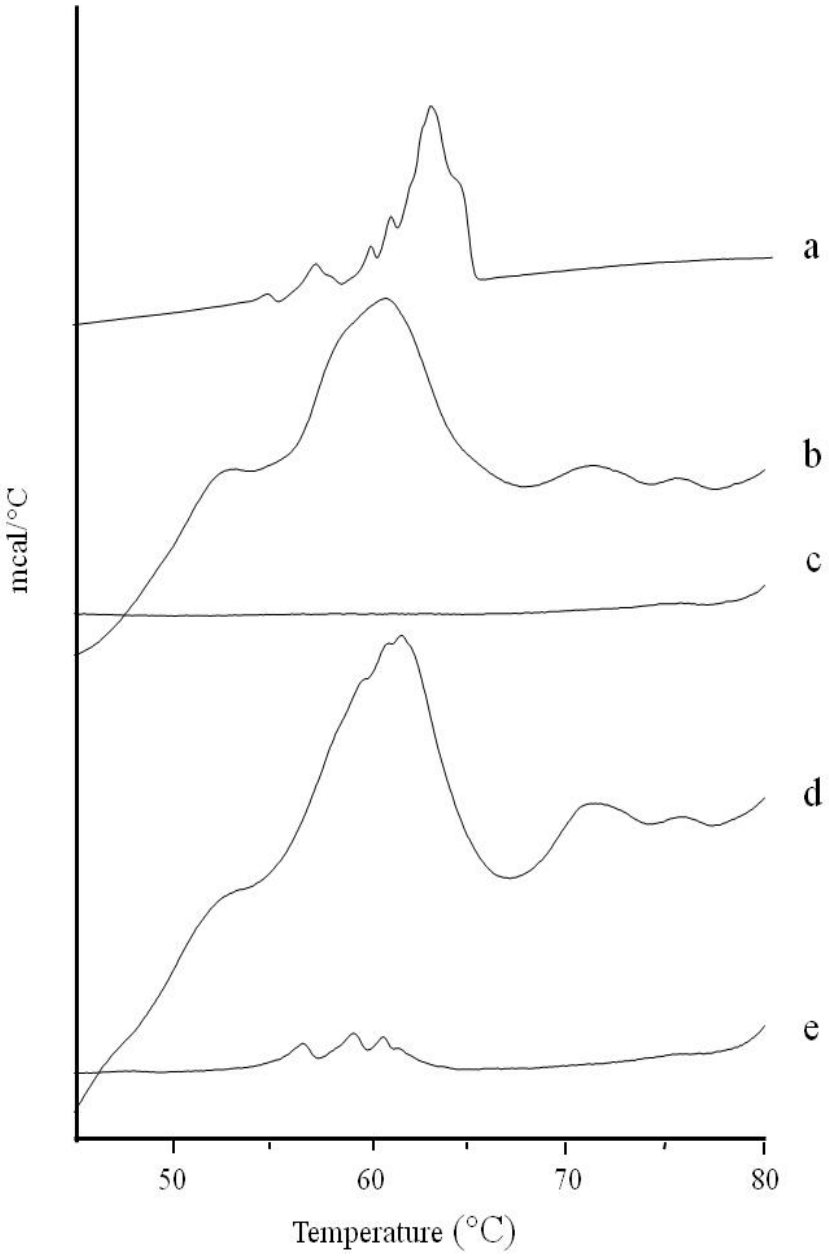

Fig. 7 The experimental curve of DSC scan.

References

1. **Pison U**, Welte T, Giersig M, Groneberg DA. Nanomedicine for respiratory diseases. Eur J Pharmacol 2006;533:341-350.
2. **Siekmeier R** and Scheuch G. Systemic treatment by inhalation of macromolecules-Principles, problems and examples. JPP 2008;59:53-79.
3. **Mühlfeld C**, Rothen-Rutishauser B, Blank F, Vanhecke D, Ochs M, Gehr P. Interaction of nanoparticles with pulmonary structures and cellular responses. Am J Lung Cell Mol Physiol 2008;294:L817-L829.
4. **Kraft KS**, Grant M. Preparation of macromolecule-containing dry powders for pulmonary delivery. Methods Mol Biol 2009;480:165-74.
5. **Tomoda K**, Ohkoshi T, Nakajima T and Makino K. Preparation and properties of inhalable nanocomposite particles: effects of the size, weight ratio of the primary nanoparticles in nanocomposite particles and temperature at a spray-dryer inlet upon properties of nanocomposite particles. Colloids Surf B Biointerfaces 2008 Jun 15;64(1):70-76.
6. **Dailey LA**, Jekel N, Fink L, et al. Investigation of the pro-inflammatory potential of biodegradable nanoparticle drug delivery system in the lung. Toxicol Appl Pharmacol 2006;215:100-108.
7. **Siekmeier R** and Scheuch G. Treatment of systemic diseases by inhalation of biomolecules aerosol. JPP 2009;60:15-26.
8. **Brandenberger C**, Muhlfeld C, Ali Z, et al. Quantitative evaluation of cellular uptake and trafficking of plain and polyethylene Glycol-Coated Gold nanoparticles. Small. 2010;6:1669-1678.

9. **Lenz AG**, Karg E, Lentner B, et al. A dose-controlled system for air-liquid interface cell exposure and application to zinc oxide nanoparticles. Particle and Fiber Toxicol 2009;6:32.
10. **Aufderheide M**, Knebel JW, Ritter D. Novel approaches for studying pulmonary toxicity in vitro. Toxicol Lett 2003;140-141:205-11.
11. **Suarez S**, O'Hara P, Kazantseva M, et al. Respirable PLGA microspheres containing rifampicin for the treatment of tuberculosis: screening in an infectious disease model. Pharm Res 2001;18:1315-1319.
12. **Bakshi MS**, Zhao L, Smith R, Possmayer F, Peterse NO. Metal Nanoparticle pollutants interfere with pulmonary surfactant function in vitro. Biophys J 2008; 94: 855-868.
13. **Erickson B**, DiMaggio S, Mulle DG, et al. Interaction of Poly(amidoamine) dendrimers with Survanta Lung Surfactant: the importance of Lipid Domains. Langmuir 2008;24:11003-11008.
14. **Zhiqing L**, Zhuge X, Fuhuan C, et al. ICAM-1 and VCAM-1 expression in rat aortic endothelial cells after single-walled carbon nanotube exposure. J Nanosci Nanotechnol 2010;10:8562-8574.
15. **Wang X**, Zang JJ, Wang H, et al. Pulmonary toxicity in mice exposed to low and medium doses of water-soluble multi-walled carbon nanotubes. J Nanosci Nanotechnol 2010;10:8516-8526.
16. **Gasser M**, Rothen-Rutishauser B, Krug HF, Gehr P, Nelle M, Yan B. Wick multi-walled carbon nanotubes (MWCNTs) is influenced by both pulmonary surfactant lipids and surface chemistry. L Nanobiotechnol 2010; 8:31.
17. **Muller RH**, Kader K, Gohla S. Solid Lipid Nanoparticles (SLN) for controlled drug delivery. A review of the state of the art. Eur J Pahrm Biopharm 2000;50:161-177.

18. **Panariti A**, Rivolta I, Lettiero B, Chirico G, Gasco P, Miserocchi G. SLN as vehicle for a model drug: a biophysical Study. AIP Conference Proceedings 2010;1275:115-117.
19. **Botto L**, Beretta E, Bulbarelli A et al Hypoxia-induced modifications in plasma membranes and lipid microdomains in A549 cells and primary human alveolar cells. J Cell Biochem 2008;105:503-513.
20. **Steinman RM**, Mellman IS, Muller WA, Cohn ZA. Endocytosis and the Recycling of Plasma Membrane The Journal of Cell Biology 1983;96:1-27.
21. **Müller RH**, Runge SA, Ravelli V, Thünemann AF, Mehnert W, Souto EB. Cyclosporine-loaded solid lipid nanoparticles (SLN): drug-lipid physicochemical interactions and characterization of drug incorporation. Eur J Pharm Biopharm 2008;68:535-544.
22. **Lepock JR**, Frey HE, Ritchie KP. Protein denaturation in intact hepatocytes and isolated cellular organelles during heat shock. J Cell Biol 1993;122:1267-1276.
23. **Masserini M**, Pitto M, Raimondo F, Cazzaniga E, Sesana S and Bellini T. Methyl-b -cyclodextrin Treatment Affects the Thermotropic Behaviour of Membranes and Detergent-Resistant Membrane Fractions of Cultured A431 Cells. Biol Pharm Bull 2005;28 2185-2188.
24. **Lv Q**, Yu A, Xi Y et al. Development and evaluation of penciclovir-loaded solid lipid nanoparticles for topical delivery. Int J Pharm 2009;372:191-198.
25. **Priano L**, Esposti D, Esposti R, et al. Solid Lipid nanoparticles incorporating melatonin as new model for sustained oral and transdermal delivery system. J Nanosci Nanotechnol 2007;7:3596-3601.

26. **Küchler S**, Radowski MR, Blaschke T, et al. Nanoparticles for skin penetration enhancement – A comparison of a dendritic core-multishell-nanotransporter and solid lipid nanoparticles. Eur J of Pharm and Biopharm 2009;71:243-250.
27. **Küchler S**, Herrmann W, Panek-Minkin G et al. SLN for topical application in skin diseases – Characterization of drug-carrier and carrier-target interaction. Intl J of Pharm 2010;390:225-233.
28. **Suresh G**, Manjunath K, Venkateswarlu V, Satyanarayana V. Preparation, characterization, and in vitro and in vivo evaluation of Lovastatin Solid Lipid Nanoparticles. AAPS PharmSciTech 2007;8:E1-E9.
29. **Yang S**, Zhu J, Lu Y, Liang B, Yang C. Body Distribution of Camptothecin Solid Lipid Nanoparticles after oral administration. Pharmaceutical Research 1999;16:751-757.
30. **Holpuc AS**, Hummel GJ, Tong M et al. Nanoparticles for local Drug Delivery to the Oral Mucosa: Proof of Principle Studies. Pharm Res 2010;27:1224-1236.
31. **Hauss DJ**, Fogal SE, Ficorilli JV, Ahuss DJ et al. Lipid-based delivery systems for improving the bioavailability and lymphatic transport of a poorly water-soluble LTB4 inhibitor. J Pharm Sci 1998;87:164-169.
32. **Cavalli R**, Bargoni A, Podio V, Muntoni E, Zara GP, Gasco MR. Duodenal administration of solid lipid nanoparticles loaded with different percentages of tobramycin. J Pharm Sci 2003; 92:1085-1094.
33. **Zara GP**, Cavalli R, Bargoni A, Fundarò A, Vighetto D, Gasco MR. Intravenous administration to rabbits of non-stealth and stealth doxorubicin loaded solid lipid nanoparticles at increasing concentrations of stealth agent: pharmacokinetics and distribution of

doxorubicin in brain and in other tissues J Drug Targeting 2002;10:327-335.

34. **Cavalli R**, Gasco MR, Chetoni P, Burgalassi S, Saettone MF. Solid Lipid Nanoparticles (SLN) as ocular delivery system for tobramycin, Int J Pharm 2002;238:241-245.
35. **del Pozo-Rodríguez A**, Delgado D, Solinís MA, Gascón AR, Pedraz JL. Solid lipid nanoparticles for retinal gene therapy: transfection and intracellular trafficking in RPE cells. Int J of Pharm 2008;360:177-183.
36. **Serpe L**, Guido M, Canaparo R et al. Intracellular accumulation and cytotoxicity of doxorubicin with different pharmaceutical formulations in human cancer cells, J Nanosci Nanotecnol, 2006;6:3062-3069.
37. **Dianzani C**, Cavalli R, Zara GP et al. Cholestryl butyrate solid lipid nanoparticles inhibit adhesion of human neutrophils to endothelial cells, Br J Pharmacol 2006;148:648-656.
38. **Brioschi A,** Zenga F, Zara GP, Gasco MR, Ducati A, Mauro A. Solid lipid nanoparticles: could they help to improve the efficacy of pharmacologic treatments for brain tumors? Neurol Res 2007;29:324-330.
39. **Cavalli R**, Caputo O, Carlotti ME, Trotta M, Scarnecchia C, Gasco MR. Sterilization and freeze-drying of drug-free and drug-loaded solid lipid nanoparticles Int J Pharm 1997;148:47-54.
40. **Küchler S**, Radowski MR, Blaschke T et al Nanoparticles for skin penetration enhancement – A comparison of a dendritic core-multishell-nanotransporter and solid lipid nanoparticles. Eur J of Pharm and Biopharm 2009;71:243-250.
41. **Cryan S.** Carrier-based strategies for targeting protein and peptide drugs to the lungs. AAPS Journal. 2005;7:E20-E41

42. **Nassimi M**, Schleh C, Lauenstein HD et al. A toxicological evaluation of inhaled solid lipid nanoparticles used as a potential drug delivery system for the lung.Eur J Pharm Biopharm. 2010;75:107-116.
43. **Kovacic P**, Somanathan R. Biomechanisms of nanoparticles (toxicants, antioxidants and therapeutics): electron transfer and reactive oxygen species.J Nanosci Nanotechnol 2010;10:7919-7930.
44. **Potter TM**, Neun BW, Stern ST. Assay to detect lipid peroxidation upon exposure to nanoparticles. Methods Mol Biol 2011;697:181-189.
45. **Nielsen MB**, Christensen ST, Hoffmann EK. Effects of osmotic stress on the activity of MAPKs and PDGFR-beta-mediated signal transduction in NIH-3T3 fibroblasts. Am J Physiol Cell Physiol 2008;294:C1046-55.
46. **Teskač K** and Kristl J. The evidence for solid lipid nanoparticles mediated cell uptake of resveratol. Intl J Pharm. 2010;390:61-69.
47. **Rejman J**, Oberle V, Zuhorn IS, Hoekstra D. Size-dependent internalization of particles via the pathways of clathrin and caveolae-mediated endocytosis. Biochem J 2004;377:159-179.
48. **Pietzonka P**, Rothen-Rutishauser B, Langguth P, Wunderli-Allenspach H, Walter E, and Merklel HP. Transfer of Lipophilic Markers from PLGA and Polystyrene Nanoparticles to Caco-2 Monolayers Mimics Particle Uptake. Pharmaceutical Research 2002;19:595-561.
49. **Küchler S**, Herrmann W, Panek-Minkin G et al. SLN for topical application in skin diseases – Characterization of drug-carrier and carrier-target interaction. Intl J of Pharm. 2010;390:225-233.
50. **Partlow KC**, Lanza GM, Wickline SA. Exploiting lipid raft transport with membrane targeted nanoparticles: a strategy for cytosolic drug delivery. Biomaterials 2008 ;23:3367-3375.

Chapter 3

Uptake of Solid Lipid Nanoparticles in a mammalian cell line: insight into the cytoplasmic distribution

Rivolta L.[1], Panariti A.[1], Collini M.[2], Lettiero B.[1], D'Alfonso L.[2], G. Miserocchi G. [1], Chirico G. [2]

[1] Dipartimento di Medicina Sperimentale, Università di Milano Bicocca, Via Cadore, 48 - 20052 Monza (I)

[2] Dipartimento di Fisica, Università di Milano Bicocca, Piazza della Scienza 3, 20126 Milano (I).

FEBS J, 2010 submitted

Keywords: solid-lipid nanoparticles, cell uptake, fluorescence microscopy, diffusion equations.

Abstract

The Solid Lipid Nanoparticles (SLN) can translocate lipophilic compounds to cell membranes and release into the cell their load. We study here the intracellular distribution of the SLN's load, which typically accumulates to the nuclear membrane, by means of fluorescence microscopy imaging. Experiments on lung epithelial cells interacting with SLNs loaded with coumarin-6, a green fluorescent dye taken here as model hydrophobic compound, indicates that the intracellular load concentration and its accumulation towards the nuclear membrane, is determined by the interplay of a mean field interaction energy, whose origin is to be searched in the actin structure of the cytoskeleton and the diffusion of the load.

.

Introduction

Solid Lipid Nanoparticles (SLNs) can be obtained by emulsification and subsequent recrystallization of a physiological matrix [1-3] whose biocompatibility prevents some of the toxicity problems often associated to other nanoparticles (NPs). These systems have been proposed as drug carriers for several administration routes [3-12] in alternative to polymeric nanoparticles, fat emulsion and liposomes [13] and they are preferentially adequate as vehicles for lipophilic and amphiphilic drugs [5] but they are also capable to load aminoglycoside antibiotics [4] and peptides [14].

Reasonable (≅10%) levels of drug entrapment in SLN have been achieved and an extremely high level of prolonged drug release, between 85% and 90%, [11, 15-17] have been reported. However, a limited amount of information is available about the drug distribution and mobility within the SLN. Due to the nanoparticles crystalline structure the drug mobility should be largely reduced and its leakage from the carrier to the solution could be controlled and prolonged in time [13, 15, 18]. Drug molecules may be adsorbed on the outer non crystalline layer of the particle, entrapped or dissolved in the lipid core. The distribution strongly depends on the physico-chemical characteristics of the drug and of the components of the SLN. Evidences taken from in vitro experiments indicate that [19] the major part of the drug is bound to the particle surface and may be released to different extent and with various kinetics depending on its partition coefficient [15, 16]. Previous works [20] suggest that the SLNs could be used for prolonged release of drugs by exploiting the drug influence on the melting point and on the enthalpy gain of the lipid matrix. Indeed, the interaction of the lipid matrix of the nanoparticles with the phosfolipid bilayer of the cell membrane [21] may modulate the physico-chemical characteristic of the drug carrier and trigger the release of the loaded compound. Nanoparticulate systems foster the delivery of active compounds to the cells either by the direct uptake of the particle or by diffusion from the carrier surface into the cells without particle internalization [21, 22]. However, even when SLN interact with leukocytes, capable to internalize by endocytosis, it is not possible to discriminate whether the whole nanoparticles entered the cells or only the load has been transferred into the cytosol [21]. In

both cases, before reaching the cytoplasm, NPs have to interact with the plasma membrane of the cells that represents a dynamic barrier separating the intra- from the extra-cellular environment. Previous results [22] obtained in our laboratory suggest that, at least in the case of the SLN built from tripalmitin, the most likely mechanism responsible for the cellular uptake of the drug exploits a partial fusion of the particle onto the cell membrane freeing the drug for further intracellular diffusion. Few studies are available on the processes that determine the ultimate intracellular fate of the drug. A number of papers report that NPs, or their load, accumulate in the perinuclear region [23-29]. None of these studies, though, contributes with a model for this behaviour that occurs despite the different chemical properties of the load and of the NPs used in the literature. The aim of the present contribution is to analyze from a biophysical point of view the cytoplasmic distribution of the SLN load, the way it is affected by the incubation temperature and by the state of the cytoskeleton. We use coumarin-6 incorporated in the SLNs as a model of a generic lipophilic drug to be delivered, and focus our efforts on the perinuclear accumulation of coumarin fluorescence signal in order to formulate a biophysical model of the load intracellular distribution.

Materials and Methods

Nanoparticles. Solid Lipid Nanoparticles (SLN) were produced by NANO-VECTOR, in the terms of the CE Contract STREP N° LSHB-CT-2006-037639-BONSAI (Bio-imaging with Smart Functional

Nanoparticles) by choosing tripalmitin as lipidic matrix. SLNs have been loaded with coumarin-6 (3-(2'-Benzothiazolyl)-7-diethylaminocoumarin -MW 350,4 Da), c-SLNs, to allow their visualization by means of fluorescence microscopy (λ_{exc} = 450 nm, λ_{em} = 505 nm). The molar ratio coumarin-6:tripalmitin was about 80 (Gasco M.R., personal communication). c-SLN dispersions have been washed four times by tangential flow filtration (Sartorius ,Vivaflow 50 Cassette, RC Membrane, Cut Off 100 kDa), followed by heat sterilization and final storage overtime at 4°C until use [22].

In experiments where coumarin-6 was used as free drug, a stock solution was prepared at a concentration of 20 μg/ml in DMSO and diluted at the desired working solution conditions. The average diameter of heat sterilised c-SLN dispersion, determined by Dynamic Light Scattering (Brookhaven 90Plus system, Brookhaven Instruments Corp.), was 116.1±15 nm, and remained essentially stable (≤130 nm) either when particles were dispersed in buffer, or in cell culture medium supplemented with 1% FBS. The Z potential of the SLN was -24 ± 2 mV (Brookhaven 90Plus system, Brookhaven Instruments Corp).

Cell culture. A30 cells [26] were grown on Petri dishes in DMEM medium supplied with 10% Fetal Bovine Serum (FBS), 1% of L-Glutamine and 1% of Penicillin/Streptomycin and incubated in a controlled environment at 37°C with 5% CO_2. During experiments cells were incubated with medium supplemented with 1% FBS to prevent NPs aggregation. For the time course experiments, the cells were incubated with the c-SLNs at 32°C.

Effect of temperature on NPs intracellular distribution. We estimated the cytoplasmic concentration of coumarin-6 by monitoring the fluorescence distribution in cells exposed to c-SLN (0.01mg/ml) for 45 minutes either at 37°C or at 4°C. In the latter case the cells were pre-cooled for 30 minutes at 4°C. At the end of the incubation period, cells were immediately fixed in PFA 4% in PBS.

Image acquisition. The experimental set up consisted of a wide field NIKON Eclipse FN1 equipped with a 63X objective motorized table (Prior Scientific, Rockland, MA, USA) and Metamorph (Molecular Device, Downington, PA, USA) software for image acquisition and analysis. We used fields of view that encompassed at least 5 cells for analysis. The fluorescence signal form the c-SLNs was discriminated by a band pass filter (λ_{em} = 505 nm) and the images were averaged over an exposure time of 400 ms. On average, 40 Z planes/field were acquired along the Z axis at 0.5 μm inter-distance, starting from top of the cell. We typically considered the overall fluorescence acquired in the wide field. In specific cases, we used the fluorescence estimated on a Z plane corresponding to the mid cell height, obtained through a deconvolution process (AutoDeblur, Media Cybernetics, Bethesda, MA, USA).

Cytochalasin D treatment: Cells were incubated with c-SLN at the concentration of 0.01 mg/ml for 45 minute at 37°C in order to reach a typical intracellular fluorescence distribution. After the wash out of the nanoparticles, cells were incubated with fresh medium containing cytochalasin D at a concentration of 2μM for 1 hour at 37°C. At the end of the incubation time the intracellular fluorescence distribution

was monitored under the microscope and the images were acquired and analyzed as described.

Statistical analysis: Statistical analysis were carried out by t-test and the significance level was set at $p<0.001$ (indicated by symbol * in the figures).

Results

In order to analyse the intracellular fluorescence distribution and uptake kinetics of the fluorophore (coumarin-6) loaded in the SLNs (c-SLNs), we used a monolayer of human lung epithelial, A30 cells, whose characteristics are very close to the more studied A549 [26], an important component of the blood-air barrier, and a sensitive site for particulate body interaction. The analysis of the coumarin-6 fluorescence was performed by selecting on individual cells a line (the emission line EL) that runs from the plasmatic to the nuclear membrane (**Fig.1A**) and four cytoplasmic regions of interest (10 pixel square ROIs) positioned along such EL at 25%, 50% and 75% of the total length. The location of the plasmatic membrane was obtained by saturating the colour levels to half the maximum colour depth in the images. We verified that this was enough to locate the cell membrane by comparing with images in which the actin filaments were specifically labelled. A minimum of ten cells was used to average the data. The cells were exposed to an estimated concentration of 1.8 x 10^{10} c-SLNs/ml, corresponding to a concentration of tripalmitin of 0.01 mg/ml, one order of magnitude lower than the toxic

concentration (0.2 mg/ml) estimated by Lactate Dehydrogenase (LDH) release assay [22].

Uptake and cytoplasmic distribution of the SLNs

We followed the kinetics of c-SLN internalization by monitoring the ROI's average fluorescence signal along the EL line at 3', 9', 15' and 30' right after the addition of NPs to the cell culture (T = 32°C during the image acquisition). The intracellular fluorescence increased as a function of the distance from the plasma membrane reaching the maximum in proximity of the nuclear membrane **(Fig.1B)**. This fluorescence spatial distribution, I(x), observed during the uptake process and at the equilibrium (**Fig.2**), can be always described by a single exponential growth as a function of the distance, x, from the cell membrane (x=100% indicates the nuclear membrane) along the EL according to:

$$I(x) = F_0 + A\exp\left[(x-100)/L\right] \qquad (1)$$

The best fit parameters of the solid lines reported in **Fig.2** are: A(15') = 135 ± 40 [a.u.], L(15') = 26 ± 5 % and F_0(15') = 12 ±5 and A(30') = 330 ± 50 [a.u.], L(30') = 29 ± 3 % and F_0(15') = 10 ±2. It is important to notice that the cell membrane value is $\cong F_0 + A\exp\left[-100/L\right]$. A single exponential trend seems to describe the data as can be gained also from the plot of the normalized fluorescence distribution along the EL and its fit to **Eq.1** (inset of **Fig.2**). This result suggests that, independent of the incubation time, once entered the cells in some

way, the load distributes according to a single mechanism through the whole cell-nucleus distance.

The only relevant difference in the time evolution of the fluorescence distribution concerns the in-homogeneity ratio A/F_0 that offers a quantification of the perinuclear accumulation of the load. This ratio varies from 12 ± 7 to 25 ± 7 when passing from 15' to 30' of SLN exposure time, indicating a progressive perinuclear accumulation. The fluorescence signal monitored at x=50% and 75% along the EL (**Fig.3**) increased at first gradually and seems to reach, after approximately 30 minutes, a saturation value that depends on the position along the EL (**Fig.3**). Such bimodal behaviour, can be fit to a sigmoidal time function of the type:

$$f(t) = f_0 + (f_1 - f_0)(1 + \exp((t - t_{1/2})/\delta)^{-1} \quad (2)$$

The mid point time $t_{1/2}$ is relatively insensitive to the position along the EL line, $t_{1/2} \cong 18'$ (**Fig.3**) while the transition is sharper ($\delta(50\%) \cong 3.5'$ compared to $\delta(75\%) \cong 7'$) as we move closer to the cell membrane through which the c-SLN carried load is internalized. This observation may be an indication that the kinetics of the load distribution in the cytoplasm is affected also by the internalization process, as discussed later.

Effect of temperature

In order to evaluate the temperature effect on the internalization and the distribution of the load, the cells were exposed to c-SLN for 45

minutes either at 4°C or 37°C, fixed as described in the Materials and Methods, and the distribution of the fluorophore was then measured **(Fig.4)**. The absolute value of the intracellular fluorescence is lower for the cells incubated with the SLNs at the lowest temperature as we find I(x=75%) = 155 ± 10 [a.u.] at T=37^{o}C and I(x=75%) = 80 ± 12 [a.u.] at T=4^{o}C. Changes in the cell thickness due to temperature do not affect substantially this conclusion since the emission I(x=75%) computed on deconvoluted images (focal plane at 50% of the cell thickness) confirms a marked difference between the two temperature investigated (350 ± 80 [a.u.] compared to 262 ± 6 [a.u.] for 37°C and 4°C respectively, $p<0.001$, 22 cells). Moreover, the total amount of fluorophore loaded by the cell at T = 37 ^{o}C, as measured by the integral under the lines reported in **Fig.4,** is approximately twice (8800 [a.u.]) as much as that measured for T = 4 ^{o}C (4800 [a.u.]).

The intensity normalized to its maximum value increases with the distance from the cell membrane independently of the experiment temperature and it can still be described by **Eq. 1**. The best fit decay length values are L = 31 ±1 % and L = 43 ± 2 % for T=37 ^{o}C and T=4 ^{o}C, respectively. For the T=37^{o}C data set, however, we observe a slight but definite deviation of the experimental data trend from the simple functional form, **Eq.1** (**Fig.4A**, inset). This finding can be taken as a direct evidence of the presence of at least two intracellular distribution processes, one of which is temperature activated.

Disruption of cytoskeleton

We investigated the role of the cytoskeleton structure on the load distribution by applying, after reaching a steady state fluorescence

distribution, cytochalasin D at a concentration (2.0 μM for 1 h) suitable to disintegrate actin bundles but low enough to avoid cytotoxic damage [28] **[Fig. 5A]**. We found that indeed the treatment led to a more homogeneous pattern of the fluorescence signal, suggesting a redistribution of the fluorophore in the cytoplasm [**Fig. 5B]**. In order to quantify the influence of the cytoskeleton on the load distribution, we normalized the ROIs' fluorescence signal to that measured at 25% of EL ($I(x)/I(25\%)$ in **Fig.5B**. While in the physiological condition the ratio increased 5 fold in proximity of the nuclear membrane, in the cytoD treated cells the ratio reached only a ≅ 1.6 plateau level [**Fig.5C]**.

Discussion

We assume that the cytoplasmic green emission [**Fig.1B]** reports the intracellular coumarin-6 accumulation. Our data indicate that when human lung A30 epithelial cells are exposed to coumarin-6 loaded SLNs, the intracellular fluorescence signal progressively increases (20-80 fold) along the EL line with a monotonic accumulation of the SLN load in the perinuclear region. As can be appreciated from **Figs. 2** and **4**, at least two processes are active in determining this inhomogeneous distribution with a cross-over at x ≅ 30% along the EL that depends on the incubation temperature.

A possible physical and chemical model for the perinuclear accumulation can be drawn by assuming an interaction between the loaded particles and the cell (cytoskeleton and membranes) that

favours the load concentration to the nuclear membrane, notwithstanding the diffusion process. The equilibrium concentration is obtained by the solution of the diffusion equation for the stationary case, and can be written as:

$$c_{eq}(x) = c_N \exp\left[\frac{\langle \Delta U \rangle}{K_B T 100}(x - 100)\right]$$

(3)

The comparison of **Eq.1** to **Eq.3** indicates that the best fit decay length, L, is a measure of the average interaction energy gain, $<\Delta U> = <U_{cell}> - <U_{nucleus}>$, that the load/dye suffers when moving from the cell membrane to the nuclear membrane ($\langle \Delta U \rangle \geq 0$):

$$\langle \Delta U \rangle = 100 \frac{K_B T}{L}$$

(4)

The L values reported in **Table I** correspond to a decrease of 0.9 (± 0.14) $K_B T$ units of $\langle \Delta U \rangle$, when decreasing the temperature from T= 37°C to T= 4°C: the load-membrane interaction energy at the nucleus is smaller at lower temperature. This may reflect a change in the cytoskeleton structure and dynamics that affects the load distribution.

By analyzing **Eq.1** we gain also information on the relative perinuclear concentration of loaded dye at the equilibrium. In fact the excess perinuclear concentration, $\Delta C = (c_N - c_C)/c_C$ can be related to the area, $\Im$,under the fluorescence distribution curves reported in **Fig.4** (normalized to the background level F_0) and the decay length as:

$$\Delta_C = \frac{(c_N - c_C)}{c_C} = (\Im + 1)\frac{100}{L} \qquad (5)$$

Here, the perinuclear and the cell concentrations of the load are c_N and c_C, respectively. The estimated perinuclear excess values, Δ_C, (**Table I**) indicate that the perinuclear excess of concentration increases by approximately 55% when increasing the temperature from T= 4^{o}C to T= 37^{o}C.

The limited changes in the load internalization that we observed when decreasing the cell temperature, suggests that endocytotic pathways, that are sensibly dependent on the temperature [30-31] in the range 4-37^{o}C, are only partially effective in the upload process of the SLNs and that the internalization is also determined by a direct interaction between the membrane and the SLN phospholipids. This picture agrees with previous analyses [22] that indicated that the internalization of the SLN load is comes along with the modification of the lipid (SLNs) physical and chemical thermodynamic parameters, probably due to their interaction with phospho-lipids (membrane). Calorimetric studies indicate [22] that the SLN interacting with the cell membrane, only partially preserve their native structure. Therefore a fraction of the intracellular fluorescence results from coumarin-6 freed from the modified SLNs.

We also tried to shed some light on the role of the cytoskeleton structure in determining the load distribution by monitoring the fluorophore intracellular signal in conditions in which the cytoskeleton structure is altered by adding cytochalasin D. Indeed we found that the inhomogenous intracellular distribution was almost

completely lost after this treatment (**Fig.5**), as we measure L as large as 80%, almost three times larger than that measured in absence of cytochalasin D, that corresponds to (see **Eq.4**) a decreased energy gain ($<\Delta U> \cong K_BT$ compared to $<\Delta U> \cong 3\ K_BT$ prior to the cyto-D treatment, **table I**). It must be noted that the analysis proposed here, based on a one dimensional diffusion process, is not substantially affected by this assumption. In fact similar, though less direct, results are obtained when generalizing this treatment by taking into account the polar symmetry of the cell.

Upload kinetics.

Regarding the origin of the hypothesized NP-cytoskeleton interaction we focus on the possibility of local overpressures generated by the cytoskeleton dynamics. In fact, it is well accepted that the cytoplasm of mammalian cells is under pressure and that this pressure is mainly determined by contractile forces exerted by cytoskeletal stress fibres [32-33]. These fibers contain, among other component, actin filaments that, in intact living cells, may shorten to generate tension as well as elongate thereby determining also cellular elasticity. Thus the cells possess tensed and elastic components simultaneously. One possible hypothesis about the generation of the fluorescence perinuclear accumulation in the cells may rely on the presence of these forces [28] that should be relaxed when treating the cells with actin filament destabilising drugs, such as cytochalasin D as indeed is found here (**Fig.5**). Information on the state of the load released in the cytoplasm can be obtained through the analysis of the uptake kinetics. In fact the

sigmoidal fit to the kinetic data (**Fig.3** and **Eq.2)** cannot easily be cast on a solid biophysical model that we delineate schematically hereafter.

If we assume the following initial conditions, $c(x,0) = c_{ext}\delta(x)$, that describe the case in which on the outer layer of the cell membrane the load is at the constant concentration c_{ext} at time t=0, the load concentration follows a simple exponential time dependence of the type:

$$c(x,t)\big|_{x=0,100} = a(x) + b(x)\exp\left[-t\Gamma_0\right] \quad (6)$$

where a(x) and b(x) are parameters that depends on the initial membrane load concentration, c_{ext}, and on the position along the EL line. The relaxation rate Γ_0 is related to the effective energy gain, $<\Delta U>$, the load diffusion coefficient, D, and the average cell thickness, Δ (from the cell to the nuclear membrane) as:

$$\Gamma_0 = \frac{D}{4\Delta^2}\left(\frac{\Delta U}{K_B T}\right)^2 \quad (7)$$

However the initial condition $c(x,0) = c_{ext}\delta(x)$ cannot describe the actual situation in which the SLNs interact with the cells. In fact we expect that the SLNs enter the cell membrane at a characteristic rate, γ, that depends on the details of nanoparticle interaction with the membrane. Moreover, the extracellular SLNs concentration, c_{ext}, should decay slowly with time due to the continuous internalization of the SLNs by the all the cells in the culture. This decay can be to first

approximation described by an exponential trend with a second relaxation rate Γ. Therefore the initial conditions for the intracellular load concentration close to the cell membrane, should be more closely described by a form of the type: $c(0,t) = c_{ext}\left(1 - \exp\left[-t\gamma\right]\right)\exp\left[-t\Gamma\right]$. The first exponential growth (the term within the round parentheses) accounts for the increase in the concentration of the load within the cell right at the cell membrane, due to the internalization process. The second exponential decay, with relaxation rate Γ, accounts instead for the overall depletion of the SLNs in the cell culture. Within such model, **Eq.6** changes to a sum of exponential decays that, with the assumption that $\Gamma << \gamma$, can be written as:

$$c(x,t) \cong B\left(\exp\left[-t\gamma\right] - \exp\left[-t\Gamma_0\right]\right) + c_\infty(x)\left(1 - \exp\left[-t\gamma\right]\right) \quad (8)$$

From **Eq.8**, we can obtain the fluorescence signal along the EL as a function of time as, $F(x,t) \cong F_\infty c(x,t)/c_\infty(x)$, that, as can be seen from **Fig.3**, can indeed fit the experimental data as well as the sigmoidal fit (**Eq.2**). We have globally fitted the two data sets in **Fig.3** by assuming common values of the Γ_0 and γ parameters, whose best fit values are: $\Gamma_0 = 0.1 \pm 0.02$ min and $\gamma = 0.07 \pm 0.02$ min^{-1}. The time delay observed in the rise of the load concentration (**Fig.3**) is determined by the relaxation rate γ and the slope of the load signal at larger times is related to the rate Γ_0. The marked sigmoidal shape of the kinetics derives then from the difference in the two relaxation rates, Γ_0 and γ, that account for the intracellular diffusion/transport and the internalization of the load.

From the diffusion relaxation rate, Γ_0, we can estimate a value of the diffusion/transport load coefficient in the cytoplasm. By taking an average value of the energy loss, $\Delta U/K_BT \cong 2.8$ (**Table 1)**, without cytochalasin D) and by assuming an average size of 5μm for the cell cytoplasm ($\Delta \cong 5$ μm), we estimate $D \cong 0.02$ $\mu m^2/s$. This value is more than four orders of magnitude less than the coumarin free dye diffusion in aqueous solution at room temperature ($D_{coum} \cong 280 \mu m^2/s$), and about two orders of magnitude lower than the diffusion coefficient of the SLNs at the same conditions. The study of the diffusion coefficient of simple chromophores in cells' cytoplasm and on the cell membrane [34], indicate that the chromophore slows its diffusivity down by about 10^2 times in the cytoplasm and about 10^4 times on the cell membrane. In the view of these literature data, our estimate of the diffusion coefficient associated with the coumarin-6 fluorescence signal suggest that the load moves within the cell cytoplasm in a form that us still reminiscent of the nanocarrier structure and not in the form of free dye.

In summary, we have undertaken a detailed analysis of the distribution and the kinetics of the fluorescence signal during SLN-mediated uptake of a hydrophobic dye in A30 cells. The analysis of the fluorescence microscopy data indicates the combined action of the diffusion of the dye in the cytoplasm and of a mean force field that act on the dye and induce its accumulation around the nucleus. Data collected in conditions in which the cytoskeleton is perturbed indicate that these forces, that correspond to an energy gain of the order of few K_BT from the cell to the nuclear membrane, originate from the

cytoskeleton dynamics. We speculate here that the cytoskeleton reacts in response to the internalization with tensive stresses that lead to intracellular overpressure. The biophysical model that we propose allows us to quantify the interaction energy gain of the load from the cell to the nucleus membrane. Regarding the state of the load after the cell internalization, the kinetics of the load uptake measured as a function of the distance from the cell membrane, indicates that the fluorescence changes according to a slow diffusivity of the load which is not fully compatible with the size of the free dye. This study sets a warning about the possibility of a strong nonspecific interactions of internalization compounds with the cytoskeleton that should be taken into account when looking for specific pharmacological targeting of intracellular compartments.

Table

Table I. Analysis of the distribution of coumarin-6 as a function of the nuclear to cytoplasmatic membranes.

	A	L (%)	F_0	A/F_0	$\frac{\langle \Delta U \rangle}{K_B T} = \frac{100}{L}$	Δ_C
T =37 °C	315± 7	31 ± 1	4 ± 2	75±6	3.2 ± 0.	21.7 ± 3
T= 4 °C	160 + 0.9	43 ± 2	2 ± 2	80 ± 8	2.3 ± 0.1	13.8 ± 2
T= 37 °C + CytoD.	86 ± 16	80 ± 40	40 ± 7	2.1 ± 1	1.2 ± 0.6	

Table 1. The characteristic distance, L, is in unit of % of the total distance between the nuclear and the cytoplasmatic membranes. Notice that the load concentration at the cell membrane is $c(x=0) = A\exp[-100/L]$. The parameter $\Delta_C = (c_N - c_C)/c_C$ indicates the relative excess of the load concentration at the nuclear membrane and is computed from **Eq.5** and the numerical integration (trapezoidal rule) of the data reported in **Fig.4**.

Figure Legends

Figure 1: Definition of the intracellular Emission Line. Panel A shows a representative image acquired after 30 min of c-SLN incubation (FITC, λ_{exc} = 488nm, integration time 400 msec). From the cell to the perinuclear region, an Emission Line (EL) was drawn (white line) and four different ROIs were selected (0, 25, 50, 75% of EL) along which the fluorescence analysis was carried out. In panel B, representative traces of the fluorescent signal along the EL recorded at 0', 9', 15' and 30' of incubation time, show a load accumulation in the perinuclear region consistent with the image in panel A. The signal has been obtained by averaging over equal area ROIs and is shown in arbitrary units.

Figure 2: Intracelullar Distribution of the Load. Fluorescence intensity as a function of the distance from the plasma membrane along the EL for two acquisition times: 15' (open squares) and 30' (open circles) from the initial addition of the c-SLN to the cells. The data are the result of the average over seven cells and the error bars represent the standard deviations. The solid lines are the best fit of **Eq.1** to the data. The inset shows the normalized fluorescence signal together with the best fit of **Eq.1** to both the sets of data.

Figure 3: Internalization kinetics. The plot represents the kinetics of the change of the fluorescence signal (in [a.u.]) measured in cells incubated with c-SLN at positions along the EL of 50% (empty symbols) and 75% (filled symbols). The data are the result of the

average over seven cells. The solid lines are obtained through the global fit of the both the data sets to **Eq.8**, F(x) = $b\left(\exp\left[-t\gamma\right]-\exp\left[-t\Gamma_0\right]\right)+ F_\infty(x) \left(1-\exp\left[-t\gamma\right]\right)$. The best fit parameters are: $F_\infty(50\%)$=76 ± 10, $b(50\%)$ = 290 ±50, $F_\infty(75\%)$= 174 ± 5, $b(75\%)$ = 630 ± 55, γ =0.07±0.03 min^{-1} and Γ_0 = 0.01 ± 0.02 min^{-1}. The dashed lines represent the individual fits of the EL=50% and EL=75% data to the sigmoidal function: $f(t)= f_0+\left(f_1-f_0\right)\left(1+\exp\left(\left(t-t_{1/2}\right)/\delta\right)^{-1}\right.$. The best fit parameters in this case are: $f_0(50\%)$ =-2.7±0.5, $f_1(50\%)$ = 58 ± 10, $t_{1/2}(50\%)$ = 17.5' ± 4' and δ = 3.5' ± 1.5', $f_0(75\%)$ = -26 ± 5, $f_1(75\%)$ = 150 ± 25, $t_{1/2}(75\%)$ = 19' ± 4' and δ = 7' ± 3'.

Figure 4: Temperature dependence of the intracellular Distribution of the Load. The main panel shows the effect of the decrease of the c-SLN incubation temperature on the intracellular fluorescence: T = 37°C (filled circles) and T = 4°C (open circles). The data are the result of the average over seven cells and the error bars represent the standard deviations. The solid lines are the best fit of **Eq. 1** to the data. The inset reports the residuals of the best fit lines (solid line for T=4°C and dashed line for T=37°C).

Figure 5: Effect of the Cytoskeleton Structure on the intracellular Distribution of the Load. Panel A: typical images acquired on A30 cells in control condition (CTRL) and after treatment with CytoD 2μM for 1 h (+ CytoD). Actin filaments are labelled in red. The treatment applied with CytoD breaks the major actin filaments in the

cells. The horizontal white bar corresponds to 20 micrometers. Panel B: images of fluorescence distribution in A30 cells after 30’ of incubation with c-SLN before (CTRL) and after (+cytoD) cytoD treatment. The fluorescence distribution is substantially changed following the cytoD treatment. The horizontal white bar corresponds to 20 micrometers. Panel C: the plot represents the trend of the fluorescence as a function of the distance from the plasma membrane, for the control (CTRL) and the cytoD treated sample (cytoD), normalized to the signal measured at EL = 25%. The data are the result of the average over ten cells and the error bars represent the standard deviations. Statistical analysis were carried out by t-test and the significance level was set at $p<0.001$ (indicated by symbol * in the plot).

Figures :

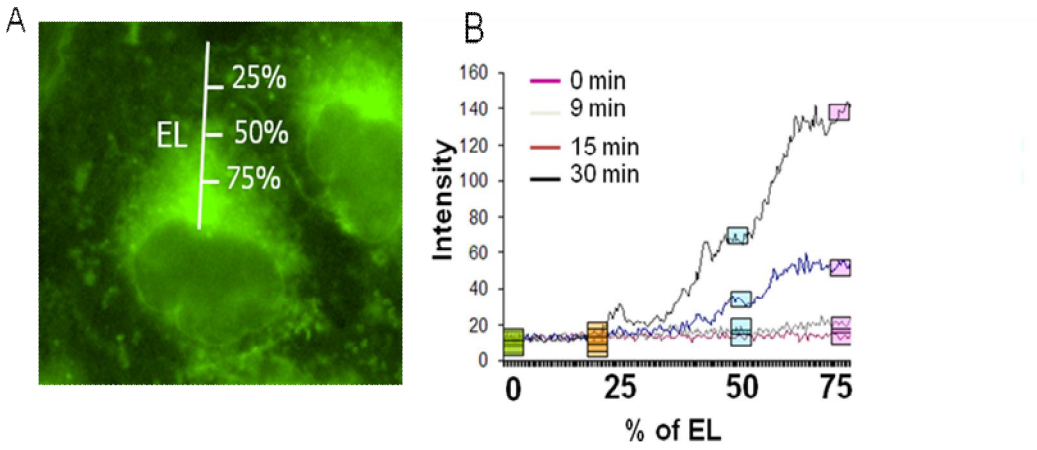

Figure 1: Definition of the intracellular Emission Line

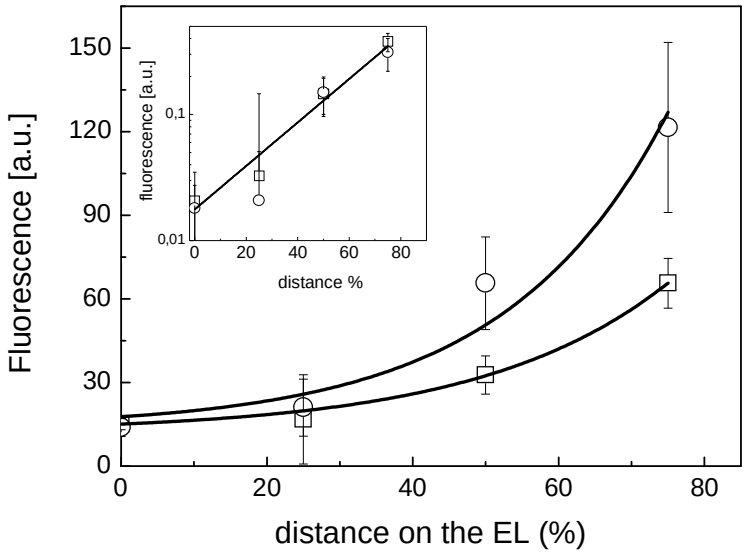

Figure 2 : Intracellular distribution of the load

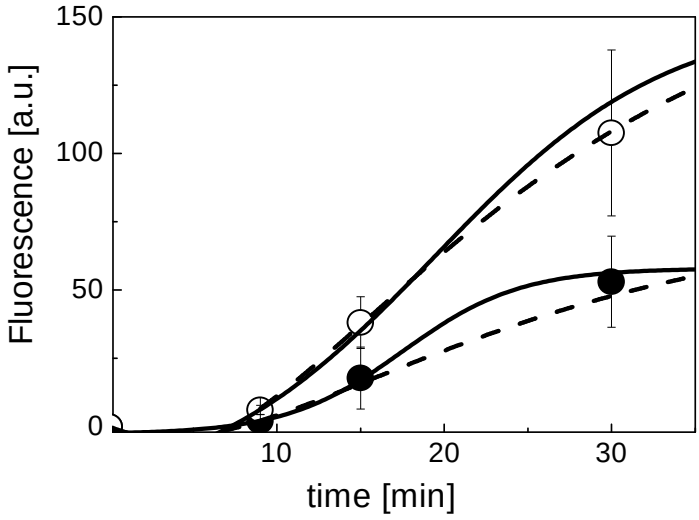

Figure 3: Internalization kinetics

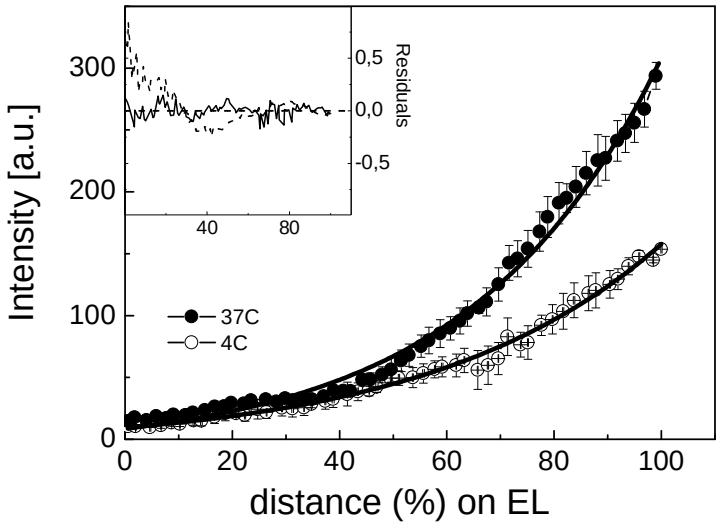

Figure 4: Temperature dependence of the intracellular Distribution of the Load

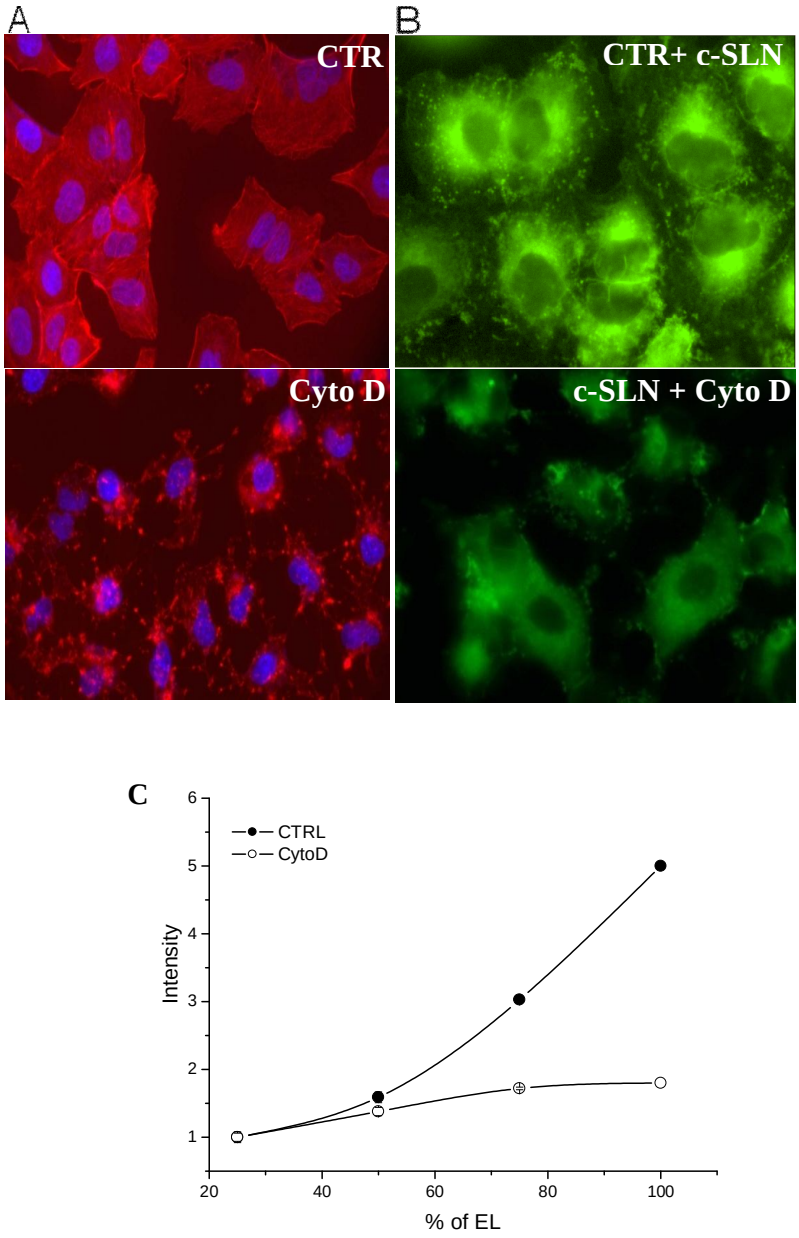

Figure 5: Effect of the Cytoskeleton Structure on the intracellular Distribution of the Load

References

1. **Gasco MR.** (1997) Solid Lipid nanospheres from warm micro-emulsion. Pharm Tech Europe. 9: 52-58.
2. **Marengo E**, Cavalli R, Rovero G, Gasco MR (2003) Scale-up and optimization of an evaporative drying process applied to aqueous dispersions of solid lipid nanoparticles. Pharmac. Devel. Tech. 8: 299-309.
3. **Suresh G**, Manjunath K, Venkateswarlu V, Satyanarayana V. (2007) Preparation, Characterization, and in vitro and In vivo evaluation of Lovastatin Solid Lipid Nanoparticles. AAPS Pharm.Sci.Tech. 8: E1-E9.
4. **Bargoni A**, Cavalli R, Zara GP, Fundarò A, Caputo O, Gasco MR. (2001) Transmucosal transport of tobramycin incorporated in solid lipid nanoparticles (SLN) after duodenal administration to rats. Part II—Tissue distribution. Pharmacol Res. 43:497-502.
5. **Yang R**, Gao R-C, Cai C-F, Xu H, Li F, He H-B, Tang X. (2010) Preparation of Gel-Core-Solid Lipid Nanoparticle: A Novel Way to Improve the Encapsulation of Protein and Peptide. Chem. Pharm. Bull. 58: 1195-1202.
6. **Jensen LB**, Magnussson E, Gunnarsson L, Vermehren C, Nielsen HM, Petersson K. (2010) Corticosteroid solubility and lipid polarity control release from solid lipid nanoparticles. Int. J. Pharmac. 390: 53-60.
7. **Teskac K**, Kristl J. (2010) The evidence for solid lipid nanoparticles mediated cell uptake of resveratrol. Int. J. Pharmac. 390: 61-69.
8. **Yang SC**, Zhu JB, Lu Y, Liang BW, Yang CZ. (1999) Body Distribution of Camptothec in Solid Lipid Nanoparticles after oral administration. Pharmaceutical Research 16:751-757.

9. **Hauss DJ,** Fogal SE, Ficorilli JV, Price CA, Roy T, Jayara AA, Keirns JJ. (1998) Lipid-based delivery systems for improving the bioavailability and lymphatic transport of a poorly water-soluble LTB4 inhibitor. J Pharm Sci. 87:164-9.
10. **Cavalli R,** Bargon A, Podio V, Munton E, Zara CP, Gasco MR. (2003) Duodenal administration of solid lipid nanoparticles loaded with different percentages of tobramycin. J. Pharm. Sci. 92:1085-1094.
11. **Manjunath K**, Venkateswarlu V. (2005a) Pharmacokinetics, tissue distribution and bioavailability of clozapine solid lipid nanoparticles after intravenous and intraduodenal administration. J. Control. Rel. 107: 215-228.
12. **Müller RH**, Mäder K, Gohla S. (2000) Solid lipid nanoparticles (SLN) for controlled drug delivery – a review of the state of the art. Eur. J. Pharm. Biopharm. 50:161-177.
13. **Müller RH**, Mehnert W, Lucks JS, Schwarz C, zur Muhlen A, Weyhers H, Freitas C and Ruhl D. (1995) Solid lipid nanoparticles – An alternative colloidal carrier system for controlled drug delivery. Eur. J. Pharm. Biopharm. 41:62-69.
14. **Hu FQ**, Hong Y and Yuan H. (2004) Preparation and characterization of solid lipid nanoparticle containing peptide. Int. J. Pharm. 273: 29-35.
15. **zur Muhlen A**, Schwarz C, Mehnert W. (1998) Solid lipid nanoparticles (SLN) for controlled drug delivery - Drug release and release mechanism. Eur. J. Pharm. Biopharm. 45: 149-155
16. **Schwarz C**, Mehnert W. (1999) Solid lipid nanoparticles as drug delivery systems J. Microencapsulation. 16: 205-213.
17. **Lv Q**, Yu A, Xi Y, Li H, Song Z, Cui J, Cao F, Zhai G. (2009) Development and evaluation of penciclovir-loaded solid lipid nanoparticles for topical delivery. Int. J. Pharm. 372:191-8.

18. **Westesen K**, Bunjes H and Koch MHJ. (1997) Physicochemical characterization of lipid nanoparticles and evaluation of their drug loading capacity and sustained release potential. J. Control Rel. 48:223-236
19. **zurMuhlen Z**, zurMuhlen E, Niehus H, Mehnert W. (1996) Atomic force microscopy study of Solid Lipid Nanoparticles. Pharm. Res. 13:1411-1416.
20. **Manjunath K**, Reddy JS, Venkateswarlu V. (2005b) Solid lipid nanoparticles as drug delivery systems. Meth. Find. Exp. Clin. Pharm. 27: 127-144.
21. **Kristl J**, Volk B, Ahlin P, Gombac K, Sentjurc M. (2003). Interactions of solid lipid nanoparticles with model membranes and leukocytes studied by EPR. Int. J. Pharm. 256:133-140
22. **Rivolta I**, Panariti A, Lettiero B, Sesana S, Gasco P, Gasco MR, Masserini M, Miserocchi G. (2011) Cellular uptake of coumarin-6 as a model drug loaded in Solid Lipid Nanoparticles (SLN). J. Physiol. Pharm. In press.
23. **Lai SK**, Hida K, Chen C, Hanes J. (2008) Characterization of the intracellular dynamics of a non-degradative pathway accessed by polymer nanoparticles. J. Control Release. 125:107-11.
24. **Chavanpatil MD**, Khdair A, Gerard B, Bachmeier C, Miller DW, Shekhar MP, Panyam J. (2007) Surfactant-polymer nanoparticles overcome P-glycoprotein-mediated drug efflux. Mol. Pharm. 4:730-8.
25. **Chakraborty SK**, Fitzpatrick JA, Phillippi JA, Andreko S, Waggoner AS, Bruchez MP, Ballou B. (2007) Cholera toxin B conjugated quantum dots for live cell labeling. Nano Lett. 7:2618-26.
26. Botto L, Beretta E, Bulbarelli A, Rivolta I, Lettiero B, Leone BE, Miserocchi G, Palestini P. (2008) Hypoxia-induced modifications in

plasma membranes and lipid microdomains in A549 cells and primary human alveolar cells. J. Cell Biochem. 105:503-13.

27. **Gemeinhart RA**, Luo D, Saltzman WM. (2005) Cellular fate of a modular DNA delivery system mediated by silica nanoparticles. Biotechnol Prog. 21:532-7.
28. **Schulze C**, Mueller K, Kaes JA, Gerdelmann JC. (2009) Compaction of Cell Shape Occurs Before Decrease of Elasticity in CHO-K1 Cells Treated With Actin Cytoskeleton Disrupting Drug Cytochalasin D. Cell motility and the Cytoskeleton. 66: 193-201.
29. **Wei W**, Ma GH, Hu G, Yu D, Mcleish T, Su ZG, Shen ZY. (2008) Preparation of Hierarchical Hollow CaCO3 Particles and the Application as Anticancer Drug Carrier. J. Am. Chem. Soc. 130:15808-10.
30. **Weigel PH** and Oka JA. (1981) Temperature dependence of endocytosis mediated by the asialoglycoprotein receptor in isolated rat hepatocytes. Evidence for two potentially rate-limiting steps. J. Biol. Chem. 256: 2615-2617.
31. **Wolkers WF**, Looper SA, Fontanilla RA, Tsvetkova NM, Tablin F, Crowe JH. (2003) Temperature dependence of fluid phase endocytosis coincides with membrane properties of pig platelets. Biochim Biophys Acta. 1612:154-63.
32. **Cai Y**, Sheetz MP. (2009) Force propagation across cells: mechanical coherence of dynamic cytoskeletons. Curr. Opin. Cell Biol. 21:47-50.
33. **Luo Y**, Xu X, Lele T, Kumar S, Ingber DEJ. (2008) A multi-modular tensegrity model of an actin stress fiber. Biomech. 41: 2379-2387.
34. **Schwille P**, et al. (1999) Molecular dynamics in living cells observed by fluorescence correlation spectroscopy with one- and two-photon excitation. Biophys. J. **77**: 2251–2265.

Chapter 4

UPTAKE AND INTRACELLULAR DISTRIBUTION OF FUNCTIONALIZED IRON OXIDE NANOPARTICLES.

Lettiero B.[1], Panariti A. [1], Morjan I.[2], Wang D.[3], Dumitrache F. [2], Alexandrescu R. [2], Miserocchi G. [1], Rivolta I. [1]

[1] Department of Experimental Medicine, University of Milano Bicocca, Monza, Italy

[2] Laboratory of Laser Photochemistry, National Institute for Lasers, Plasma and Radiation Physics, Bucharest, Romania.

[3] Ian Wark Research Institute, University of South Australia, Adelaide, Australia.

In preparation

Abstract

Due to their attractive magnetic properties, iron oxide nanoparticles (NPs) has been widely studied as potential tools for several biomedical applications such as bioimaging and gene delivery. For these purposes detailed information of the early stages of interaction between iron oxide NPs and cells is essential. Accordingly, this study aimed at characterizing the mechanisms underlying the uptake and intracellular distribution of biocompatible iron oxide NPs coated with L-Dihydroxyphenylalanina (L-dopa)–TRITC in lung epithelial cells. Our data revealed that the particles crossed the plasma membrane with an energy-dependent process, since the incubation at low temperature (4°C) prevented their entrance. Moreover, specific compounds (amiloride and EIPA) together with inhibitors of cytoskeleton integrity dramatically abolished NPs entrance, suggesting a potential role of macropinocytosis in NPs uptake. Furthermore, once cellular internalization occurred, TRITC-NPs movement followed a centripetal direction and, over time, NPs accumulated at the perinuclear level, but no evidence of specific colocalization with subcellular organelles was found, except for a close proximity with acidic compartments (late endosomes and lysosomes).

Introduction

In the last years iron oxide nanoparticles (usually magnemite, Fe_2O_3 and magnetite, Fe_3O_4) have been considered as attractive tools for an increasing number of imaging and therapeutic purposes [1-2], such as Magnetic Resonance Imaging (MRI), site specific drug-delivery, local hyperthermia, as well as magnetic-based cell transfection or "magnetofection" [3]. Interestingly, the high magnetic responses, exclusively displayed upon an external magnetic field, along with the unique features related to the nanoscale size, make iron oxide NPs suitable to potentially act at cellular or even at molecular level [4]. However, due to the combination of spontaneous magnetic attraction and hydrophobic interactions, these particles tend to aggregate in colloidal suspensions, thus dramatically preventing any biological application. Hence, surface modification via several types of coating materials, such as dextran, albumin, silicones, poly(ethyleneglycol) (PEG) and dopamine [5-7] have been performed in order to provide NPs steric stability in physiological buffers. Moreover, surface properties of iron oxide NPs may govern their cell fate in terms of efficiency of cellular uptake and potential toxicity [8]. For instance, iron oxide NPs either functionalized with the nonionic polysaccharide pullulan [9] or polyvinyl alcohol (PVA) [10] showed higher biocompatibility (>90%) than the uncoated counterpart presumably due to surfactant capability to prevent unfavorable interactions between reactive iron surfaces and cells. This effect, in turn, could reduce cellular uptake leading to lower toxicity. Likewise, the absence of known binding centers for dextran-iron oxide NPs on the plasma

membrane [11] most likely limited the capability of cell uptake to fluid phase endocytosis [12].

In the literature very few data are available about the effects of iron oxide-NP at cellular level [12-14] and are mainly focused on morphological cell modifications and cytoskeletric reorganization. Indeed, in view of their future application in biomedicine, gaining detailed information on cellular fate of iron oxide NPs is a crucial starting point to prevent potential cytotoxicity.

In light of this considerations, we sought to thoroughly evaluate the *in vitro* behavior of a new formulation of magnetic nanoparticles sterically stabilized with the dispersant L-Dihydroxyphenylalanine (L-dopa) [RSF39@L-dopa], on alveolar epithelial cell line, in terms of biocompatibility, likely mechanism of cellular uptake, intracellular NPs movement and distribution.

Materials and Methods

Synthesis of RSF39. Nano-sized iron oxide particles have been directly synthesized by the laser induced pyrolysis of a mixture containing iron pentacarbonyl and air, as carbon and oxygen precursors, respectively. Ethylene was used as sensitizer (energy transfer agent). The iron oxide sample (RSF39) was obtained at the laser power of 55 W. The work pressure was maintained at 300 mbar. The morphology and composition of the iron oxides nanopowder were characterized by transmission electron microscopy (TEM).

Synthesis fluorescent-labeled RSF39@L-dopa-TRITC NPs. Bare RSF39 NPs were first stabilized with L-dopa. For this, in a 15 ml plastic tube 5 ml of aqueous-solution of (L-dopa) (c=5 mg/ml, pH 8) was added to 100 mg of dry RSF39 and immediately vortexed. Subsequently, the mixture was sonicated for 1 hour in a 60°C water bath. The RSF39@L-dopa NPs were then precipitated and washed with acetone, dried under vacuum and re-dispersed in water. The NPs dispersions were centrifuged at 4000*g* or filtered through 100 nm syringe filters before use. Secondly, 200 mg RSF39@L-dopa NPs were disperse in 9 ml of H2O and the pH of the dispersion was adjusted with NaOH to pH 9-10. Then, in separate vial, 10 mg (0.02 mmol) of tetramethylrhodamine-5/6-isothiocyanate (TRITC) was dissolved in 50µl of DMF and then diluted with 500 µl of H2O. The TRITC solution was mixed with the RSF@L-dopa dispersion and the mixture was stirred for 24 hours. After 24 hours, the NPs were precipitated in excess acetone and washed several times with acetone, until the acetone was colorless. The precipitate was dispersed in 5 ml of H2O. The particle dispersion was then dialysed against H2O for 3 days (MWCO 1000). Finally, the dispersion was centrifuged at 4000g to remove the aggregates. The emission wavelength maximum of the NPs was around 580 nm.

Size measurements of RSF39 @L-dopa NPs-TRITC in culture medium were performed by Dynamic Light Scattering (DLS) (Malvern, Zetasizer 3000 HSA instrument) at a fixed angle of 90°C and at temperature of 25°C in triplicate.

Cell culture. A30 cells were cultured on Petri dishes in Dulbecco's modified Eagle's medium (DMEM), supplemented with 10% Fetal bovine serum (FBS) and 1% (v/v) of an antibiotic cocktail made of Penicillin/Streptomycin at 37°C using a humidified 5% CO_2 incubator. For the experimental conditions cells were incubated with medium supplemented with 1% FBS in order to reduce significantly any serum interference in the toxicity assay.

Cell viability assay. The level of cell toxicity related to plasma membrane damages after incubation with RSF39@L-dopa-TRITC NPs was evaluated by measuring the release of the cytosolic Lactate Dehydrogenase (LDH) enzyme in the culture medium (LDH assay). A30 were seeded on 96-well microplates and, at confluence, incubated with increasing concentration of RSF39@L-dopa-TRITC NPs (from 10 ng up to 100 μg/ml) for 6 hrs and 24 hrs. The analysis was performed according to the direction of the manufacturer (Clonetech). The cell membrane damage was calculated through the following formula, in order to obtain a curve dose-response :

$$\text{Cytotoxicity} = \frac{\text{Triplicate absorbance} - \text{Low control}}{\text{High control - Low control}}$$

Study of NPs uptake. The effect of temperature was studied incubating the cells with iron oxide NPs (100μg/ml) either at 37°C or 4°C for 1hr. For the latter condition 30 min of sample pre-cooling at 4°C was performed before starting the incubation. In other experiments A30 cells were pre-treated with amiloride (3mM) and its

analogous EIPA (50μM) at 37°C before the incubation with RSF39@L-dopa-TRITC NPs (at 100μg/ml) for 30 min at 37°C in presence of the chemicals. In a third set of experiments, cells were treated with cytochalasin D (cyto D, 1μM) and nocodazole (10 μM) before or after incubation with NPs at 37°C.

Analysis of NPs distribution. To evaluate the intracellular movements of RSF39@L-dopa-TRITC NPs over time, A30 cells were incubated with iron oxide NPs (100μg/ml) for 20 min at 37°C , then washed with PBS, and incubated in DMEM supplied with 1% FBS for a specified period of time (up to 4 hrs). After cell fixation in paraphormaldehyde 4% at room temperature (RT) for 30 min, the quantitative analysis of NPs distribution was performed by measuring their distance from the nucleus in a significant number of cells (n=15).

Immunofluoresce cell staining. To characterize the intracellular distribution of RSF39@L-dopa-TRITC, antibodies directed against established marker of subcellular organelles were used: mouse monoclonal antibodies against early endosomes antigen 1 (EEA1), goat polyclonal antibodies against Lysosomal-associated membrane protein 1 (LAMP1), monoclonal antibodies against a Golgi matrix protein (GM130) and antibodies against the GTPase RAB7 protein to identify late endosomes. Cells were grown on glass coverslips in DMEM supplemented with 10% FBS at 37°C until 80% of confluence was achieved. They were incubated with 100 μg/ml of RSF39@L-dopa-TRITC, and fixed with paraformaldehyde 4% at different time points (up to 1h). Control samples were processed in parallel in

absence of any NPs incubation. Cells were then washed three times with Phosphate Buffered Saline (PBS), Low Salt PBS (LS) and High Salts PBS (HS) respectively and permeabilized with a gelatin dilution buffer GDB2X containing 0,01% (v/v) digitonin, for 30 min at RT. Subsequently, cells were incubated with primary antibody diluted in GDB2X (dilution 1:500 for LAMP1 and GM130; 1:700 for EEA1 and 1:100 for RAB7) for 2h at 37°C, then washed three times with HS and incubated with Alexa fluor-488 conjugated secondary antibodies (dilution 1:100) for 1 hr at 37°C. Finally, cells were washed with HS and LS three times respectively and nuclear staining was performed using 4',6-diamidino-2-phenylindole (DAPI) at concentration of 1μM in PBS for 5 min. Coverslips were mounted onto slides with glycerol.

Images acquisition and analysis. Fluorescence images were acquired at a magnification of 100X with Olympus BX51 wide field fluorescent microscope equipped with CELL-R software. Immunostained cells were also imaged using a confocal microscope (LSM 510 Meta), with the use of a 63X magnification PlanApo lens (NA 1.4). Single confocal sections are shown.

Statistical analysis. The statistical analysis of experimental data was performed using the Student's t-test and data were presented as mean ± SD. Statistical significance was considered at $p < 0,01$.

Results

Nanoparticles characterization.

TEM analysis of sample RSF39 reveals an almost polycrystalline morphology **[Fig.1a]**. The nanoparticles show coalescent features. Cross-linked chains may be sometimes observed. The image displays mostly faceted particles. **Figure 1b** presents the histogram of the particle size distribution. By a lognormal fit, rather sharp particle diameter distributions is found, with the maximum at about d_m = 5 nm. Changes in the NPs suspension from water to culture medium caused an evident increase in the NPs hydrodynamic diameter from 115-120 nm up to 180-250 nm respectively.

In vitro cell viability

The biocompatibility of RSF39@L-dopa-TRITC nanoparticles was tested by the *in vitro* quantification of LDH enzyme release in the extracellular medium which is an early sign of plasma membrane damage. A30 cells were incubated with increasing concentrations of NPs (from 10 ng up to 100 μg/ml) for 6 hrs and 24 hrs. Indeed, our data suggested a dose-dependent reduction in cell viability, though it remained as high as 80% even at the maximal concentration tested (100 μg/ml), regardless the time of incubation **[fig.2]**. Therefore, since this last concentration resulted in a low cell perturbation, we decided to use it for the incubation of the cells in further experiments. In fact, 100μg/ml ensured the best fluorescence signal to noise ratio.

Study of cellular uptake

As RSF39@L-dopa NPs were covalently conjugated to Tetramethylrhodamine isothiocyanate (TRITC) dye, the fluorescent NPs appeared as punctate red spots in the cytoplasm of A30 cells (λ_{exc} 557 nm, λ_{em} 576 nm) **[fig.3a]**. To characterize whether NPs internalization was an energy-dependent process, A30 cells were incubated with L-dopa-coated iron oxide NPs for 1h either at 37°C or 4°C. Lowering the temperature down to 4°C completely abolished NPs uptake **[fig.3b]**, thus suggesting the involvement of active transports in particle internalization.

Due to the NPs diameter (180-250nm), among active transports, macropinocytosis seemed to be the likely mechanism that drove NPs internalization and in order to assess its possible involvement in L-Dopa-coated iron NPs uptake experiments were carried out by testing two specific macropinocytosis pharmacological inhibitors: amiloride (3mM), its derivate EIPA (50 μM). All the treated samples showed a significant block of NPs uptake compared to the control condition **[Fig.4]**.

To further confirm our hypothesis about a macropinocytosis-mediated iron oxide NPs uptake pre-conditioned A30 cells were incubated for 30 min with cytochalasin D (1μM) and nocodazole (10 μM), that are specific inhibitors of actin and microtubules polymerization respectively. Our data clearly showed that both the cell treatments against cytoskeleton functionality were able to prevent iron NPs from crossing the plasma membrane **[Fig.5]**.

Intracellular movement and distribution of RSF39@L-dopa-NPs

After 10 minutes of incubation of RSF39@L-dopa-TRITC a typical red dotted staining appeared in peripheral regions of the cells **[Fig.6a]** indicating that the NPs crossed the plasma membrane in few minutes. Indeed, upon longer incubation time, the intracellular distribution of the fluorescence changed significantly. We decided to monitor this phenomenon carrying out a quantitative analysis of the localization and the dimension of the NPs clusters over a window of time going from 10 minutes up to 4 hours of incubation **[Fig.6a-d]**. We were able to monitor a slow NPs-TRITC movement towards the nucleus, being 5.8±1.4μm far from the nuclear membrane at the shorter time of incubation, and 2.7±1μm after 4 hours **[Fig.6e]**. Interestingly, with increasing exposure time, NPs clusters size was scaled up to larger fluorescent intracellular aggregates (form 0.75±0.1 up to 1.91±0.5μm going from 10 minutes to 4 hours of incubation at 37°C, $p<0.01$) **[Fig.6f]**. To verify any potential role of cytoskeleton in the observed dynamic of NPs movements, the analysis was conducted in presence of RSF39@L-dopa-TRITC and subsequent treatment with cytochalasin D or nocodazole for 1h at 37°C. Our results showed a major capability of nocodazole in interfering with NPs progression towards nuclei than cytochalasin D that, in turn, seemed to have a role in the formation of the larger NPs aggregates ($p<0.001$) **[Fig.6e-f]**.

Immunofluoresce colocalization experiments

As iron-NPs movement tended to follow a centripetal direction *over time,* immunofluoresce experiments were performed to identify any

possible localization with some subcellular structures and organelles such as Golgi apparatus, early endosomes, late endosomes or lysosomes. We were not able to demonstrate a specific co-localization of NPs with any of these organelles, but only a close proximity between fluorescent signal and acidic compartments (late endosomes and lysosomes) after 1hr of incubation **[Fig.7]**.

Discussion

Among all biomedical applications, magnetic nanoparticles have been extensively studied as alternative systems for *in vitro* transfection of genetic material (e.g. small interfering RNA, siRNA) [3] and cellular magnetic labeling [15]. Accordingly, in addition to the development of appropriate NPs surface modifications, the knowledge of the cellular dynamics in response to NPs exposure is one of the major prerequisite for the design of effective and safer devises. Indeed, physicochemical properties (especially size and surface charge) have significant implications in the cellular uptake and biological processes of nanoparticles [16].

Here, we proposed an example of *in vitro* investigation of iron oxide NPs (RSF39) interaction with epithelial alveolar cells (A30 cells). The low molecular dispersant L-dopa was used as a steric NPs stabilizer because of its strong binding to the iron core and to functional molecules on NP surface [17]. We could monitor intracellular movements of RSF39@L-dopa by means of the fluorescent dye TRITC stably conjugated to the particles.

Despite the increase in the particles size in culture medium (150-250nm) RSF39@L-dopa-TRITC NPs were stable over the whole duration of the incubation time (24h) as assessed by DLS measurements and were also rather biocompatible up to high exposure level (100μg/ml) where an approximately 20% of LDH enzyme release, thus cellular membrane damage occurred **[fig.2]**. This is in agreement with some previous studies that have generally found low cytotoxic rate for a range of magnetic NPs with varying coatings (e.g. pullulan, dextran), even at higher NPs concentrations [9,12].

The uptake of exogenous molecules (e.g. engineered NPs) from the cell surface may generally occur through several pathways which are directly related to both composition and size of solutes [18,19] and, thus to the volume of fluid internalized. Indeed, particles can cross the plasma membrane by passive diffusion, that does not require membrane transport and metabolic energy consumption or undergo to active endocytosis, by which solutes are transported against the thermodynamic equilibrium. In our experiments, the total block of RSF39@L-dopa-TRITC NPs uptake in A30 cells at 4°C **[fig.3]** suggested the likely role of active transports in particle internalization, since they are sensibly temperature-dependent pathways [20].

Because of the size of iron oxide NPs, we evaluated the contribution of macropinocytosis in the cellular uptake. Indeed, macropinocytosis is a nonselective type of endocytosis responsible for the engulfment of large volumes of extracellular fluid. It is a cytoskeleton-driven mechanism that primarily requires the formation of plasma membrane protrusions, or ruffles, via the assembly of localized actin filaments. Then they fuse back with the plasma membrane and give rise to

relatively large-sized vesicles with diameters ranging from 0.2 to 1 μm, called macropinosomes [21]. Generation of macropinosomes can be uniquely affected by the inhibition of Na^+/H^+ exchangers (NHEs). Indeed, NHE1 activity is required to control the critical pH in the immediate vicinity of the plasma membrane, that presumably promotes actin polymerization during macropinocytosis [22]. Amiloride, a guanidinium-containing pyrazine derivative, and its strong and selective analogous 5-(N-ethyl-N-isopropyl) amiloride (EIPA) have been extensively used for this purpose [22,23]. With this regard, we found that the uptake of iron oxide NP was completely abolished when cells incubation was carried out in presence either of amiloride or EIPA **[fig.4]**.

Moreover, as macropinocytosis is an actin-dependent process, a further proof of its involvement in iron–based NPs uptake consisted in the treatment of A30 cells with the chemical cytochalasin D (Cyto D), whose primary action is to inhibit association and dissociation of actin monomers, thus preventing actin polymerization. Again, our data demonstrated that incubation of A30 cells with RSF39@L-dopa-TRITC NPs in presence of a non toxic concentration of cyto D could significantly block NPs uptake **[Fig.5b]**. Likewise, even the inhibition of microtubule functionality by nocodazole totally prevented iron oxide NPs internalization **[Fig.5c]**. Indeed, an intact microtubule network is necessary for the coordination of cell ruffling and membrane movements that drive the formation of macropinosomes [24]. Therefore, all the results presented so far strongly suggested that the most likely mechanism of RSF39@L-dopa-TRITC NPs uptake in A30 cells occurred through macropinocytosis.

Subsequently, we investigated the intracellular distribution of RSF39@L-dopa-TRITC NPs over time in order to define their fate following an acute exposure. Indeed, A30 cells were incubated with iron oxide NPs and, after washing order to avoid a continuous iron loading from the extracellular medium, their movements were analyzed up to 4 hrs. The capability of NPs to move slowly from cell peripheral regions (at 10 min) towards a perinuclear region (at 4hrs) presumably resembled the known centripetal movement of macropinosomes, already described in macrophages [25]. Moreover, iron oxide NPs movement was likely to be controlled by microtubules since treatment with nocodazole significantly affect NPs intracellular distribution, with a clear slowing of the time of progression towards the nucleus **[fig.6]**.

Another feature of the intracellular behavior of iron oxide NPs consisted on the tendency to give rise to larger aggregates with the increasing of the incubation time. It is known that macropinosomes can fuse each other and culminate with the formation of large vacuolar structures [26]. Therefore, it is plausible that NPs aggregates are generated for some extent by the progressive mixing of macropinosome contents following membrane fusion.

Actin filaments were likely implicated in the progressive NPs aggregation, since incubation with cyto D significantly prevented this process. A possible explanation for this phenomenon could be the presence of actin filaments surrounding the surface of macropinosomes deep in the cytoplasm [27], which could control dynamics and morphology of both vesicles and iron oxide NPs.

Finally, despite NPs showed a perinuclear accumulation, the analysis of fluorescently labeled subcellular organelles and structures showed that RSF39@L-dopa-TRITC NPs did not colocalize with early endosomes and Golgi apparatus, but there was only a partial overlap with late endosomes and lysosomes **[Fig.7]**.

Hence, further studies are necessary to clarify whether iron oxide NPs require longer period of incubation to accumulate in acidic compartments, since sequestration and degradation of NPs in lysosomes is one of the crucial barriers to an effective *in vitro* delivery of a variety of macromolecules (e.g. DNA, oligonucleotides, small interfering RNA).

Conclusion

Our study demonstrated that RSF39@L-dopa-TRITC NPs did not cause evident signs of acute toxicity, due to the low level of plasma membrane damage observed up to 24h of incubation with A30 cells. Macropinocytosis was the most likely mechanism involved in NPs internalization which led to a perinuclear NPs accumulation over time remarkably driven by cytoscheletric structures. However, such accumulation did not correspond to a specific colocalization with subcellular acid compartments which are known to be highly concentrated in proximity of the nuclear region. Therefore, our study provided useful information about NPs trafficking and cellular processes that occurred after an acute NPs incubation. This is a necessary starting point for proceeding with a further analysis of the long-term fate of NPs exposure, still poorly investigated.

Figure Legends :

Figure 1: **Characterization of RSF39@L-dopa-TRITC Nanoparticles**. Panel (a) represents TEM analysis of the iron oxide sample. In panel (b) particle size distribution as determined from TEM measurements.

Figure 2: **LDH release of RSF39@L-dopa-TRITC treated cells**. Dose-response curve for A30 cells incubated with progressively increasing TRITC-NPs concentration from 10 ng/ml up to 100 μg/ml for 6hrs and 24hrs. Data are presented by means ± SD (n=6).

Figure 3: **Effect of temperature on NPs uptake.** Panel (a) and (b) shows intracellular distribution of RSF39@L-dopa-TRITC (red spots) after 1h of incubation at 37°C or at 4°C, respectively. Lowering the temperature prevented NPs internalization. Nuclear staining (blue) was performed using DAPI. Scale bar, 20 μm.

Figure 4: In panel (a), cells in control condition showing NPs perinuclear accumulation (red spots). In panel (b) and (c), the treatment with amiloride and EIPA respectively, prevents NPs entrance, suggesting a role of macropinocytosis in cells uptake. Scale bar, 20μm.

Figure 5: **Role of the cytoskeleton in the cellular uptake of NPs**. In panel (a) control cells incubated with RSF39@L-dopa-TRITC (red spots) for 30 min at 37°C. Pre-treatment with cyto D (panel b) and

nocodazole (panel c) caused a significant inhibition of cellular uptake. Scale bar 20μm.

Figure 6: **Analysis of intracellular progression and aggregation of NPs (red) over time** (panel a-d). The treatment of RSF39@L-dopa-TRITC incubated cells with nocodazole (panel e) and with cyto D (panel f) prevented NPs progression towards the nucleus and their aggregation, respectively. Scale bar, 20 μm.

Figure 7: **Intracellular TRITC-NPs localization**. No clear colocalization of RSF39@L-dopa-TRITC (red) with early endosomes (EEA1, green) and Golgi (GM130, green), but only a close proximity with lysosomes (LAMP1, green) and late endosomes (RAB7, green). Scale bar, 10 μm

Figures:

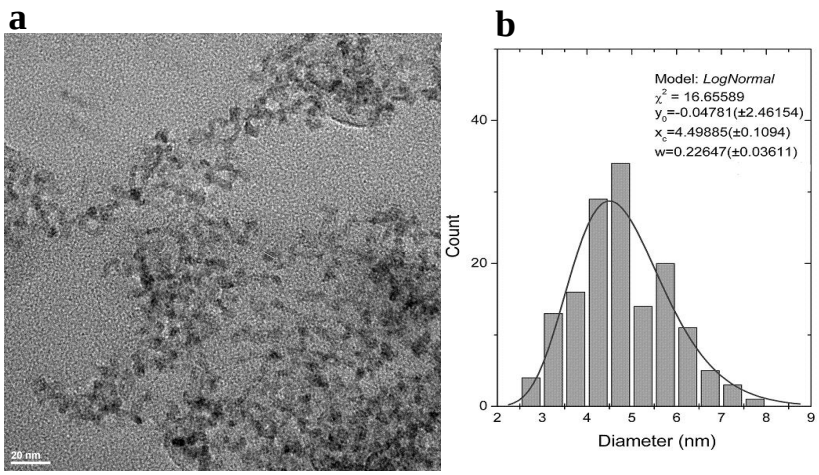

Figure 1: Characterization of RSF39@L-dopa-TRITC Nanoparticles

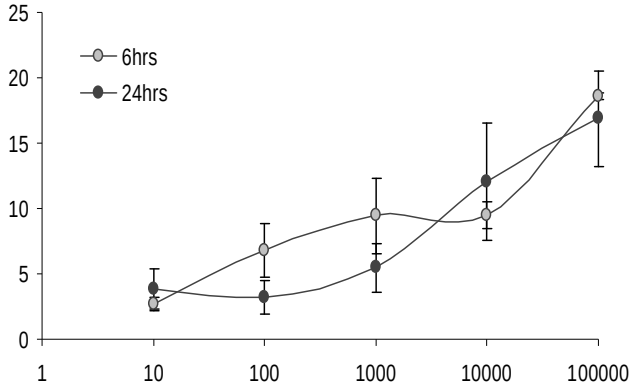

Figure 2 : LDH release of RSF39@L-dopa-TRITC treated cells

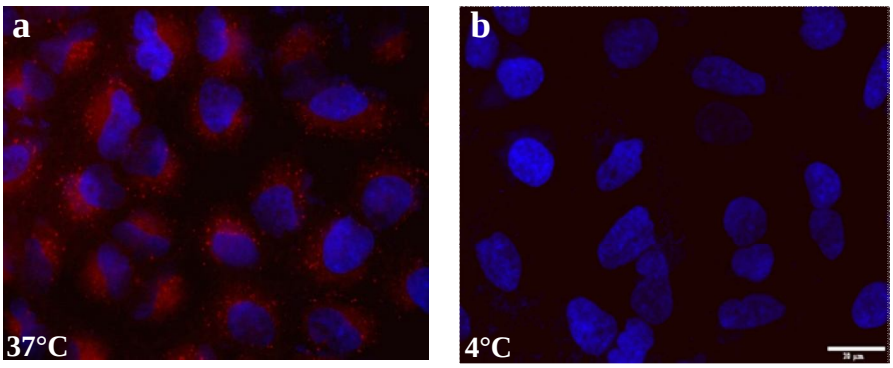

Figure 3: Effect of temperature on NPs uptake.

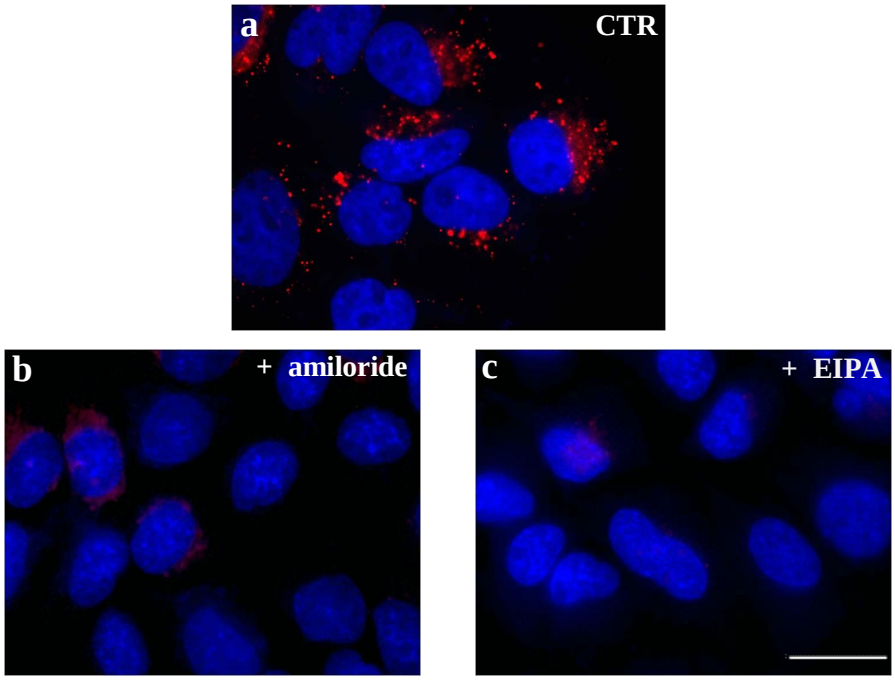

Figure 4 : Inhibition of TRITC-NPs uptake

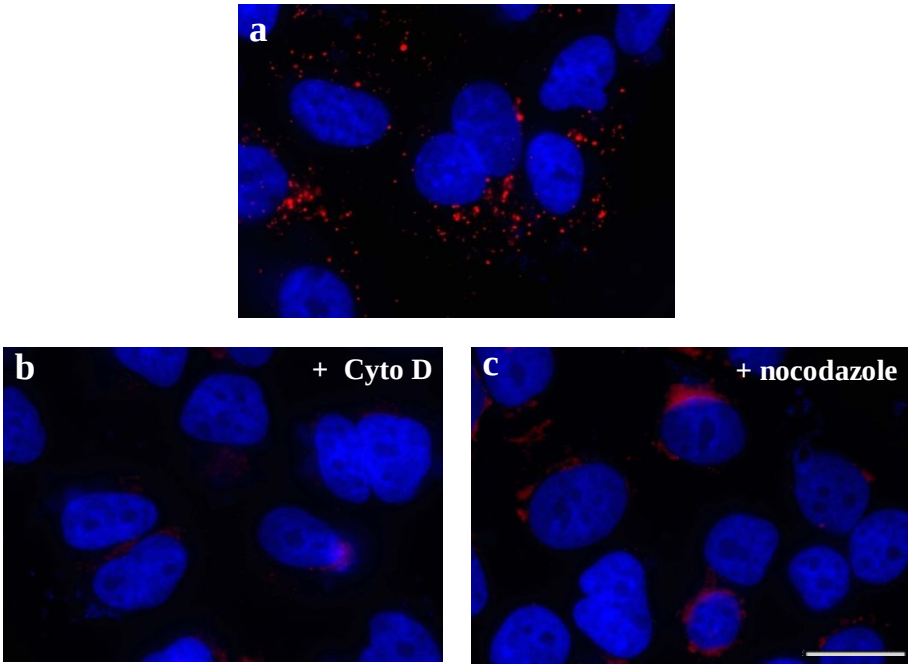

Figure 5: Role of the cytoskeleton in the cellular uptake of NPs

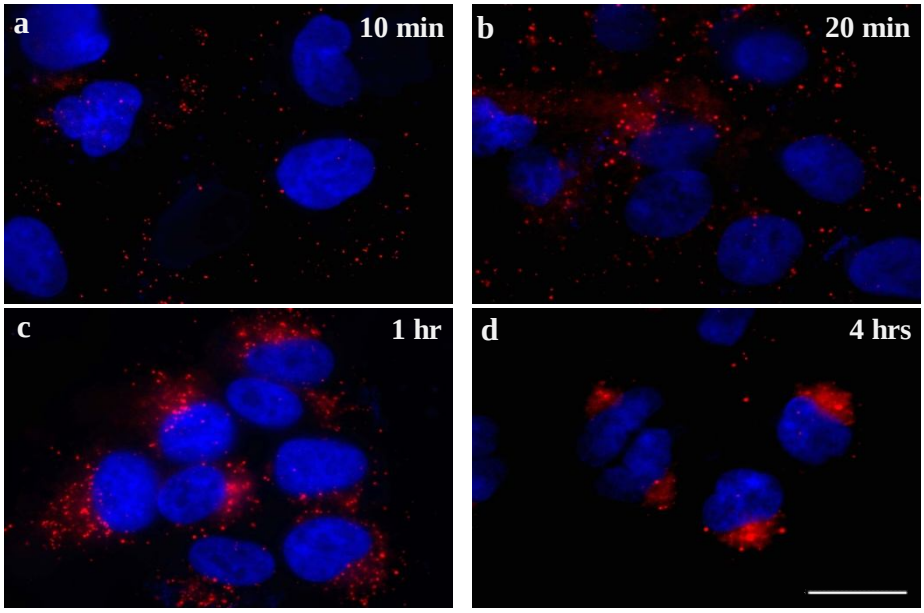

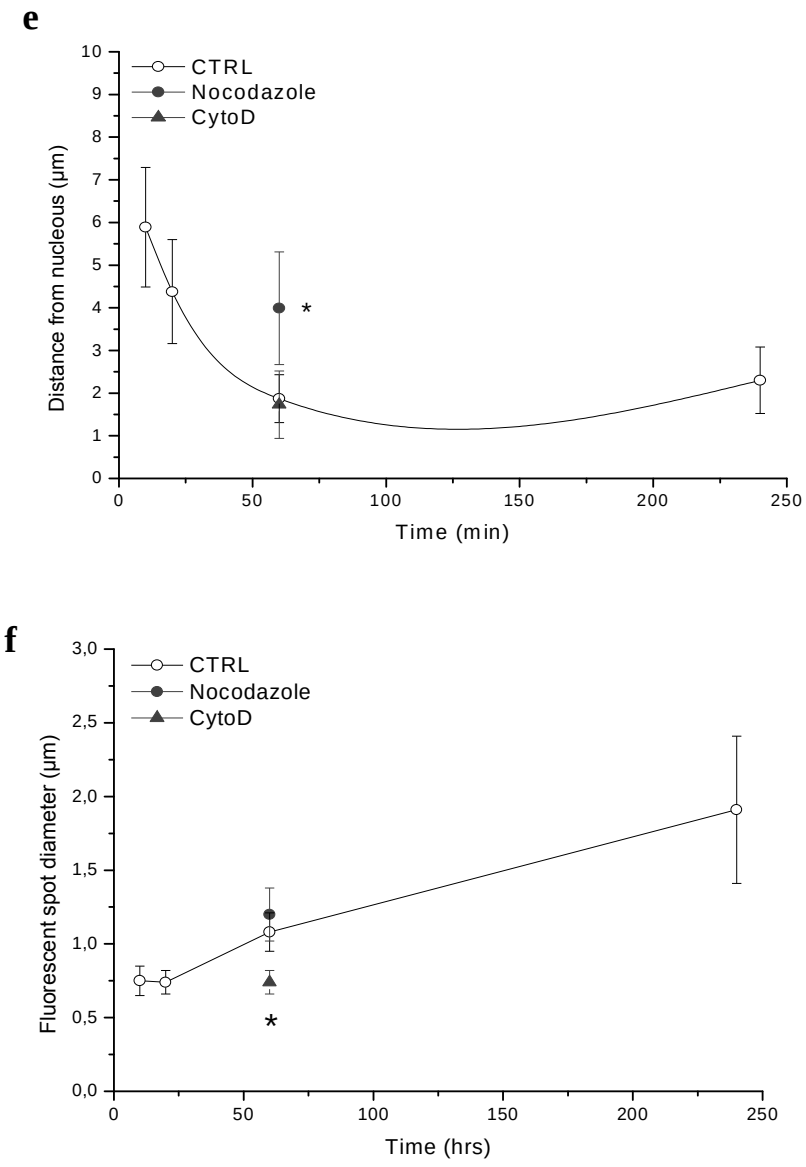

Figure 6 : Analysis of intracellular progression and aggregation of NPs (red) over time

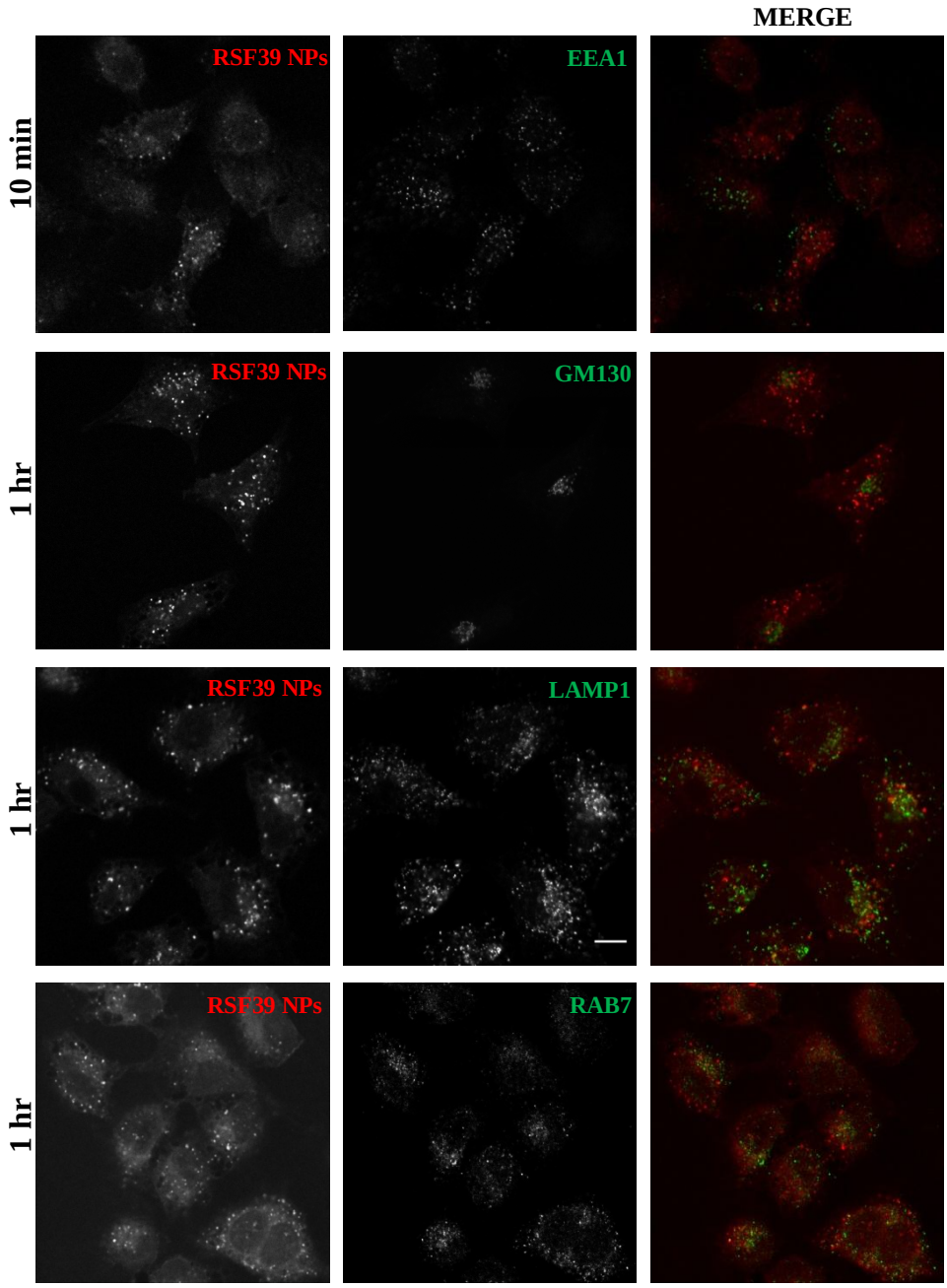

Figure 7: Intracellular TRITC-NPs localization

References

[1] **Xu C.** and Sun S.(2009) Superparamagnetic nanoparticles as targeted probes for diagnostic and therapeutic applications. Dalton Trans. 7(29): 5583–5591.

[2] **Gupta A.K.** and Gupta M.(2005) Synthesis and surface engineering of iron oxide nanoparticles for biomedical application. Biomaterials 26: 3995-4021.

[3] **Dobson J.** (2006) Gene therapy progress and prospects: magnetic nanoparticle-based gene delivery. Gene Therapy 13:283–287.

[4] **Lee J.H.**, Huh Y.M., Jun Y., Seo J., Jang J., Song H.T., Kim S., Cho E.J., Yoon H.G., Suh J.S. and Cheon J.(2007) Artificially engineered magnetic nanoparticles for ultra-sensitive molecular imaging. J. Nat. Med. 13(1):95-99.

[5] **Berry C.C.**, Wells S., Charles S., and Curtis A.S.G.(2003) Dextran and albumin derivatised iron oxide nanoparticles: influence on fibroblasts in vitro. Biomaterials 24: 4551–4557.

[6] **Lacava L.M.**, Lacava Z.G.M., Da Silva M.F., Silva O., Chaves S.B., Azevedo RB, Pelegrini F, Gansau C, Buske N, Sabolovic D, and Morais PC. (2001) Magnetic resonance of a dextran-coated magnetic fluid intravenously administered in mice. Biophys J 80:2483–2486.

[7] **Amstad E.**, Gillich T., Bilecka I., Textor M., and Reimhult E. (2009) Ultrastable iron oxide nanoparticle colloidal suspension using dispersants with catechol-derived anchor groups. Nano Letters 9(12):4042-4048.

[8] **Duguet E**, Vasseur S, Mornet S, and Devoisselle JM.(2006) Magnetic nanoparticles and their applications in medicine. Nanomedicine (Lond) 1: 157-168.

[9] **Gupta A.K**. and Gupta M. (2005) Cytotoxicity suppression and cellular uptake enhancement of surface modified magnetic nanoparticles. Biomaterials 26: 1565-1573.

[10] **Mahmoudi M.,** Simchi A., Imani M., Shokrgozar M.A., Milani AS, Hafeli UO, et al.(2010) A new approach for the in vitro identification of the cytotoxicity of superparamagnetic iron oxide nanoparticles. Colloids Surf B Biointerfaces 75:300-309.

[11] **Moore A.**, Weissleder R., and Bogdanov A.(1997) Uptake of dextran-coated monocrystalline iron oxides in tumor cells and macrophages. J.Magn Reson Imaging 7:1140–1145.

[12] **Berry C.C.**, Wells S., Charles S. and Aitchinson G. (2004) Cell response to dextran-derivatised iron oxide nanoparticles post internalization. Biomaterials 25:5405–5413.

[13] **Hilger I.**, Fruhauf S, Linss W, et al. (2003) Cytotoxicity of selected magnetic fluids on human adenocarcinoma cells. J Magn Magn Mater.261(1–2):7–12.

[14] **Zhang Y**., Kohler N, and Zhang M. (2002) Surface modification of superparamagnetic magnetite nanoparticles and their intracellular uptake. Biomaterials 23(7):1553–1561.

[15] **Boutry S.**, Brunin S., Mahieu I., Laurent S., Elst L.V. and Muller R.N. (2008) Magnetic labeling of non-phagocytic adherent cells with iron oxide nanoparticles: a comprehensive study. Contrast Media Mol. Imaging 2008, 3 223–232.

[16] **Karlsson H.L.,** Gustafsson J., Cronholm P., and Möller L. (2009) Size-dependent toxicity of metal oxide particles. A comparison between nano- and micrometer size. Toxicology Letters 188 (2009) 112–118.

[17] **Xu C.**,Xu K.,Gu H., Zheng R., Liu H.,Zhang X.,Guo Z.,and Xu B. (2004) Dopamine as A Robust Anchor to Immobilize functional Molecules on the Iron Oxide Shell of Magnetic nanoparticles.J. AM. CHEM. SOC. 126, 9938-9939.

[18] **Nam H.Y**., Kwon S.M., Chung H., Lee S.Y., Kwon S.H., Jeon H., Kim Y., Park J.H., Kim J., Her S., Oh Y.K., Kwon I.C., Kim K., and Jeong S.Y.(2009) Cellular uptake mechanism and intracellular fate of hydrophobically modified glycol chitosan nanoparticles.J Control Release 5;135(3):259-267.

[19] **Chavanpatil A.K.M.D**., and Panyam J. (2006) Nanoparticles for cellular drug delivery: mechanism and factors influencing delivery. J. Nanosci. Nanotechnol. 6: 2651-2663.

[20] **Steinman R.M.,** Mellman I.S., Muller W.A., and Cohn Z.A. (1983) Endocytosis and the recycling of plasma membrane. J. Cell Biol. 96:1-27.

[21] **Swanson J.A.** (2008) Shaping cups into phagosomes and macropinosomes. Nat Rev Mol Cell Biol 9:639–649.

[22] **Koivusalo M**., Welch C., Hayashi H.,Scott C.C., Kim M.,1 Todd Alexander T., Touret N., Hahn K.M., and Grinstein S. (2010) Amiloride inhibits macropinocytosis by lowering submembranous pH and preventing Rac1 and Cdc42 signaling. J. Cell Biol. 188(4): 547-563.

[23] **Masereel B.**, Pochet L., and D. Laeckmann D. (2003) An overview of inhibitors of Na(+)/H(+) exchanger. Eur. J. Med. Chem. 38:547–554.

[24] **Racoosin E.L**. and Swanson J.A.(1992) M-CSF-induced macropinocytosis increases solute endocytosis but not receptor-mediated endocytosis in mouse macrophages. J. Cell Science 102: 867-880.

[25] **Racoosin E.L.**, and Swanson JA. (1993) Macropinosome maturation and fusion with tubular lysosomes in macrophages. J Cell Biol. 121:1011–1020.

[26] **Hewlett L.J.**, Prescott A.R., and Watts C. (1994) The coated pits and micropinocytic pathways serve distinct endosome populations. J Cell Biol. 124: 689-703.

[27] **Willingham M.C**., Yamada S.S., Davies P.J.A., Rutherford A.V., Gallo M.G., and Pastan I. (1981) Intracellular localization of actin in cultured fibroblasts by electron microscopic immunocytochemistry. J. Histochem Cytochem 29(1): 17-37.

Chapter 5

Complement activation cascade triggered by PEG-PL engineered nanomedicines and carbon nanotubes: challenges ahead

SM Moghimi[a,‡], AJ Andersen[a], SH Hashemi[a], B Lettiero[a], AC Hunter[b], TL Andresen[c], J Szebeni[d]

[a]*Centre for Pharmaceutical Nanotechnology and Nanotoxicology, Department of Pharmaceutics and Analytical Chemistry, University of Copenhagen, Universitetsparken 2, DK-2100 Copenhagen Ø, Denmark*

[b]*Molecular Targeting and Polymer Toxicology Group, School of Pharmacy, University of Brighton, Brighton BN2 4GJ, UK*

[c]*Department of Micro- and Nano-Technology, DTU-Nanotech, Technical University of Denmark, Frederiksborgvej 399, DK-4000 Roskilde, Denmark*

[d]*Department of Nanomedicine, Institute of Nanotechnology, Bay Zoltán Foundation for Applied Research, Milskolc, Hungary*

Journal Controlled Release 146 (2010) 175-181

Keywords: Carbon nanotube; Complement activation; Liposome; Micelle; Poly(ethylene glycol); Pseudoallergy

Abstract

Since their introduction, poly(ethylene glycol)-phospholipid (PEG-PL) conjugates have found many applications in design and engineering of nanosized delivery systems for controlled delivery of pharmaceuticals especially to non-macrophage targets. However, there are reports of idiosyncratic reactions to certain PEG-PL engineered nanomedicines in both experimental animals and man. These reactions are classified as pseudoallergy and are associated with cardiac anaphylaxis and rapid haemodynamic collapse. Recent studies suggest that complement activation may be a contributing, but not a rate limiting factor, in eliciting hypersensitivy reactions to such nanomedicines in sensitive individuals. This is rather surprising since PEGylated structures are generally assumed to suppress protein adsorption and blood opsonization events including complement. Here, we examine the molecular basis of complement activation by PEG-PL engineered nanomedicines and carbon nanotubes and discuss the challenges ahead.

Introduction

MethoxyPEG$_{2000–5000}$-phosholipid (mPEG-PL) conjugates are versatile molecules with numerous biomedical applications. These conjugates were initially incorporated in to the liposomal bilayer for conferring longevity to vesicles in the systemic circulation; this eventually led to the development of Doxil® approved for treatment of HIV-related Kaposi's sarcoma and refractory ovarian carcinoma [1-3]. PEGylated vesicles, through prolonged circulation times in the blood, can ultimately target many vascular elements following conjugation of targeting ligands to the distal end of the projected PEG chains bearing a reactive functional group [1,2,4]. Apart from targeting ligands, contrast agents or bio-sensors have also been coupled to the distal end of the PEG chain for engineering of multifunctional vesicles applicable to a wide range of pathologies [2,4-6]. PEG-phospholipid conjugates exhibit low critical micelle concentration values and form a stable micellar structure of approximately 30 nm in size, allowing drug solubilization and are amenable for additional functionalization and parenteral administration [7]. The application of PEG-phospholipid conjugates in steric stabilization and generation of long circulating oil-in-water nanoemulsions is also noteworthy [8]. Finally, apart from nanomedicine design and development, PEG-phospholipids can further stabilize entities such as carbon nanotubes through surface adsorption and enhance their dispersion in aqueous media; such modifications also affect nanotube pharmacokinetics following intravenous injection for biological and mechanistic studies [9].

There are indications that certain PEG-phospholipid bearing nanomedicines may be Janus-faced; indeed, there are clinical reports of acute hypersensitivity reactions to infusion of long circulating regulatory-approved PEGylated liposomes in sensitive individuals [10-12]. These reactions, classified as pseudoallergy, are often associated with flushing and circulatory disturbances [13]. Recent studies in pigs have suggested that cardiopulmonary distress caused by Doxil® and other liposomes strongly correlate with complement activation [14]. The complement system **[Fig.1]**, consisting on over 30 soluble plasma and cell-surface bound proteins, serves as an important effector of both innate and acquired immunity [15]. Accordingly, complement activation by PEGylated vesicles is an unexpected phenomenon since surface mPEG coverage is generally believed to dramatically suppress particle-protein interaction and blood opsonization events, including fixation [1,16]. Similar to the binding of allergens to IgE on the surface of mast cells and basophiles, complement anaphylatoxins (and particularly C5a) can trigger immediate release of a plethora of proinflammatory mediators from these cells and macrophages. This cascade of secondary mediators substantially amplifies effector immune responses and may induce anaphylaxis in sensitive individuals [13,17]. In addition to PEGylated vesicles, unexplained acute adverse reactions such as ataxia, restlessness and trembling, respiratory abnormalities, frothing at the mouth, collapse and even death have also surfaced in veterinary senarios (cattle, sheep and swine) following administration of intravenous medicines containing high PEG content [18]. Anaphylaxis has further been reported in some patients and animals who have received intravenous formulations

containing the block co-polymer poloxamer 188, which is structurally similar to PEG [19,20]. Remarkably, these polymers (at concentrations relevant to their designated applications) also activate complement system [18,20].

It is the purpose of this article to examine the molecular basis of complement activation by PEG-PL engineered nanomedicines and other entities (e.g. PEGylated carbon nanotubes), highliting the modulatory role of interfaces in which PEG-PL molecules are located, and discuss the challenges ahead.

The porcine model of anaphylaxis

Intravenous administration of minute amounts of Doxil® (0.1 mg lipid/kg body weight) induces reproducible haemodynamic changes and ECG alterations in the porcine model as depicted in **Fig.2a**. These include an abrupt drop in systemic arterial pressure (SAP) that is associated with massive pulmonary hypertension, decreased cardiac output and decreased end-tidal PCO_2 [14]. During the nadir of the blood pressure curve (lasting ~4 min), a transient tachyarrhythmic episode followed by ST depression and T-wave elevation is noticeable. However, the ECG is normalized after 12–15 min. A more severe reaction (a deeper and longer hypotensive period) occurs by doubling the Doxil® dose **[Fig.2a]**. An interesting feature of the systemic pressure response that the reduction of systolic pressure is greater compared with that of diastolic pressure, resulting in a substantial reduction of pulse pressure amplitude. These changes can

be associated with severe bradycardia (which is not of sinus origin), arrhythmia and the presence of incomplete as well as complete atrioventricular block with asystole. The ECG traces suggest that the bradycardia is a reflection of slowed atrioventricular conduction. Since the physiological baroreflex to hypotension is tachycardia the bradycardia associated with hypotension represents “paradoxical bradycardia”. Follow up studies suggested that acute adenosine release within the heart could explain the paradoxical bradycardia via A_1 receptors [14]. Larger liposome doses (0,5 mg lipid /kg body weight) are lethal in the porcine model; ventricular fibrillation and cardiac arrest occurs within 3 min of liposome injection [14] .

Activation of mast cells in the coronary arterial intima, and perivascularly, in close proximity to myocytes can induce cardiac anaphylaxis [21,22]. These cells express high-affinity receptors for anaphylatoxins C3a and C5a, and triggering of anaphylatoxin receptors induces the release of a variety of inflammatory mediators and vasoactive molecules from mast cells [13]. For instance, eicosanoid release (particularly thromboxane A2) could induce pulmonary and coronary vasoconstriction, which may be combined with microthrombus formation and microembolization of capillaries by neutrophil-platelet aggregates [13]. In addition, C3a can further activate platelets, enhancing their aggregation and adhesion, but C5a is 100-fold more potent than C3a, and enhance blood thrombogenicity through upregulation of tissue factor and plasminogen activator inhibitor-1 expression on various cell types [23,24]. Overall, the resultant falls in cardiac preload and coronary flow lead to myocardial ischemia, decreased contractibility and reduced cardiac output and

hypotension. If not resolved spontaneously, this may lead to circulatory collapse and death [14].

Recent studies have provided further evidence for the role of complement-derived anaphylatoxins in Doxil®-induced anaphylaxis [14]. Firstly, in heparinized (10 IU/ml, which has no major impact on controlling complement activation) pig plasma, Doxil® addition was able to elevate C5a levels by 300- to 400-fold **[Fig.2b]**, thus confirming complement activation [14]. In comparison, multilamellar vesicles composed of DMPC:DMPG:cholesterol (50:5:45 mole ratios) not only generated more C5a in the pig serum than Doxil® treatment **[Fig.2b]**, but also induced more severe cardiac abnormalities in the porcine model that were similar to those induced by administration of zymosan (a potent complement activating agent). These observations support the notion that the anaphylatoxin C5a plays a causal role in the cardiac abnormalities caused by liposome administration, and severe liposome reactions may involve a considerable rise of plasma C5a in pigs. Indeed, bolous administration of recombinant human C5a (rhC5a) at a dose of 330 ng/kg (normal pig plasma C5a level is ~20 ng/ml and the plasma volume is ~33 ml/kg) led to a mild reaction with transient reduction of pulse pressure and slight reversible hypertension **[Fig.2c]**. In sharp contrast, higher doses of rhC5a (e.g., equivalent to 600- to 700-fold higher than the baseline C5a level in pig) caused a short-lived transient hypertension followed by massive hypotension in association with bradyarrhythmia, pulmonary hypertension and marked decrease of end-tidal PCO2 **[Fig.2c]**. This treatment mimicked the severe cardiac abnormalities associated with multilamellar vesicles and zymosan. Furthermore, the severity of liposome-induced cardiac

abnormalities in the porcine model can be significantly reduced with complement inhibitors such as the recombinant truncated soluble form of complement receptor type-1 and anti-porcine C5a antibody GS1 [14]. However, we can not exclude a possible and significant role for other complement-derived anaphylatoxins (e.g., C3a) in the most severe or lethal reactions.

Doxil®-mediated complement activation in human serum

Doxil® was shown to trigger complement and generate complement opsonic fragments from radiolabelled C3 in human serum [16,25]. As shown in **Fig. 3** C3b deposition and degradation (65 and 40/43 kDa fragments) reaches the plateau within 5 min. This further confirms that surface-bound mPEG molecules do not interfere with C3b inactivation by factors H and I [16]. Another notable feature is generation of high molecular weight C3b- and iC3b-containing complexes (C3-X), a phenomenon typical of complement activation by immune aggregates. Doxil® has also been shown to activate complement in 21 out of 29 cancer patients, as reflected by significant elevation of SC5b-9 (the terminal complex activation marker of complement system) levels in plasma within 10–30 min of infusion [12]. In this study [12], cute allergic reactions were reported in 13 patients, where 12 had elevated plasma SC5b-9 levels. However, among the 16 non-responding individuals, 9 had elevated plasma SC5b-9 levels.

Vesicles of the same size and composition as Doxil®, but without encapsulated doxorubicin, also trigger complement in human serum through both classical and alternative pathways, but the extent of complement activation is less than that of Doxil® [25]. The mechanisms of complement activation by PEGylated liposomes, however, are poorly understood. Surface projected mPEGs may trigger complement through the classical pathway in the presence of reactive antibodies to PEG. Indeed, some 25% of the general populations are believed to be positive for IgG2 and IgM antibodies that recognize four to five repeat ethoxy units [26,27]. In our hands, none of the tested human sera were positive for anti-PEG antibodies, therefore complement activation by PEGylated liposomes can proceed in the absence of such antibodies. Nevertheless, anti-PEG antibodies through complement activation may play an important role in liposome clearance from the blood in protocols involving repeated administration of PEGylated vesicles [28,29].

Alternatively, PEG may act directly on complement proteins (e.g., C3) or indirectly through water activity to further enhance fluid phase complement turnover [18]. It is well established that the extent of water clustering increases with PEG size; the hydration increases from two molecules of water per PEG monomer for a tetramer to five molecules of water per PEG monomer for 45-mer [30,31]. Therefore, if C3 binds to or become trapped between surface PEG 'brushes', C3 hydration conformational changes ("C3 tickover") may become accelerated, leading to the assembly of fluid phase C3Bb convertases **[Fig.1]**. However, our studies with endotoxin free near monodispersed PEG2000 at a final concentration of 2.5 mg/ml in serum (this PEG

concentration far exceeds that of surface attached PEG in complement activation studies with PEGylated liposomes) did not raise serum levels of complement activation products C4d (a marker of calcium-sensitive classical and lectin pathways), Bb (a marker of the alternative pathway) and SC5b-9 above the background [32]. However, complement activation by PEG is concentration-dependent; for PEG2000 this translates to a concentration of ≥ 10 mg/ml but with higher molecular weight PEGs complement activation proceeds with lower concentrations [18]. The role of alternative pathway and lectin pathway in PEG-mediated triggering of complement cascade has been demonstrated [18]. These observations are therefore relevant to scenarios where intravenous PEG is used as a therapeutic agent; examples include spinal cord injury and traumatic axonal brain injury, where PEG is believed to seal the membrane of damaged axons through membrane fusion [33,34].

We further determined that mPEG-PL conjugates in micellar form were incapable of activating complement [32]. Thermodynamically, micellar solution is at equilibrium, the concentration of monomers being equal to the critical micelle concentration. This further suggests that mPEG-PL monomers are also ineffective in triggering complement. Remarkably, methylation of the phosphate-oxygen moiety of mPEG-lipid prevented complement activation by PEGylated vesicles [32]. This is illustrated in **Fig.4** with mPEG-prodrug ether lipid conjugate-based liposomes of different sizes and was further confirmed in vivo, using the rat model. Methylation not only removes the anionic charge on the phosphate-oxygen (anionic liposomes, and depending on their phospholipid headgroup, are

complement activators [15,35]), but may sterically block the simultaneous binding of naturally occuring anti-phospholipid antibodies to both liposomal phospholipid head group and the phosphate-oxygen moiety of the PEGylated conjugate. Additionally, methylation may interfere with spatial organization of surface-bound antibodies for correct recognition by the three modules of the globular C1q domain. On the basis of these observations, we ascribe the inability of mPEG-PL micelles to activate complement to their small hydrodynamic size and other geometrical factors that restrict the surface assembly of complement convertases. Indeed, complement convertases are in a similar size range (~20 nm) to these micelles. In marked contrast to this statement, we have also shown complement activation by poloxamer 188 and 407 micelles, which share similar size ranges to mPEG-PL micelles [16,20]. We are currently investigating the responsible mechanisms with these micelles. Collectively, these observations demonstrate the importance of interface characteristics, in which PEG-PL molecules are accumulated, resulting in triggering the complement cascade. Therefore, it would be interesting to examine the complement activating properties of methylated mPEG-PL incorported liposomes containing anionic phospholipids.

Complement-fixed PEGylated liposomes interact poorly with macrophage complement receptors (CRs) [32]. This is most likely due to steric hinderance by the projected mPEG chains to the binding of C3b- and iC3b-opsonized vesicles to their corresponding receptor (CR3) [32]. This process is most likely responsible for the blood longevity of PEGylated liposomes, which are opsonized.

Complement policing of carbon nanotubes

There is interest among material scientists to utilize non-biodegradable carbon nanotubes for site-specific drug delivery (as in targeting of solid tumours and nucleic acid delivery) and other biological interventions, which partly arises from their unique spectroscopic and thermal properties [36]. These entities can be single-walled or multi-walled, but for biological studies carbon nanotubes must be solubilized. This may be achieved either by covalent functionalization of their surface with different chemical groups or by adsorption of amphiphilic molecules, such as PEG-lipids.

Non-functionalized carbon nanotubes, whether single- or multi-walled, are activators of the human complement system [37]. For instance, with single-walled entities complement activation is exclusively due to adsorption of C1q and is independent of antibodies [37]. Complement activation also occurs with covalently functionalized nanotubes (e.g., ε-caprolactam or L-alanine functionalized) albeit to a lesser extent when compared with non-functionalized entities (uncoated nanotubes) [38].

Coating of carbon nanotubes (250 nm in length and 1–5 nm in width) with PEG5000-phospholipid conjugates affords excellent solubilization and stability in biological milieu [9]. These non-bodegradable entities potentially provide another interesting platform/model to assess the role of PEG-PL interfaces in modulating the activity of complement system and compare them to PEGylated nanomedicines. Accordingly, through a series of functional studies involving healthy and C1q-depleted sera we showed that PEG-PL-

stabilized carbon nanotubes can activate the human complement system through lectin pathway **[Fig.5]**. Indeed, nanotube-mediated complement activation was blocked by N-acetylglucosamine, a substrate for mannose-binding lectin (MBL) and ficolin, as well as in the presence of antibodies against MBL-associated serine protease-2, MASP-2 (the zymogen associated with MBL/ficolin) [39]. Mixed responses were in complement activation was noted in rats following nanotube administration (Fig. 5). These observations were based on thromboxane B2 measurements (an established and direct marker for thromboxane A2) [39]. Complement anaphylatoxins induce thromboxane A2 release from blood cells and demonstration of increased serum thromboxane B2 levels provides evidence of in vivo complement activation. The observed mixed responses may be due to differences in the blood concentration of lectin pathway components (e.g., mannose-binding lectin and/or ficolin; MASP-2 activity) among different rats. Nevertheless, our findings [39] are consistent with deposition of a significant fraction of intravenously injected PEGylated carbon nanotubes in hepatic Kupffer cells [9], which is presumably complement-mediated. Finally, the demonstrated adjuvanticity of carbon nanotubes (whether uncoated or surface-modifed) [40] is also consistent with their complement activating nature, bearing in mind that C3 split-products like C3d can induce B lymphocyte activation [41].

The exact mechanism for PEG-lipid stabilized carbon nanotubes-mediated triggering of lectin pathway remains unclear. Both mannose-binding lectin and ficolin express affinity for sugars with N-acetylated groups, but these structures are absent from native nanotubes. We

suggest that complement activation either arises from direct binding of mannose-binding lectin and/or ficolin to unprotected regions of PEGylated nanotubes (and indeed, atomic force microscopy studies have indicated that surface coating is not homogenous [39], **Fig. 6**) or indirectly via adsorption of mannose-rich serum components such as certain apo-lipoproteins. Our recent studies (unpublished observations) have further shown that nanotubes with covalently grafted mPEG molecules can still trigger the complement cascade and therefore resolving nanotube-mediated complement activation remains a challenge.

Concluding remarks

We have noted three modes of complement-related responses with PEG-phospholipid engineered entities **[Fig.6]** and discussed the likely driven forces and interfacial determinants that trigger complement. Comprehensive mapping of these events is expected to pave the way toward design and development of immunologically safer nanomedicines for clinical use. This has already begun with liposomes and micellar systems; from nanoengineering and 'structure-activity' relationship studies to clinical practice (i.e., dosing regimen, infusion time, desensitization with placebos). Indeed, mPEG-PL micelles seem to have an immunological safety edge for biomedical and therapeutic applications as they do not activate human complement; however, pharmaceutical aspects must also receive equal considerations in designing viable formulations. We are also paying attention to additional biological and design considerations that may trigger

complement in different body compartments [42,43] using a wide range of bionanotechnology tools and methodologies such as quartz crystal microbalance [44]. Our attempts include the pathology and microenvironmental factors regulating local complement activation (e.g., as in solid tumours and Alzheimer's disease), and also the effect of coupling of potentially complement-activating ligands (such as monoclonal antibodies and virally-derived peptides) to both PEGylated and non-PEGylated nanomedicines.

Resolution of carbon nanotube-mediated complement activation is largely hindered by the poorly-defined surfaces of nanotubes and lack of their reproducible production [45]. However, a clear understanding of molecular mechanisms that orchestrate complement activation by both native and surface-modified carbon nanotubes will have impact in the nanotoxicology field. Indeed, complement activation may be relevant to reported pro-inflammatory reactions following environmental exposure to carbon nanotubes and related carbon particles and fibers [46–48].

Clinical evidence from PEGylated liposome administration clearly attests that complement activation per se cannot solely explain vesicle-induced pseudoallergy. The involvement of other biological factors in pseudoallergy must not be ignored and should be investigated. Among many factors, there may be genomic differences between sensitive and non-sensitive individuals and future immunogenomic studies are expected to have an impact in pseudoallergy research. However, parallel development of in vitro tests are still needed to differentiate between immunologically (at least from complement immunology point of view) "potent" and "safe"

nanomedicines and/or sensitive and non-responding individuals [17]. This is especially relevant to clinical scenarios where cardiovascular stress is not acceptable.

Figure Legends:

Figure 1: Complement activation pathways. C4d, Bb and SC5b-9 are established activation markers (〰) for calcium sensitive (CP & LP), AP and terminal pathways, respectively. Activation markers for anaphylatoxins (✹) are also shown.

Figure 2: Cardiopulmonary and electrocardiogram changes in pigs after bolus injection of Doxil® (a) or recombinant human C5a (c) and C5a production in pig serum following liposome challenge. SAP = systemic arterial pressure; PAP = pulmonary arterial pressure; PRL = standard poorly reactive liposomes (they do not induce significant haemodynamic and cardiorespiratory abnormalities) in pigs; HRL = highly reactive liposomes (multilamellar vesicles formed from DMPC:DMPG:cholesterol, mole ratios 50:5:45 that induce dramatic and extended declines in SAP, pulse amplitude, end-tidal PCO_2 and major rise in PAP) in pigs. Modified after Szebeni et al., [14] with permission.

Figure 3: Doxil®-mediated complement activation in human serum. For clarity and interpretation of the SDS-PAGE profile in (b), the schematic structure of C3 is also presented (a). C3 convertases initially cleave the α chain at arrow head 1, generating anaphylatoxin C3a and a conformationally changed C3b frgament (α′ chain and the uncleaved β chain), where the reactive thiolester moiety in C3dg portion can form covalent bonds with the complement activating surface/particle P. Only a small portion of C3b binds to the complement activating surface and the thiolester of the majority of C3b reacts with water to form iC3b. C3b is sequentially catalyzed (two stages) by factor I (arrow heads 2 & 3), resulting in the release of C3f (and the formation of iC3b) and C3c. This leaves C3dg bound to the target (see also **Fig.1**). Modified after Moghimi & Szebeni [16] with permission.

Figure 4: Effect of liposome composition and size on complement activation in human serum. Liposmes were composed of DPPC and designated mPEG-lipids (a) in molar ratios of 95:5, unless stated otherwise. Modified after Moghimi et al., [32] with permission.

Figure 5: Complement activation by single walled carbon nanotubes (SWNT) in human serum and in vivo in rats. Detailed experimental procedures are presented elsewhere. Modified after Hamad et al., [39] with permission.

Figure 6: Summary of complement cascade triggering by PEG-PL engineered nanomedicines and carbon nanotubes.

Figures:

Fig. 1

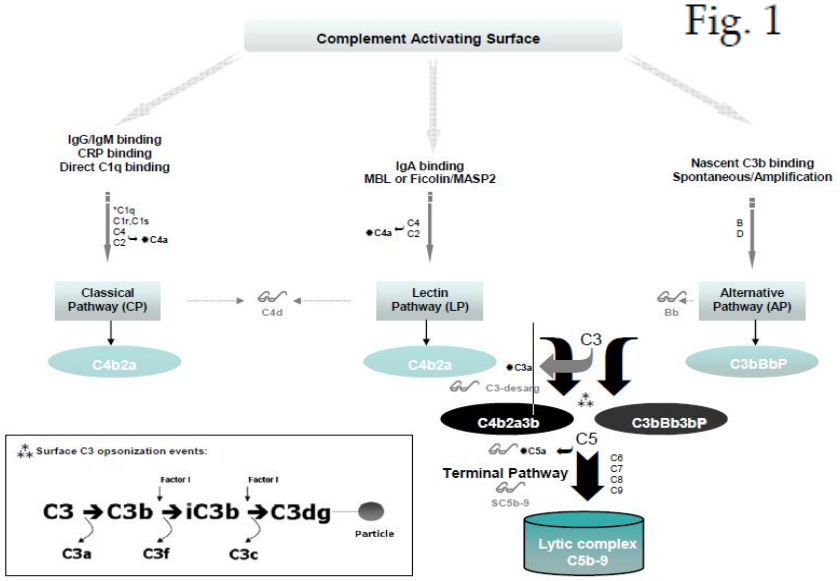

Fig. 2

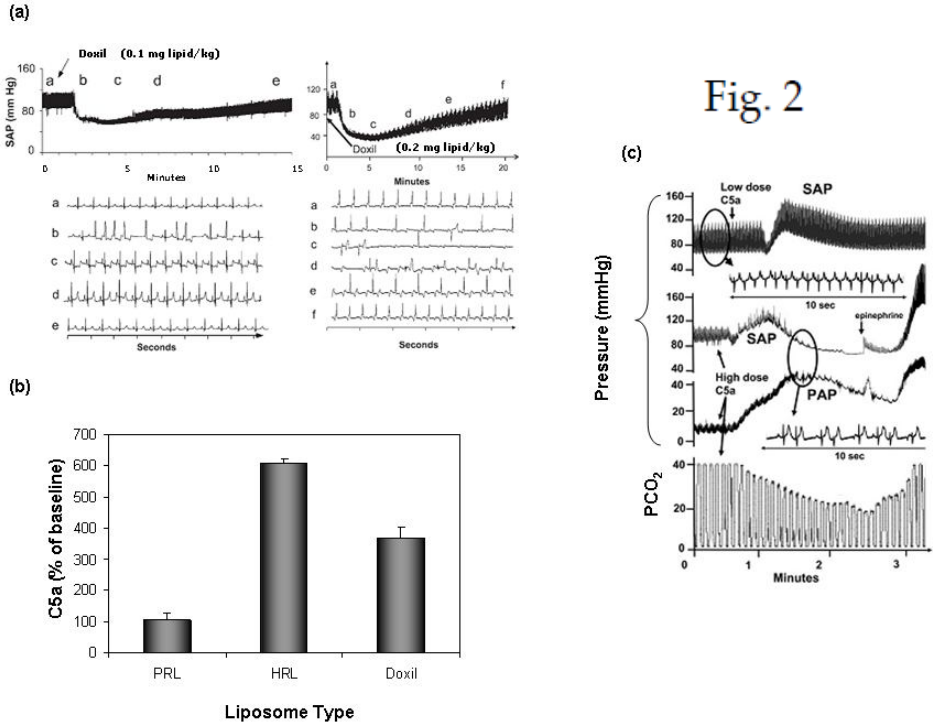

Fig. 3

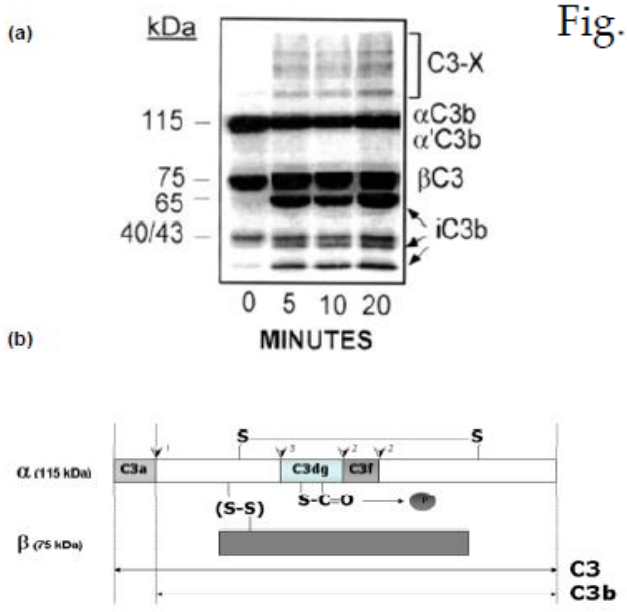
(a)
kDa
115
75
65
40/43
C3-X
αC3b
α'C3b
βC3
iC3b
0 5 10 20
MINUTES
(b)
α (115 kDa)
β (75 kDa)
C3a
C3dg
C3f
S
S
(S-S)
S-C=O
C3
C3b

Fig. 4

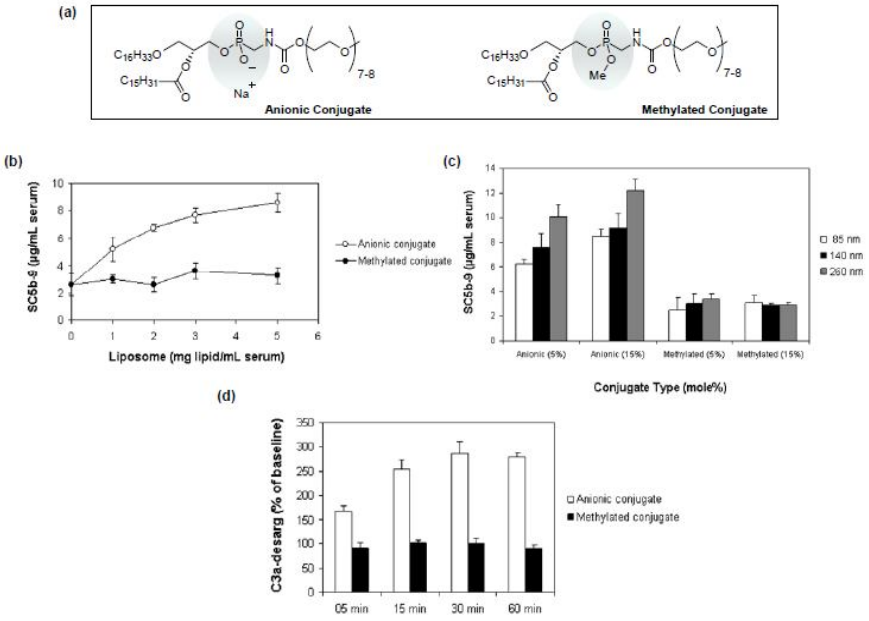
(a)
Anionic Conjugate
Methylated Conjugate
(b)
SC5b-9 (µg/mL serum)
Liposome (mg lipid/mL serum)
Anionic conjugate
Methylated conjugate
(c)
SC5b-9 (µg/mL serum)
85 nm
140 nm
260 nm
Anionic (5%)
Anionic (15%)
Methylated (5%)
Methylated (15%)
Conjugate Type (mole%)
(d)
C3a-desarg (% of baseline)
Anionic conjugate
Methylated conjugate
05 min
15 min
30 min
60 min

Fig. 5

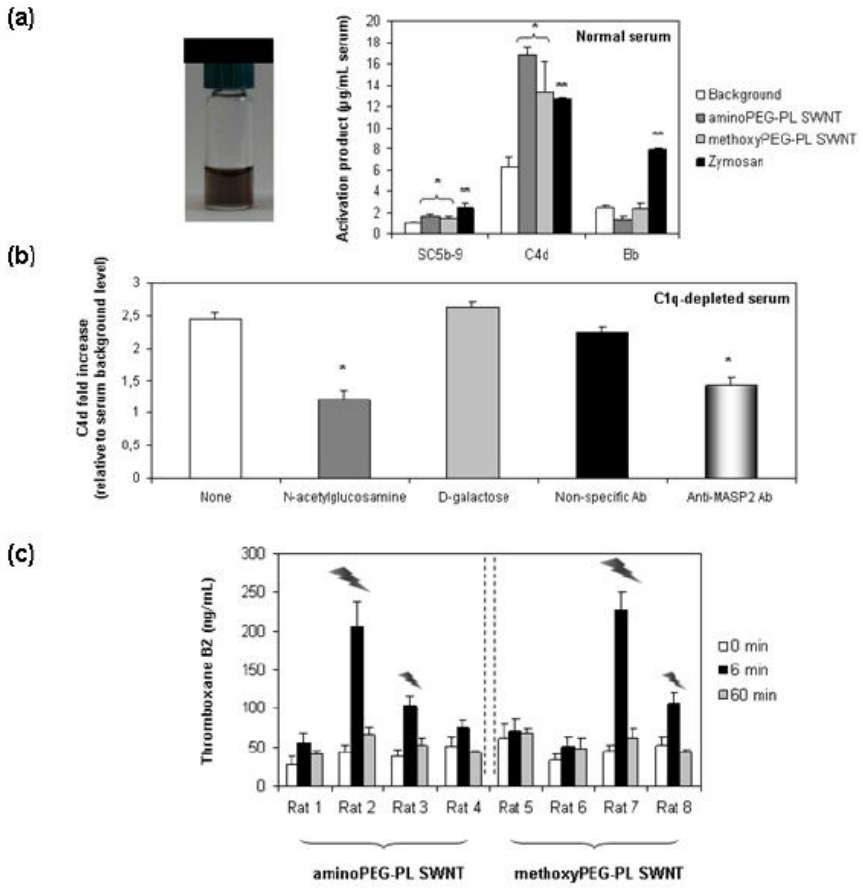
(a)
Normal serum
Activation product (μg/mL serum)
SC5b-9
C4d
Bb
Background
aminoPEG-PL SWNT
methoxyPEG-PL SWNT
Zymosan
(b)
C1q-depleted serum
C4d fold increase
(relative to serum background level)
None
N-acetylglucosamine
D-galactose
Non-specific Ab
Anti-MASP2 Ab
(c)
Thromboxane B2 (ng/mL)
0 min
6 min
60 min
Rat 1
Rat 2
Rat 3
Rat 4
Rat 5
Rat 6
Rat 7
Rat 8
aminoPEG-PL SWNT
methoxyPEG-PL SWNT

Fig. 6

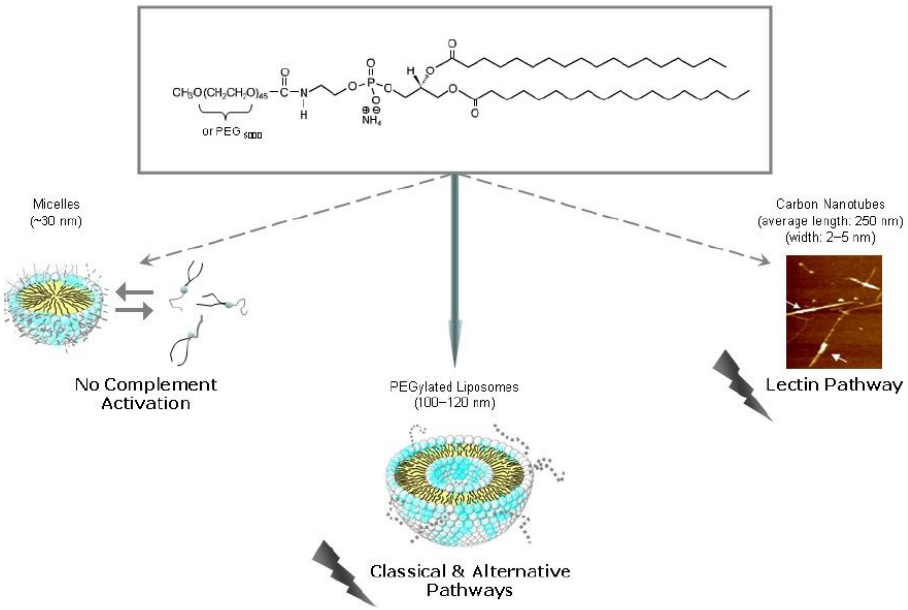
Micelles
(~30 nm)
No Complement
Activation
PEGylated Liposomes
(100–120 nm)
Classical & Alternative
Pathways
Carbon Nanotubes
(average length: 250 nm)
(width: 2–5 nm)
Lectin Pathway

References

1. **S.M. Moghimi**, A.C. Hunter, J.C. Murray, Long-circulating and target-specific nanoparticles: theory to practice, Pharmacol. Rev. 53 (2001) 283–318.
2. **S.M. Moghimi**, A.C. Hunter, J.C. Murray, Nanomedicine: current status and future prospects, FASEB J. 19 (2005) 311–330.
3. **T.M. Allen**, P.R. Cullis, Drug delivery systems: entering the mainstream, Science 303 (2004) 1818–1822.
4. **V.P. Torchilin**, Recent advances with liposomes as pharmaceutical carriers, Nat. Rev. Drug Discov. 4 (2005) 145–160.
5. **S.M. Moghimi**, T. Kissel, Particulate nanomedicines, Adv. Drug Deliv. Rev. 58 (2006) 1451–1455.
6. **V.P. Torchilin**, Multifunctional nanocarriers, Adv. Drug Deliv. Rev. 58 (2006) 1532–1555.
7. **V.P. Torchilin**, Structure and design of polymeric surfactant-based drug delivery systems, J. Control. Rel. 73 (2001) 137–172.
8. **F. Liu**, D. Liu, Long-circulating emulsions (oil-in-water) as carriers of lipophilic drugs, Pharm. Res. 12 (1995) 1060–1064.
9. **Z. Liu**, C. Davis, W. Cai, L. He, X. Chen, H. Dai, Circulation and long-term fate of functionalized, biocompatible single-walled carbon nanotubes in mice probed by Raman spectroscopy, Proc. Natl. Acad. Sci. U.S.A. 105 (2008) 1410–1415.
10. **B. Uziely**, S. Jeffers, R. Isacson, K. Kutsch, D. Wei-Tsao, Z. Yehoshua, E. Libson, F.M. Muggia, A. Gabizon, Liposomal doxorubicin: activity and unique toxicities during two complementary phase I studies, J. Clin. Oncol. 13 (1995) 1777–1785.
11. **D.S. Alberts**, D.J. Garcia, Safety aspects of pegylated liposomal doxorubicin in patients with cancer, Drugs (Suppl.) 54 (1997) 30–45.

12. **A. Channan-Khan**, J. Szebeni, S. Savay, L. Liebes, N.M. Rafique, C.R. Alving, F.M. Muggia, Complement activation following first exposure to pegylated liposomal doxorubicin (Doxil): possible role in hypersensitivity reactions, Annal. Oncology 14 (2003) 1430–1437.
13. **J. Szebeni**, Complement activation-related pseudoallergy: a new class of drug-induced acute immune toxicity, Toxicology 216 (2005) 106–121.
14. **J. Szebeni**, L. Baranyi, S. Savay, M. Bodo, J. Milosevits, C.R. Alving, R. Bunger, Complement activation-related cardiac anaphylaxis in pigs: role of C5a anaphylatoxin and adenosine in liposome-induced abnormalities in ECG and heart function, Am. J. Physiol. Heart Cir. Physiol. 290 (2006) H1050–H1058.
15. **S.M. Moghimi**, I. Hamad, Liposome-mediated triggering of complement cascade, J. Liposome Res. 18 (2008) 195–209.
16. **S.M. Moghimi**, J. Szebeni, Stealth liposomes and long circulating nanoparticles: critical issues in pharmacokinetics, opsonization and protein-binding properties, Prog. Lipid Res. 42 (2003) 463–478.
17. **J. Szebeni**, S.M. Moghimi, Liposome triggering of innate immune responses: a perspective on benefits and adverse reactions, J. Liposome Res. 19 (2009) 85–90.
18. **I. Hamad**, A.C. Hunter, J. Szebeni, S.M. Moghimi, poly(ethylene glycol)s generate complement activation products in human serum through increased alternative pathway turnover and a MASP-2-dependent process, Mol. Immunol. 46 (2008) 225–232.
19. **R. Lustig**, N. McIntosh-Lowe, C. Rose, J. Haas, S. Kransnow, M. Spaulding, L. Prosnitz, Phase I/II study of Fluosol-DA and 100% oxygen as an adjuvant to radiation in the treatment of advanced squamous cell tumours of the head and neck, Int. J. Radiat. Oncol. Biol.16 (1989) 1587-1593.
20. **S.M. Moghimi**, A.C. Hunter, C.M. Dadswell, S. Savay, C.R. Alving, J. Szebeni, Causative factors behind poloxamer 188 (Pluronic F68,

Flocor™)-induced complement activation in human sera. A protective role against poloxamer-mediated complement activation by elevated serum lipoprotein levels, Biochim. Biophys. Acta 1689 (2004) 103–113.

21. **G. Marone**, M. Bova, A. Detoraki, A.M. Onorati, F.W. Rossi, G. Spadaro, The human heart as a shock organ in anaphylaxis, Novartis Found. Symp. 257 (2004) 133–149.
22. **G. Marone**, V. Patella, G. de Crescenzo, A. Genovese, M. Adt, Human heart mast cells in anaphyaxis and cardiovascular disease, Int. Arch. Allergy Immunol. 107 (1995) 72–75.
23. **M.M. Markiewski**, B. Nilsson, K.N. Ekdahl, T.E. Mollnes, J. D. Lambris, Complement and coagulation: strangers or partners in crime? Trend. Immunol. 28 (2007) 184–192.
24. **A.J. Andersen**, A.H. Hashemi, T.L. Andresen, A.C. Hunter, S.M. Moghimi, Complement: alive and kicking nanomedicines, J. Biomed. Nanotechnol. 5 (2009) 364–372.
25. **J. Szebeni**, L. Baranyi, S. Savay, H.U. Lutz, E. Jelezarova, R. Bunger, C.R. Alving, The role of complement activation in hypersensitivity to pegylated liposomal doxorubicin (Doxil), J. Liposome Res. 10 (2000) 469–481.
26. **J. K. Armstrong**, G. Hempel, S. Koling, L.S. Chan, T. Fisher, H.J. Meiselman HJ, G. Garratty, Antibody against poly(ethylene glycol) adversely affects PEG-asparaginase therapy in acute lymphoblastic leukemia patients, Cancer 110 (2007) 103–111.
27. **A.W. Richter**, E. Akerblom, Polyethylene glycol reactive antibodies in man: titer distribution in allergic patients treated with monomethoxy polyethylene glycol modified allergens or placebo, and in healthy blood donors, Int. Arch. Allergy Appl. Immunol. 70 (1984) 124–131.
28. **A. Ludge**, K. McClintock, J.R. Phelps, I, MacLachlan, Hypersensitivity and loss of disease site targeting caused by antibody responses to PEGylated liposomes, Mol. Ther. 13 (2006) 328–337.

29. **T. Ishida**, S. Kashima, H. Kiwada, The contribution of phagocytic activity of liver macrophages to the accelerated blood clearance (ABC) phenomenon of PEGylated liposomes in rats, J. Control. Rel. 126 (2008) 162–165.

30. **V. Crupi**, M.P. Jannelli, S. Magazu, G. Maisano, D. Majolino, P. Migliardo, R. Pontiero, Raman spectroscopic study of water in the poly(ethylene glycol) hydration shell, J. Mol. Struct. 381 (1996) 207–212.

31. **M. Kozielski**, Conformational changes in the chains of polyoxyethyleneglycols, J. Mol. Liquid 128 (2006) 105–107.

32. **S.M. Moghimi**, I. Hamad, T.L. Andresen, K. Jørgensen , J. Szebeni, Methylation of the phosphate oxygen moiety of phospholipid-methoxy(polyethylene glycol) conjugate prevents PEGylated liposome-mediated complement activation and anaphylatoxin production, FASEB J. 20 (2006) 2591–2593.

33. **P.H. Laverty**, A. Leskovar, G.J. Breur, J.R. Coates, R.L. Bergman, W.R., Widmer, T.J. Toombs, S. Shapiro, R.B. Borgens, A preliminary study of intravenous surfactants in paraplegic dogs: polymer therapy in canine clinical SCI, J. Neurotrauma 21 (2004) 1767–1777.

34. **A.O. Koob**, R.B. Borgens, Polyethylene glycol treatment after traumatic brain injury reduces β-amyloid precursor protein accumulation in degenerating axons, J. Neurosci. Res. 83 (2006) 1558–1563.

35. **S.M. Moghimi**, A.C. Hunter, Recognition by macrophages and liver cells of opsonized phospholipid vesicles and phospholipid headgroups, Pharm. Res. 18 (2001) 1–8.

36. **K. Kostarelos**, A. Bianco, M. Prato, promises, facts and challenges for carbon nanotubes in imaging and therapeutics, Nat. Nanotechnol. 4 (2009) 627–633.

37. **C. Salvador-Morales**, E. Flahaut, E. Sim, J. Sloan, M.L. Green, and R.B. Sim, Complement activation and protein adsorption by carbon nanotubes, Mol. Immunol. 43 (1996) 193–201.

38. **C. Salvador-Morales**, E.V. Basiuk, V.A. Basiuk, M.L.H. Green, R.B. Sim, Effects of covalent functionalization on the biocompatibility characteristics of multi-walled carbon nanotubes, J. Nanosci. Nanotechnol. 8 (2008) 2347–2356.

39. **I. Hamad**, A.C. Hunter, K.J. Rutt, Z. Liu, H. Dai, S.M. Moghimi, Complement activation by PEGylated single-walled carbon nanotubes is independent of C1q and alternative pathway turnover, Mol. Immunol. 45 (2008) 3797–3803.

40. **D. Pantarotto**, C.D. Partidos, J. Hoebeke, F. Brown, E. Kramer, J.P. Briand, S. Muller, M. Prato, A. Bianco, Immunization with peptide-functionalized carbon nanotubes enhances virus-specific neutralizing antibody responses, Chem. Biol. 10 (2003) 961–966.

41. **D.T. Fearon**, M.C. Carroll, Regulation of B lymphocyte responses to foreign and self-antigens by the CD19/CD21 complex, Ann. Rev. Immunol. 18 (2000) 393–422.

42. **M.M. Markiewski**, R.A. De Angelis, F. Benencia, S.K. Ricklin-Lichtsteiner, A. Koutoulaki, C. Gerard, G. Coukos, J. D. Lambris, Modulation of the antitumor immune response by complement, Nat. Immunol. 9 (2008) 1225–1235.

43. **S.M. Moghimi**, T.L. Andresen, Complement-mediated tumour growth: implications for cancer nanotechnology and nanomedicines, Mol. Immunol. 46 (2009) 1571–1572.

44. **A.C.Hunter**, Application of quartz crystal microbalance to nanomedicine, J. Biomed. Nanotechnol. 5 (2009) 669–675.

45. **M.C. Hersam**, Progress towards monodisperse single-walled carbon nanotubes, Nat. Nanotechnol. 3 (2008) 387–394.

46. **C. Salvador-Morales**, P. Towensend, E. Flahaut, C. Venien-Bryan, A. Vlandas, M.L.H. Green, R.B. Sim, Binding of pulmonary surfactant proteins to carbon nanotubes; potential for damage to lung immune defense mechanisms, Carbon 45 (2007) 607–617.
47. **L.A. Mitchell**, F.T. Lauer, S.W. Burchiel, J.D. McDonald, Mechanisms for how inhaled multiwalled carbon nanotubes suppress systemic immune function in mice, Nat. Nanotechnol. 4 (2009) 451–456.
48. **C.A. Poland**, R. Duffin, I. Kinloch, A. Maynard, W.A.H. Wallace, A. Seaton, V. Stone, S. Brown, W. MacNee, K. Donaldson, Carbon nanotubes introduced into the abdominal cavity of mice shows asbestos-like pathogenicity in a pilot study, Nat. Nanotechnol. 3 (2008) 423–428.

Chapter 6

Summary, conclusions and future perspectives

The research papers presented in this dissertation have first evaluated different mechanisms of interaction between Nanoparticles and cells, especially alveolar epithelial cells, which are remarkably related to composition and size of the nanocarrier taken into account. Indeed, the most likely route of NPs entry into the body is the inhalation. Therefore, in addition to a systemic administration engineered NPs could act as useful carriers of drugs and macromolecules for topic pulmonary delivery. However, despite a number of advantages derived from the application of nanotechnology to biomedicine, the issue associated to NPs acute and late toxicity still remain a major unsolved drawbacks. Accordingly, our studies fit well in this context as they provide an essential starting point for understanding the basics of cell biology, in terms of cellular dynamics occurring in response to NPs exposure, thus gaining insight of any potential acute cytotoxicity.

On the one hand, it is most likely that SLN, a class of lipid-based NPs in a size range of 130-150 nm, facilitated transfer of loaded lipophilic compounds (e.g. the fluorescent dye 6-Coumarin) directly from the donor particle to the receiving cell cytoplasm following inter-membranes close apposition and lipid exchange. Our hypothesis was pointed out by several findings: modifications in SLN structure upon contact with cell plasma membrane, no significant impairment of 6-Coumarin uptake even at temperatures as low as 4°C and absence of co-localization with endocytic and cytoplasmic proteins [see Chapters 2 and 3]. On the other hand, our data clearly suggested a macropinocytosis-mediated uptake of iron oxide NPs sterically stabilized with the dispersant L-Dihydroxyphenylalanine (L-dopa) by virtue of their size which can approximately reach 260 nm in the

culture medium and scale up to intracellular aggregates, with increasing exposure time. Likewise, the incubation with specific inhibitors of macropinocytosis (e.g. amiloride and its derivative EIPA) along with nocodazole and cytochalasin D prevented nanoparticles from entering the cells, intimating a potential role of the cytoskeleton in NPs crossing the plasma membranes [see Chapter 4]. Although these particles differ in composition and mechanisms of cellular internalization, they showed a common feature of perinuclear accumulation over time. Either absence or minimal co-localization with intracellular compartments and organelles might partly exclude particle trafficking to lysosomes in the early stages of NPs exposure in favour of the idea that a mean force field, driven by cytoskeleton, could act on intact particles or on their cargo, thus inducing their accumulation around the nucleus. Focusing the analysis over prolonged period of time could provide more information to clarify the biological role of the perinuclear NPs accumulation.

Indeed, the thorough knowledge of the intracellular dynamics in response to NPs is the initial step to further modify particle properties for optimizing their targeted delivery. For instance, different approaches, such as *in vitro* magnetic-mediated transfections of macromolecules (e.g. DNA, siRNA) and drug delivery in cancer treatment, require the design of functionalized NPs both to promote cellular uptake and to circumvent lysosomal degradation.

Gaining insight into NPs fate also means understanding both the mechanisms and the products of NPs degradation because even "biocompatible coatings' that are considered initially stable may

eventually generate toxic products or expose the NPs core, thereby eliciting adverse cellular responses.

Moreover, other investigations should monitor the effect of intracellular NPs concentration over time. It is most likely that cells possess an intrinsic threshold of particles accumulation above which dramatic alterations on cell physiology may occur, regardless the type of NPs used. Indeed, high concentrations of nondegradable particles, such as carbon nanotubes and iron oxide NPs, have been shown to affect cell proliferation [1-2] and functionality [3], through remarkable cytoskeletal reorganization, even without causing acute cell death. Likewise, our results have demonstrated that even SLN, that are generally accepted as biocompatible formulations, showed clear signs of toxicity at higher concentrations probably due to either cell osmotic stress or destabilization of cellular membranes, as already described for cationic magnetoliposomes [4].
This scenario highlights the need for new tests aimed at monitoring long lasting cytotoxicity since acute, though inert, sub-cellular alterations could generate long-term irreversible cell damages.

The last part of the research work addressed the immunological aspect of the potential NPs toxicity, in terms of activation of the Complement cascade in human sera following challenge with NPs. Although this issue is of primary importance to minimize the risk of developing non IgE-mediated hypersensitivity reactions, it has received poor consideration so far. More relevantly, NPs stably coated with inert moieties (e.g. PEG phospholipid conjugates) and generally believed as "stealth" entities might elicit Complement activation.

A clear example is Doxil, a Pegylated liposomal formulation, whose capability to generate acute pseudoallergy after infusion was most likely associated to the release of complement-derived anaphylatoxins (C3a and C5a), as demonstrated in pigs. Indeed, C5a together with c3a may promote the release of inflammatory mediators, especially tromboxane A, and vasoactive molecules via the binding to mast cells, basophiles and macrophages. Since other factors, such as the inter-individual genetic differences among sensitive and non sensitive subjects may play a role in developing adverse reactions, future *in vitro* screening of complement activation together with immunogenomic studies are expected to clarify the mechanism of NPs-mediated pseudoallergy.

In conclusion, our *in vitro* studies, working synergically with future *in vivo* experiments, will provide key information for design of biologically and immunologically safer nanocarriers for therapeutic and diagnostic applications.

References

[1] **Holt B.D**., Short P.A., Rape A.D., Wang Y-l. and Dahl K.N., (2010) Carbon Nanotubes Reorganize Actin Structures in Cells and *ex Vivo*. ACSNano 4(8):4872-4878.

[2] **Soenen S.J.H.**, Nuytten N., De Meyer S.F., De Smedt C., and De Cuyper M., (2010) High intracellular iron oxide nanoparticle concentrations affect cellular cytoskeleton and focal adhesion kinase-mediated signaling. Small 6(7): 832-842.

[3] **Kostura L**., Kraitchman D., Mackay A.M., Pittenger M.F., and Bulte J.W., (2004) Feridex labeling of mesenchymal stem cells inhibits chondrogenesis but not adipogenesis or osteogenesis. NMR Biomed.17:513-517.

[4] **Soenen S.J.H**., Brisson A.R., and De Cuyper M. (2009) Addressing the problem of cationic lipid-mediated toxicity: the magnetoliposome model. Biomaterials 30: 3691-3701.

Publications

1. Cellular uptake of coumarin-6 as a model drug loaded in Solid Lipid Nanoparticles (SLN).
   Rivolta I., Panariti A., Lettiero B., Sesana S., Gasco P., Gasco MR., Masserini M., Miserocchi G.
   J. Physiol. Pharmacol, 2011 (in press)

2. Uptake of Solid Lipid Nanoparticles in a mammalian cell line: insight into the cytoplasmic distribution.
   Rivolta L., Panariti A., Collini M., Lettiero B., D'Alfonso L., G. Miserocchi G., Chirico G.
   FEBS J., 2011 (submitted)

3. Uptake and intracellular distribution of functionalized iron oxide nanoparticles.
   Lettiero B., Panariti A. , Morjan I., Wang D., Dumitrache F., Alexandrescu R., Miserocchi G., Rivolta I.(in preparation)

4. Complement activation cascade triggered by PEG-PL engineered nanomedicines and carbon nanotubes: challenges ahead.
   SM Moghimi, AJ Andersen, SH Hashemi, B Lettiero, AC Hunter, TL Andresen, J Szebeni
   J. Control. Release 146 (2010) 175-181